ISSN number 0971 - 9709

The Journal of Indian Geophysical Union

VOLUME 23, ISSUE 2 I MARCH 2019

AN OPEN ACCESS BIMONTHLY JOURNAL OF IGU

EDITORIAL OFFICE

Indian Geophysical Union, NGRI Campus, Uppal Road, Hyderabad- 500 007
Telephone: +91 -40-27012799; 27012734; Telefax:+91-04-27171564
E. mail: jigu1963@gmail.com, website: www.j-igu.in

The Open Access Journal with six issues in a year publishes articles covering
Solid Earth Geosciences; Marine Geosciences; and Atmospheric, Space and Planetary Sciences.

Annual Subscription

Individual ₹ 1000 per issue and Institutional ₹ 5000 for six issues

Payments should be sent by DD drawn in favour of "The Treasurer, Indian Geophysical Union", payable at Hyderabad, Money Transfer/NEFT/RTGS (Inter-Bank Transfer), Treasurer, Indian Geophysical Union, State Bank of India, Habsiguda Branch, Habsiguda, Uppal Road, Hyderabad- 500 007
A/C: 52191021424, IFSC Code: SBIN0020087, MICR Code: 500002318, SWIFT Code: SBININBBHO9.

For correspondence, please contact, Hon. Secretary, Indian Geophysical Union, NGRI Campus, Uppal Road, Hyderabad - 500 007, India; Email: igu123@gmail.com; Ph: 040 27012799, 272012734

ISSN: 0257-7968 (Clarivate Analytics)
ISSN: 0971-9709 (NISCAIR)
Approved as bimonthly ESCI journal by Clarivate Analytics
Cited in Indian Citation Index (ICI), New Delhi
Evaluated by NISCAIR, New Delhi

CONTENTS

Research Articles

Invited Tutorial

J. Ind. Geophys. Union (March 2019)
v.23, no.2, pp: 109-119

Delineation and sustainable development of groundwater resources in granitic terrain using electrical resistivity tomography

S.N. Rai* and S. Thiagarajan
CSIR-National Geophysical Research Institute, Hyderabad-500007, India
*Corresponding author: snrai_ngri@yahoo.co.in

ABSTRACT
Hard rock's possess negligible primary porosity but due to inherent secondary porosity in the form of geological structures such as faults, fractures, joints etc, these rocks are rendered permeable to allow movement and storage of groundwater in limited quantity. Because of sporadic distribution of these water bearing geological structures, their delineation is a challenging task. Groundwater saturated geological formations/ structures are characterized with appreciably lower resistivity in comparison to those devoid of groundwater. Because of this, resistivity method is found to be most suitable among all the geophysical methods in delineation of groundwater bearing zones in all types of geological formations in general and hard rock terrains in particular. This paper discusses the efficacy of 2D Electrical Resistivity Tomography (ERT) to delineate groundwater bearing zones in complex hydrogeological environs like granitic terrains with the help of case studies from sites located in and around Hyderabad (Telangana state, India). ERT results have also been used to identify suitable sites for managing recharge of groundwater resources. This study has helped in establishing some criterion about the possibility of occurrence of potential groundwater resources in similar geological environs.

INTRODUCTION

A major part of southern Indian territories consisting of Telangana, Andhra Pradesh, Karnataka and Tamil Nadu states is occupied by various types of hard rock such as granites, granitic gneisses, granulites, charnokites etc. Hard rock terrains exhibit weathered formation and structural features such as fractures, joints, faults and fissures developed as secondary porosity within them. These geological formations/structures are capable of storing ground water and allow its movement through them, if these are interconnected. These geological formations/ structures are referred as aquifers in hydrological term. Acute shortage of groundwater in hard rock terrains is well known because of their limited groundwater storage capacity. In hard rock terrains, ground water occurs under phreatic condition in the top weathered formation and under semi-confined to confined conditions in fractures, faults and joints at relatively deeper level. Because of withdrawal of groundwater in excess to recharging of groundwater system to meet the ever increasing demand of water supply, groundwater level has been declining year by year beyond the recovery limit. As a result, groundwater in many areas has been almost depleted in the upper weathered formations, which happen to be the main sources of water supply to the dug wells penetrating shallower aquifers. Thus, the possibility of availability of groundwater lies in the fractures, faults, joints etc at deeper levels within the hard rock unites. Delineation of groundwater potential zones and suitable sites for managing aquifer recharge are prerequisite for the sustainable development and management of groundwater resources to ensure safe and secured water supply.

Geophysical Electrical resistivity methods with different types of electrode configurations are widely used for groundwater prospecting because of noticeable contrast in resistivity value of water saturated geological formations/ structures in comparison to those devoid of groundwater. These methods are described in detail in different text books on geophysical methods (Kirsch, 2006; Dobrin and Savit, 1988; Kearey and Brooks, 2002; Todd and Mays, 2013 etc). A 2D model of the sub-surface terrain can provide information about the distribution of different units of geological formations/structures in the vertical as well as in lateral directions below the entire spread of the survey line. This becomes possible by development of 2D electrical resistivity tomography (ERT) (Griffiths et al., 1990; Griffiths and Barker, 1993; Loke, 2000) and effective data processing softwares based on inversion techniques (Loke and Barker, 1996; Loke, 1997). The main advantages of the ERT are: (i) fast and large amount of computer controlled data acquisition, (ii) increased resolution of the computed 2D images of the resistivity variation of subsurface geological formation, and (iii) presentation of resistivity variation in vertical and horizontal directions below the entire survey line. In fact, electrical resistivity tomography is now being used worldwide for delineation of groundwater resources for various purposes such as groundwater exploration to meet water supply demand, dewatering of mines to prevents land slide and collapsing of mines, extraction of geothermal energy etc (Loke, 2000; Dutta et al., 2006; Hamzah et al., 2006; Anthony and John, 2010; Kumar et al., 2011; Rai et al., 2019). Electrical resistivity tomography has further been used in Deccan traps covered draught prone Vidarbha and Marathwada regions of Maharashtra state, India (Ratnakumari et al, 2012; Rai et al., 2015; Thiagarajan et

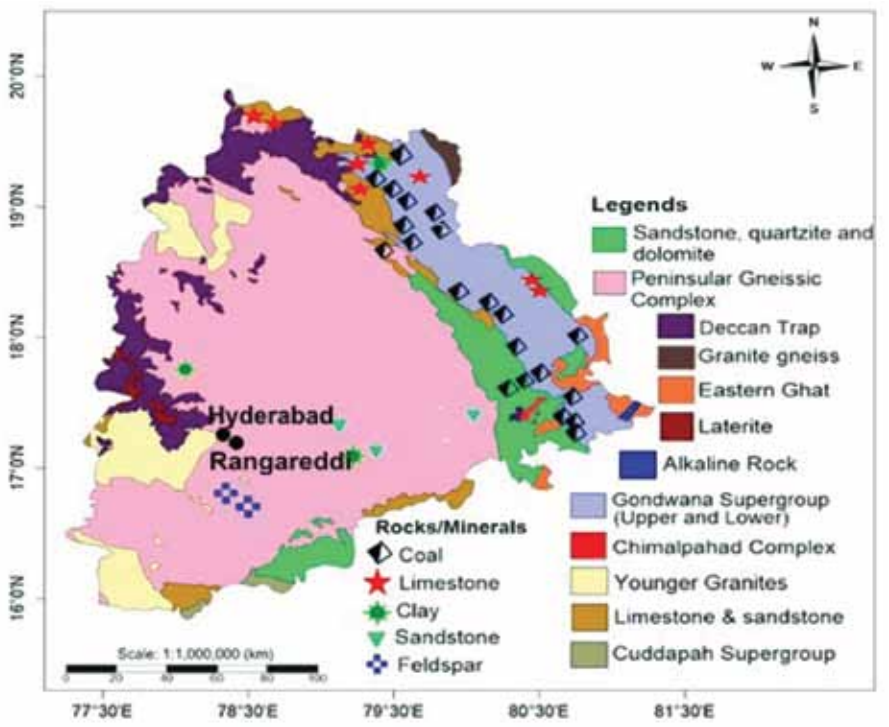

Figure 1. Geological map of Telangana (source Google).

al., 2018). The present study is aimed for delineation of aquifers and suitable sites for managing aquifer recharge using electrical resistivity tomography. The reason for failure of bore wells in short span of time and the corrective measures to overcome this problem are also discussed. The case studies presented in this paper may serve as a role model for the delineation and sustainable development of groundwater resources in other parts of hard rock terrains in order to achieve the preset objectives of management of the groundwater resources.

STUDY AREAS

The areas under investigation are located in Hyderabad city and adjoining Rangareddi district of Telangana state. Location of Hyderabad in Telagana state is shown in Figure 1. One of the investigated sites lies in the CSIR-Centre of Cellular and Micro Biology (CCMB) colony and further two sites are located in the campus of CSIR-Indian Institute of Chemical Technology (IICT). Both institutes are located in the Habshiguda area of Hyderabad. Figure 2 presents aerial view of CSIR-CCMB colony and its surroundings, together with the location of ERT profile. The colony is surrounded by Peddacheruvu (lake) from northern side, CSIR-National Geophysical Research Institute (NGRI) campus from southern side, HMT colony and CSIR-IICT colony from western side. It spreads in an area of over 14 acres. About 65% area is occupied by staff quarters. Slope of the landscape is northwards. Similarly, Indian Institute of Chemical Technology (IICT) campus is located by the side of Uppal road between Tarnaka and Habshiguda areas of Hyderabad (Figure 3). Electrical resistivity tomography is carried out along two profiles, P1 and P2, using Wenner configuration. Locations of P1 and P2 profiles are marked in figure 3. The P1 profile runs in east-west direction from staff quarter to the IICT boundary along the Uppal road through Diamond Jubilee Park (D.J. Park) and premise of Director's bungalow. The P2 profile is located in front of Lipid Science Center between IICT boundaries with Snehapuri colony in East and Nagarjunanagar colony in west. Other two ERT sites are located in a farmland under Raviryal village in Mahesharam mandal of Rangreddi district and one ERT site is located near Himayat sagar lake in the Aziz nagar under Moinabad thesil of Rangareddi district. Locations of Raviryal and Aziz nagar are shown in figures 4 and 5, respectively.

The regions under investigations are covered by the Archean granites and granite gneisses. These rocks are the major constituents of peninsular gneissic complex which occupies more than 70% surface area of Telangana state, as shown in figure 1. Gray and pink color granites are cropped out at several locations. Red soil of varying thicknesses forms top layer within the CCMB colony and IICT campus, while black soil forms top layer in the farmlands under Raviryal village and Aziz Nagar. Top soil layer is underlain by weathered granitic formation of considerable thickness followed by massive granite units which may or may not be fractured/ faulted. In granitic terrain, the groundwater

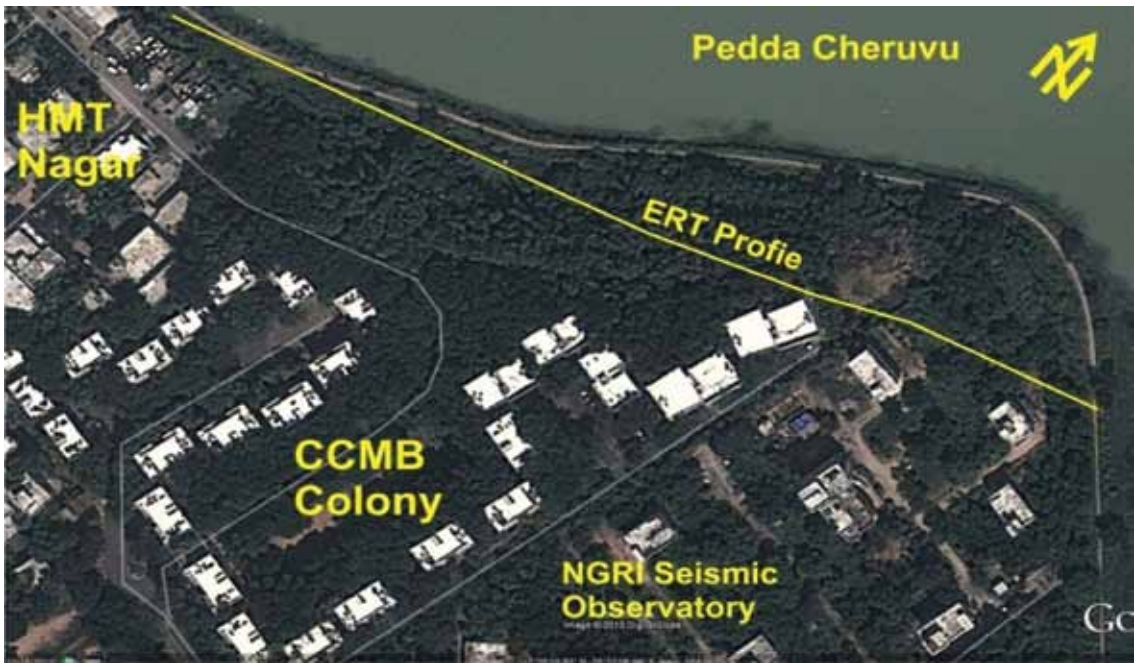

Figure 2. Aerial view of CSIR-CCMB colony along with location of ERT profile.

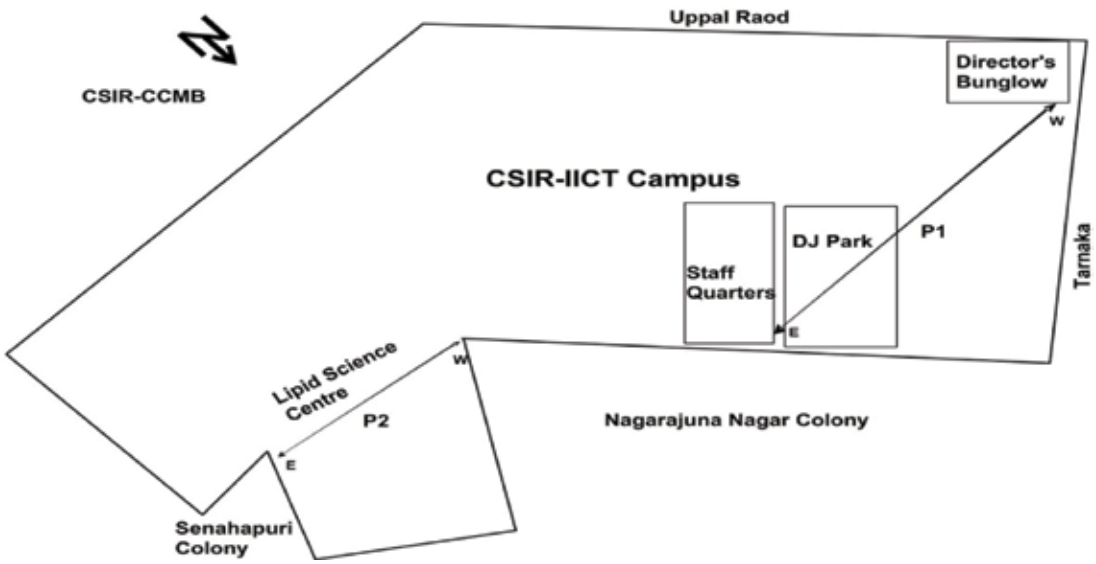

Figure 3. Location map of CSIR-IICT campus along with P1 and P2 ERT profiles

is confined mainly to the weathered and semi-weathered layers at shallower depths and in fractures and joints in massive rock units. The climatic condition in the region is of semi-arid nature. Temperature varies mostly between 16°C in winter season to 44°C in peak summer season. The annual rainfall varies between 750-850 mm. The area receives more than 80% of its rainfall from the SW monsoon, mostly during rainy season from June to September. Precipitation is the main source of groundwater recharging. Estimated groundwater recharge is less than 10% of the total precipitation.

Two decades earlier, dug wells penetrating up to the depth of weathered zone were mostly used for groundwater supply. But because of exploitation of ground water resources, in excess to their recharging the groundwater level, has been continuously declining beyond its recovery limit. As a result availability of groundwater remains mostly confined to the fractured/faulted granitic rock at deeper level throughout the year, except during short period of rainy season. Thus, the possibility of availability of ground water is mainly confined to the geological structures like fractures, faults and joints at deeper level. Such water bearing geological

Figure 4. Location of Raviryal village (Source Google map)

Figure 5. Location map of Aziz Nagar (Source Google map)

structures are distributed sporadically and are of finite areal extent. Therefore, delineation of their exact locations is a challenging task. This task has now becomes possible only with the development of 2D electrical resistivity tomography (ERT) which is capable of mapping 2D images of subsurface geological formations/structures (Loke, 2000). This task is accomplished by inversion of surface measured apparent resistivity data in form of layered resistivity model, followed by its interpretation in term of geological formations. It helps in delineation of groundwater potential zones. A brief description of ERT set up used for field survey is presented below.

Electrical Resistivity Tomography

Electrical Resistivity Tomography is carried out by using multi-electrode resistivity imaging system. In this system, many electrodes are connected with multi core cables to form a multi-electrode setup. The number of electrodes differs from system to system. In the present study, the ABEM made Terrameter Lund Imaging System with 64 electrodes is used. For demonstration purpose, figure 6 shows field setup of an ERT survey with four multi-core cables. In each multi-core cable, 16 electrodes are placed at equal spacing of 10 meters. Spacing between two electrodes can be reduced during survey depending on the availability of space for ERT survey. Multi-core cables are connected to an electronic switching unit. The switching unit is connected to a resistivity meter and the resistivity meter is connected to a laptop. Laptop based software together with the electronic switching unit is used to select automatically four relevant electrodes (two current electrodes and two potential electrodes) for each measurement. Provision is made for resistivity survey using different electrode configurations such as Wenner, Wenner-Schlumberger, Dipole-Dipole, Pole-dipole, Pole-Pole etc. Information regarding the sequence of measurements to take, the type of array to be used and other survey parameters such as the intensity of current to be used is entered into a text file which can be read by a computer program uploaded in a laptop. After reading the control file, the computer program then automatically selects the appropriate electrodes (two current electrodes and

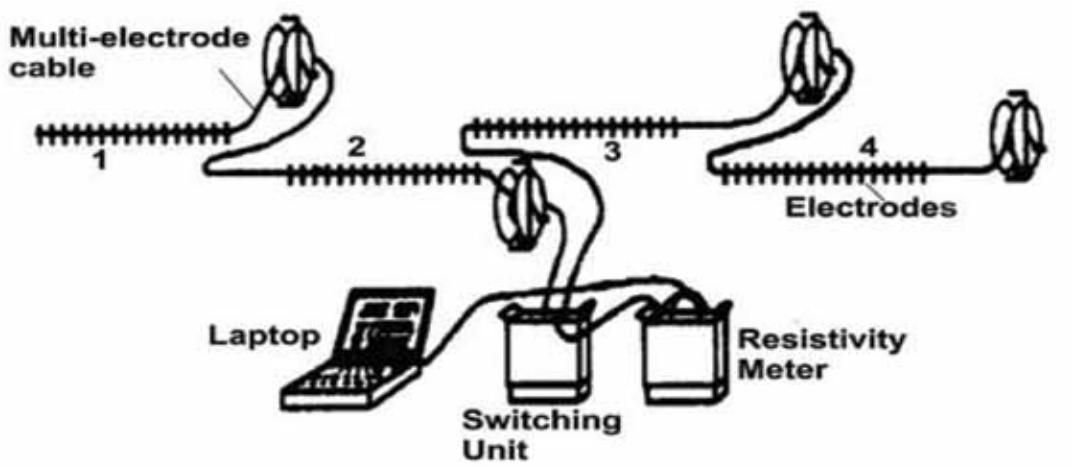

Figure 6. A sketch diagram showing field layout of ERT system

two potential electrodes) for each measurement. After that, the measurements are taken automatically and stored in the laptop. For the first measurement with 10 m electrode spacing, electrodes 1, 2, 3 and 4 are used. Electrode 1 is used as the first current electrode, electrode 2 as the first potential electrode, electrode 3 as the second potential electrode and electrode 4 as the second current electrode. For the second measurement, electrodes number 2, 3, 4 and 5 are used for first current electrode, first potential electrode, second potential electrode and second current electrode, respectively. This is repeated until electrodes 61, 62, 63 and 64 are used. After completing the sequence of measurements with 10 m spacing, the next sequence of measurements with 20 m electrode spacing is conducted. For the first measurement, electrodes 1, 3, 5 and 7 are used. For the second measurement, electrodes 2, 4, 6 and 8 are used. This process is repeated down the line until electrodes 58, 60, 62 and 64 are used for the last measurement with electrode spacing 20 m. The same process is repeated for measurements with electrode spacing 30 m, 40 m, etc. As the electrode spacing increases, the number of measurements decreases.

In ERT survey the depth of investigation is maximum below the central portion of the survey line and gradually decreases towards both ends of the survey line. Therefore, after completing the sequence of measurement for one field setup, the cable is moved along the survey profile past one of its end by several units of electrode spacing in such a way that in the next sequence of measurements, the depth coverage left over in the previous sequence of measurement is completed. By this way, it is possible to achieve the complete depth coverage of the resistivity measurements for a desired segment of the survey line. Shifting of the full length of a cable to the new position along the survey line is more convenient for this purpose. This procedure is known as roll-along (Loke, 2000; Rai et al., 2019). In present work ERT is conducted using Wenner configuration for measurement of apparent resistivity values on ground surface. The apparent resistivity value is computed by using mathematical expression $\rho_a = 2\pi a\ (\Delta V / I)$ in which ρ_a is the apparent resistivity, a is the spacing between the two consecutive electrodes, ΔV is the potential difference between the two potential electrodes, and I is the current induced in to ground through current electrodes (Wenner, 1912).

The next step is to convert the measured apparent resistivity values in to a 2D true resistivity model, which can be used for geological interpretation in order to identify water bearing geological formations and structures. This task is accomplished by using inverse modeling. Inverse modeling of the measured apparent resistivity data is carried out using RES2DINV program (Loke, 1997). This program automatically creates a 2D model by dividing the subsurface into rectangular blocks. To initiate modeling, some resistivity values will be assigned to the model blocks. Thereafter, the program calculates the apparent resistivity values of the model blocks and compares them to measured apparent resistivity values. The resistivity values of model are adjusted iteratively until the calculated apparent resistivity values of the model are in close agreement with the measured apparent resistivity values. The final output is a 2D inverse resistivity model in the form of 2D distribution of true resistivity values and thicknesses of respective geological formations. The model also presents root mean square (RMS) error value. RMS values should be preferably <10% or close to it. Then, the quality of field data and computed model are considered to be good. The inverse resistivity model is interpreted in terms of geological formations by correlating resistivity values with the corresponding geological formations. It helps in identifications of groundwater potential zones and suitable sites for managing aquifer recharge. Central Ground Water Board (CGWB) of the Government of India has published resistivity values of different litho units of granitic terrains in its website. These values are given in Table 1. The same

Table 1. Geological units and their respective resistivity values

Geological formations	Resistivity values in ohm m
Soil cover	< 20
Highly weathered granite saturated with water	20–50
Semi weathered granite	50–120
Moderately fractured/jointed granite	120–200
Massive granite	> 300

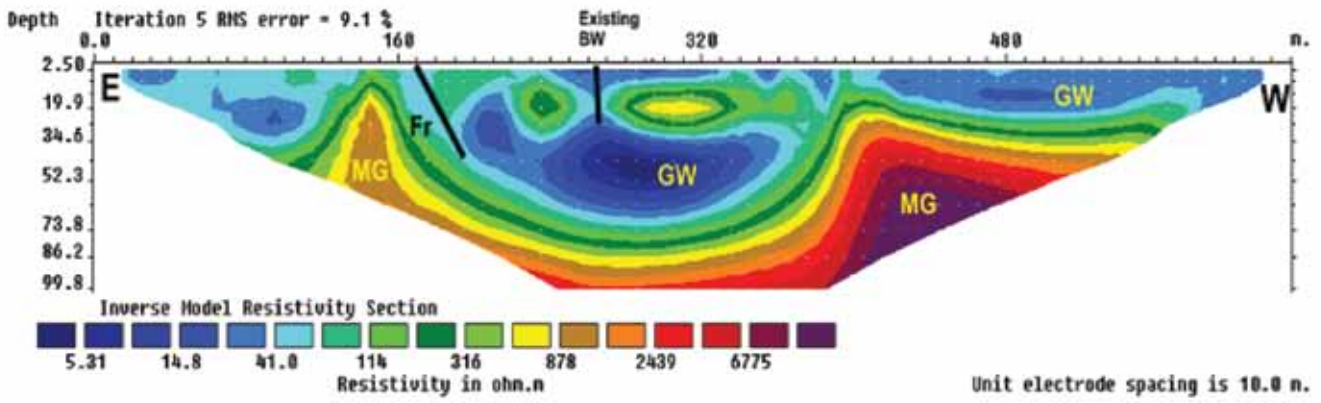

Figure 7. Resistivity model for the site in CSIR-CCMB colony; GW - groundwater zone, Fr - fracture, MG - Massive granite

values are used for interpretation of inverse resistivity models. Hereafter, inverse resistivity model will be referred as resistivity model.

RESULTS AND DISCUSSION

CSIR- CCMB Colony

Electrical Resistivity Tomography is carried out along a profile running in east to west direction along the boundary with Peddacheruvu as shown in figure 2. Profile is extended outside the boundary of CCMB Colony on both sides. Four multi-core cables each having 16 electrodes are used. Spacing between two electrodes is 10 m. For this electrode spacing, the length of this profile is 630 m. The first electrode is positioned at 78.5540°E, 17.4185°N and the last 64th electrode is positioned at 78.5499°E, 17.4219°N. Centre of the profile is located at 78.5520°E, 17.4199°N. The 2D resistivity model for the survey profile is presented in figure 7. Small vertical lines on top of the resistivity model indicate the positions of electrodes starting from 1st electrode at zero distance to the 64th electrode at 630 m. Distances are measured from E to W direction. The colored index of resistivity variation is presented below the model. The resistivity model indicates the presence of a bowl shaped set up of geological formations between 150 m and 400 m distances, which are bounded by elevated two arms of massive granites basement (> 300 Ohm). This bowl shaped set up of geological formation lies in front of CCMB colony, adjacent to the lake boundary. Within this segment of resistivity model, ~15-20 m thick two units of semi-weathered granite layer (50-120 ohm m) between 170-400 m can be seen below a thin soil cover (<20 Ohm m). Both the units are separated by a fracture zone located at 250 m. The model indicates another fracture zone near 160 m distance as marked by *Fr*. The semi-weathered granitic layer is underlain by water saturated semi weathered granitic formation (20-120 Ohm m) which is extended to a maximum depth of 80 m in the centre of the bowl structure. It's thickness decreases with the distance away from the centre of the profile towards both elevated arms of the massive granite. The resistivity model also shows the presence of a low resistivity zone (<20 ohm m) within the highly weathered formations. This indicates the leaching of the clay minerals from the host granite. This is a common feature in the granitic terrain due to alteration of alkali feldspar which is chief constituent of clay. This drastically lowers the resistivity values. This water saturated zone is the main source of water supply to the CCMB colony using a bore well whose location is shown in the model. Two units of similar geological setup can also be seen towards both ends of the profile which are separated from the central unit of geological formation by both elevated arms of the massive granite. The entire area in front of CCMB colony is a low lying area and is bounded by a bund from the lake side. This area receives run off from the remaining part of CCMB colony situated on elevated ground surface and serves as a recharge pit.

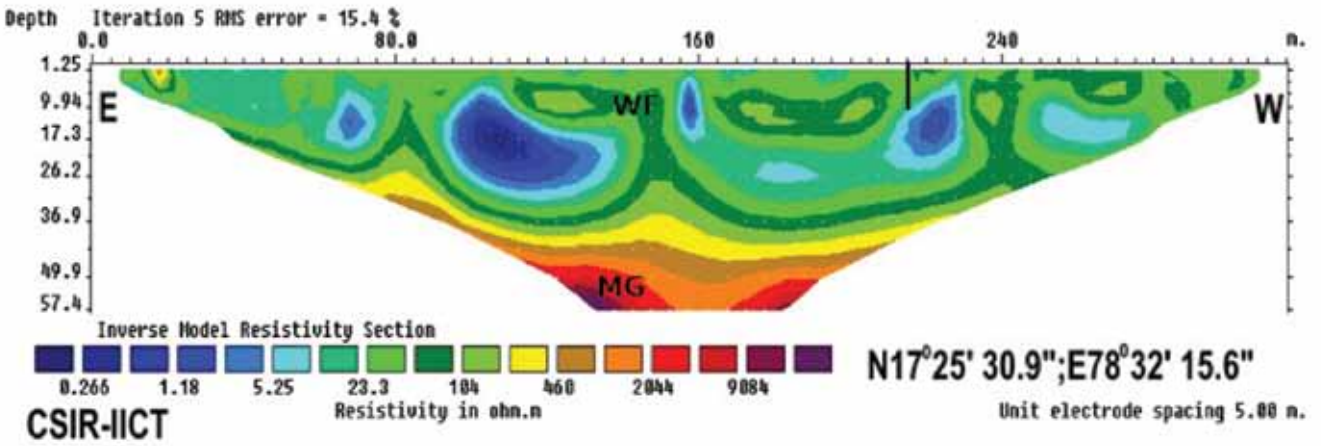

Figure 8. Inverse resistivity model along P1 profile in CSIR-IICT campus.

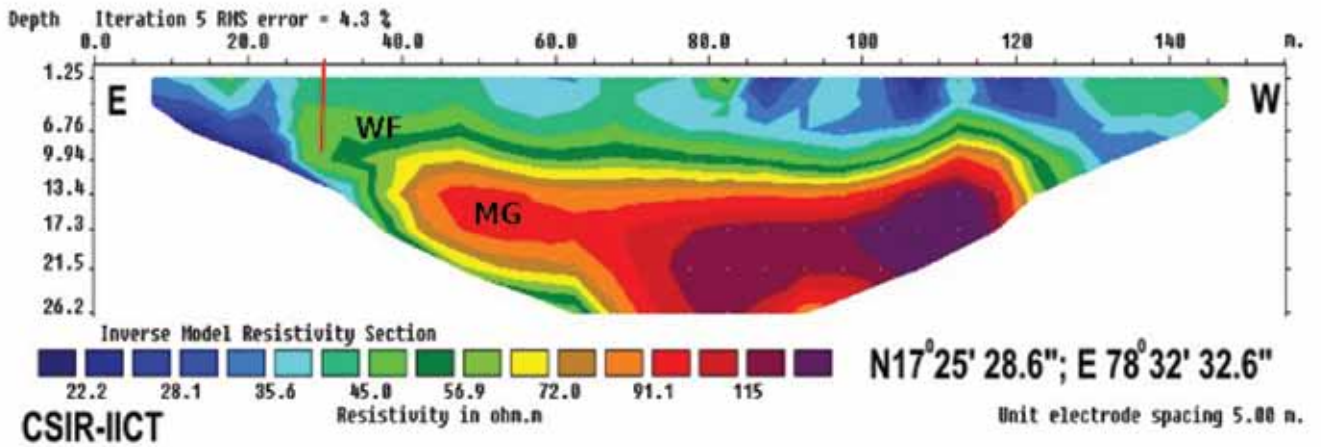

Figure 9. Inverse resistivity model along P2 profile in CSIR-IICT campus.

CSIR-IICT campus

Locations of two ERT profiles in CSIR-IICT campus marked by P1 and P2 are shown in figure 3. Profile P1 with centre at 17°25′30.9″N, 78°32′15.6″E runs in east to west direction from the corner of the staff quarter to the IICT boundary along Uppal road. This profile passes though the Diamond Jubilee Park marked as DJP in the map and the backyard of the Director's bungalow. Because of lack of space, length of this profile is restricted to 315 m only. ERT was conducted with 5m electrode spacing. Inverse resistivity model along this profile is shown in figure 8. Geological interpretation of this resistivity model suggests the presence of a composite layer of weathered and semi-weathered granitic formation (20-120 ohm m) in the depth range of ~25 to 35 m below soil cover. This layer is a water bearing. A suitable site for bore well drilling is suggested between 210 to 225 m distances where highly weathered formation is exposed on ground surface. Because of less thickness of this composite layer, its water storage capacity is too less to maintain the required demand of water supply. This resistivity model suggests the suitable site for managing aquifer recharge between 80 to 100 m distances where highly weathered granitic formation is exposed to ground surface and is low lying where run off can be diverted in to a proposed recharge structure in the form of injection well. Another suitable site for construction of injection well for groundwater recharge is between 210 to 230 m distances. Groundwater recharging from these two injection wells can increase the groundwater storage.

The second profile P2 with its centre at 17°25′28.6″ N, 78°32′32.6″ E is located in front of Lipid Science Centre. The profile is in east to west direction and lies between the two IICT boundary walls running along Snehapuri colony and Nagarjunanagar colony, as shown in figure 3. Length of the profile is only 115 m and electrode spacing used in this survey is 5 m. Resistivity model of this profile is presented in Figure 9. In this case, the depth of investigation is only 26.2 m. This resistivity model indicates the presence of highly weathered formation (<50 ohm m) on top in two units. The first unit is extended up to 25 m distance from eastern edge of the profile. The second unit is spread over in between 50 to 125 m distances. This second unit is underlain by a layer of

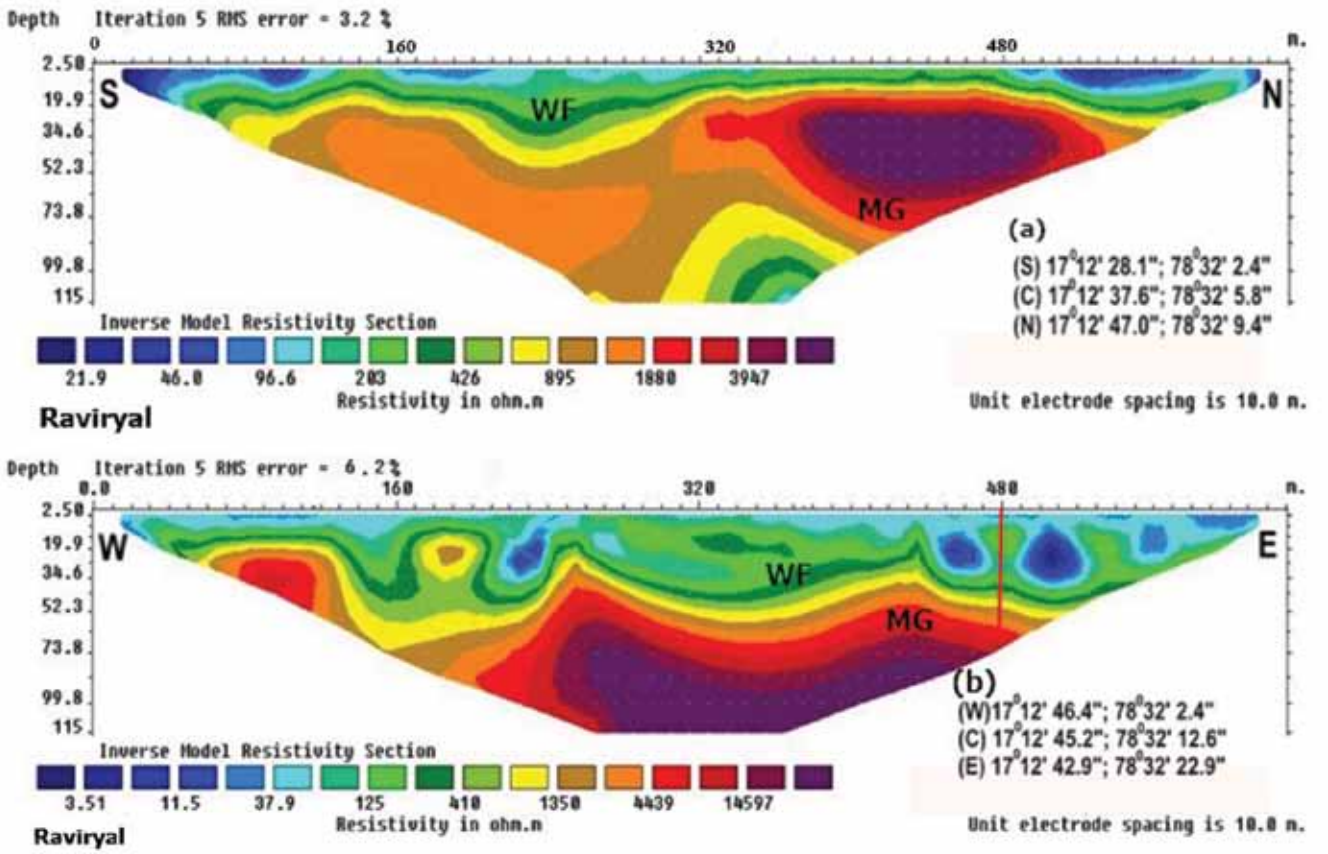

Figure 10. Resistivity models (a) and (b) in farm land under Raviryal village

semi-weathered granite which is extended up to a depth of ~ 10 m and is exposed to the ground surface between 25 m to 50m separating both units of highly weathered formation. The semi-weathered formation is underlain by massive granite unit (>300 Ohm m) between 40 m to 120 m distances. The first unit of highly weathered formation dips downwards below the massive granite unit. Similarly, the second unit of highly weathered formation is dipping downwards adjacent to the massive granite unite. Both the segments of highly weathered formations appear to be water bearing at deeper level. Suitable sites for bore well drillings are at 30 m and 130 m distances. A bore well is drilled in the first segment of the highly weathered formation and confirms the presence of groundwater. This bore well is currently in use to augment the water supply requirement of IICT. This resistivity model indicates two sites suitable for developing recharge pits for managing groundwater recharge by diverting surface runoff in to recharge pit. One site could be between eastern edge of the profile up to 20 m distance and the other one between 115 m to 130 m towards western edge of the profile. At both sites the highly weathered formation appears to be extending downwards to a greater depth.

Raviryal Village

Resistivity models presented in figures 10 (a) and (b) are along two profiles in a farm land falling under Raviryal village of Rangareddi district. This farm land is located adjacent to the Nehru outer ring road (ORR) as shown in figure 4. The profile of figure 10(a) is in south to north direction with the centre located at 17°12′45.2″N, 78°32′12.6″E. Geographical locations of the southern and northern ends of the profile are also given in the model. Length of this profile is 630 m. This model shows a thin layer of soil cover, which is underlain by massive granite unit along the entire stretch of the profile. This model does not indicate presence of any groundwater bearing zone. The profile of figure 10(b) is in west to east direction with the centre located at 17°19′51′8″ N, 78°32′12.6″ E. Geographical location of the first and last electrodes are also given in the model. Resistivity model of this profile also indicates the presence of a layer of soil on top. This is underlain by a composite layer of highly to semi-weathered granite in the depth range of 5 to 30 m. Patches of clayey formation can be seen within the soil layer which reduces its resistivity value <10 ohm m. This composite layer is

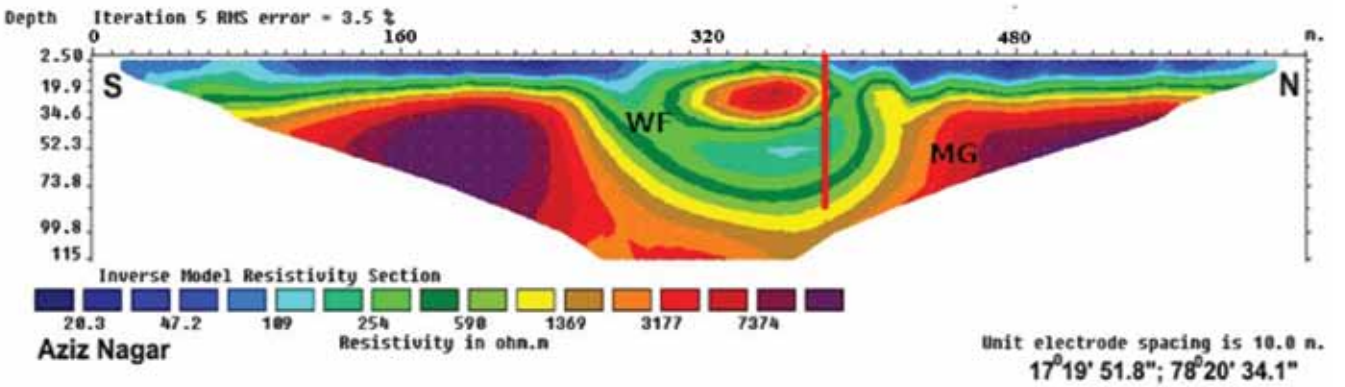

Figure 11. Inverse resistivity model in a plot in Aziz Nagar

underlain by massive granite. This profile indicates the possibility of groundwater occurrence in small quantity between 440 to the eastern edge of the profile at deeper level within the weathered granite layer. At this site development of a large diameter dug well is suggested between 480 to 550 m distances for both purposes, i.e. withdrawal of ground water for irrigation as well as managing aquifer recharge by diverting run off in to the well.

Aziz Nagar

Figure 11 presents resistivity model along a profile in a plot located near Himayat Sagar Lake in Aziz Nagar. This model indicates presence of massive granite below a thin cover of soil and weathered formation along the entire length of the profile. The massive granite unit is exposed to the ground surface between 270 m to 360 m distances. This model does not show any groundwater bearing zone.

In order to establish a criterion about the most likely possibility of occurrence of groundwater potential zones in hard rocks, in this case granitic terrain, the resistivity model of figure 9 is compared with three resistivity models obtained from ERT conducted in CSIR-NGRI campus (Rai et al., 2013). These three models are presented in figure 12. All the four models show a similar geological set up in which weathered formation is dipping downwards against the massive granite units. Presence of massive granite unit will restrict the lateral movement of groundwater beyond the interface between the massive granite and the weathered formation. In such situation the ground water will percolate down to get stored in the contact zone. Groundwater collected in the contact zone further percolate down in to fractures, faults and joints within the granite units in case if these geological structures are connected to the contact zone. In spite of less depth of investigation, occurrence of potential groundwater zones have been confirmed by bore well drilled at much deeper level in contact zone between the weathered formation and the massive granite units. This confirms more possibility of occurrence of groundwater potential zone in such geological set up.

Sustainable development

Generally in hard rock terrains, casing of bore well is done only up to the depth of weathered zone. Remaining portion of the bore well is left without casing. As a result sediment particles along with flowing groundwater water enter in to the well and get deposited around and inside the well. It leads to continuous reduction in the bore yield which ultimately resulted in to failure of bore well after few years inspite of presence of groundwater in the aquifer system. To prevent the deposition of sediments in and around the well, casing should be done for entire depth of the bore well. Slotted pipes should be used within the top layer of weathered formation to capture infiltrating rain water and within the zones of fracture, faults, joints etc of the granite unit to allow sediment free groundwater flow in to the wells as shown in figure 13. Slots of 10 to 12 cm length can be made around the periphery of pipes by pipe cutter. This measure helps in sustaining the bore yield. This is being experienced from a bore well drilled in the NGRI campus. Information about the depth of water bearing geological formations/structures beyond the depth of investigation can be obtained from the driller during drilling operation. This can be further verified by sonic log. The sonic log presents two parallel plots; one plot of travel time of an elastic wave through the geological formation and another plot of corresponding velocity of the elastic wave in that formation. If the elastic wave passes through water bearing geological formation/structures, it will be reflected in the decrease of velocity and corresponding increase in the travel time in comparison to the velocity and travel time for the same geological formations/structures devoid of water. Thus by sonic log and information collected from the driller the presence of water bearing zones delineated by interpretation of ERT data is confirmed (Rai et al., 2013).

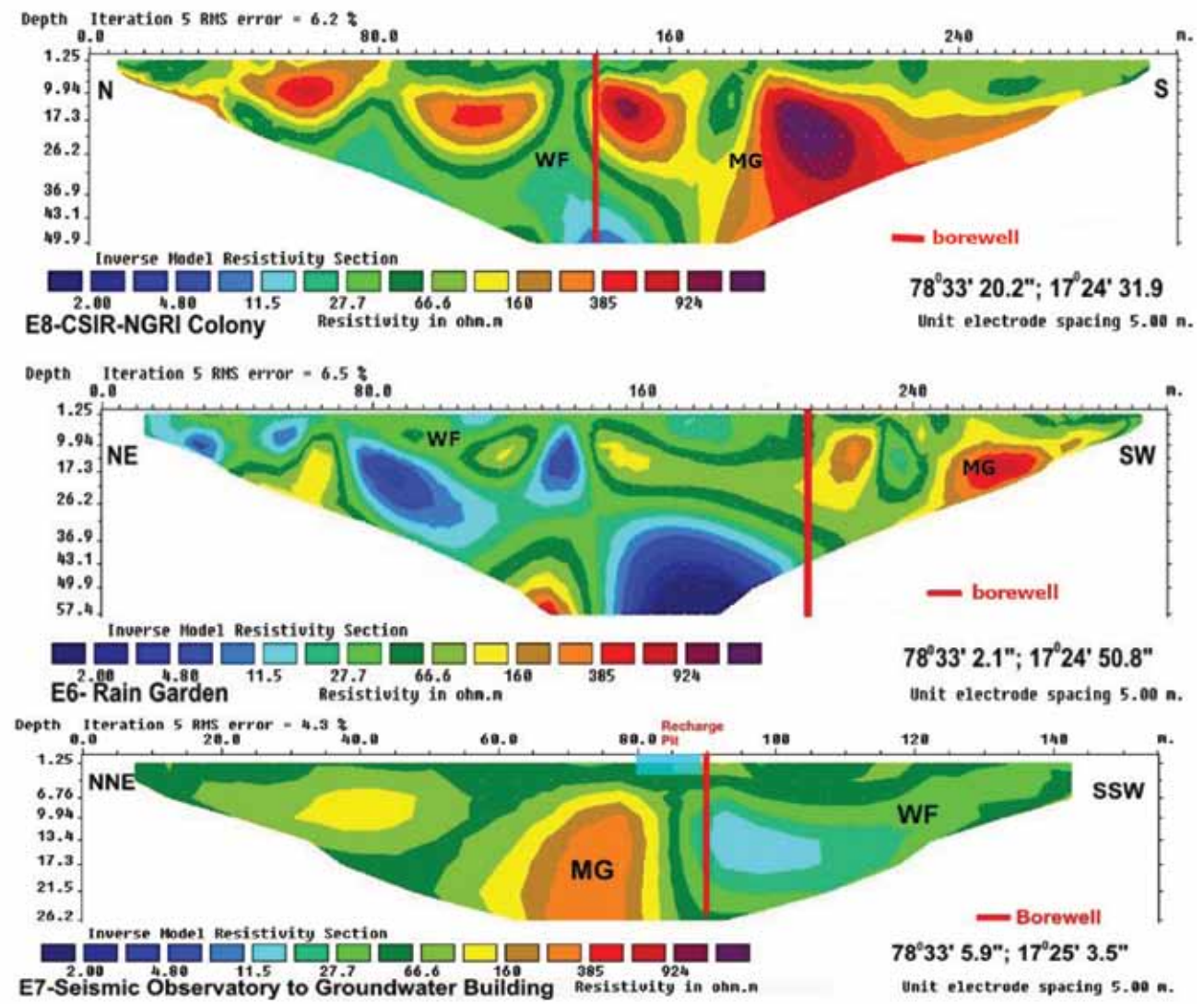

Figure12. Resistivity models from CSIR-NGRI campus. (after Rai et al., 2013)

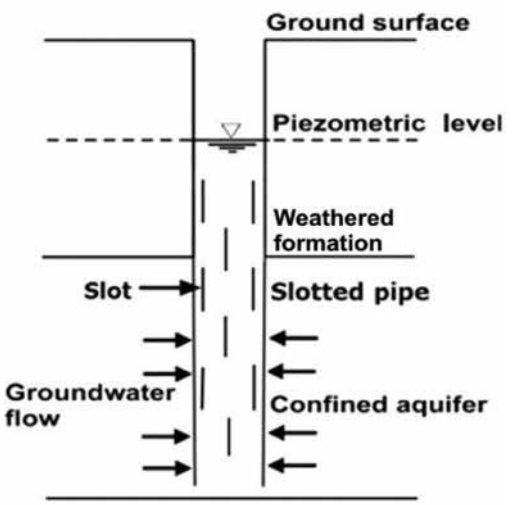

Figure 13. Bore well casing with slotted pipe within water bearing aquifers.

CONCLUSIONS

Electrical resistivity tomography has been carried out along 8 profiles, namely one in CCMB colony, two in the premise of IICT, two profiles in a farm land under Raviryal village and one profile in Aziz Nagar to delineate groundwater potential zones and sites suitable for managing groundwater recharge to increase the storage of groundwater. Interpretation of resistivity models indicates the occurrence of potential groundwater zone in CCMB colony and at the site of P2 profile in front of Lipid Science centre of IICT. One resistivity model in the farm land under Raviryal village indicates the presence of aquifer. Other resistivity models of Raviryal and Aziz Nagar do not show presence of ground water resources along the surveyed profiles. Sites for bore well drilling and for managing groundwater recharging have been also suggested. Development of one dug well at one site in the farm land of Raviryal village is also suggested, which can be used to store the groundwater. This study demonstrates the efficacy of ERT in delineation of groundwater potential zones and suitable sites for managing aquifer recharge. The use of slotted pipes for bore well casing within the weathered formation at shallower depth and in water bearing geological structures such as fracture, faults etc within the granites at deeper level is suggested to secure the bore well yield for a longer period. This work also suggests very strong possibility of occurrence of potential groundwater zone in the contact zone between weathered formation and massive hard rock unit.

ACKNOWLEDGEMENT

Authors express sincere thanks to M. Sateesh Kumar for his support in the field work. Director's permission to carry out this study is gratefully acknowledged.

Compliance with Ethical Standards

The authors declare that they have no conflict of interest and adhere to copyright norms.

REFERENCES

Anthony, A.A. and John, R.O., 2-D Electrical imaging and its application in groundwater exploration in parts of Kumbani river basin, Zaria, Nigeria, World Rural Observation, 2(2), 72-82.

Central Ground Water Board (CGWB), 2010. Geophysical studies, website, http://cgwb.gov.in/CR/achi_geo_stu.html, Govt. of India, p. 5

Dobrin, M.B. and Savit, C.H., 1988. Introduction to geophysical prospecting. 4th Edition, McGraw-Hill, Inc, p. 867.

Dutta, S., Krishnamurthy, N.S., Arora, T., Rao, V.A., Ahmed, S. and Baltass at, J.M., 2006. Localization of water bearing fractured zones in a hard rock area using integrated geophysical techniques in Andhra Pradesh, Hydrogeol. J., 14, 760–766.

Griffiths, D.H., and Barker, R.D., 1993. Two-dimensional resistivity imaging and modeling in areas of complex geology, J. Applied Geophys., 29, 211-226.

Griffiths, D. H., Turnbull, J. and Olayinka, A.I., 1990. Two dimensional resistivity mapping with a computer controlled array. First Break, 8, 121–129.

Hamzah, U., Yaacup, R., Shamsudin, A.R. and Ayub, M.S., 2006. Electrical imaging of the groundwater aquifer at Banting, Selagore, Malaysia. Environ. Geol., 49, 1156-1162.

Kearey, P., Brooks, M and Hill, I., 2002. An introduction to Geophysical Exploration., 3rd Edition, Blackwell Science Lt., p.257

Kirsch, R., 2006. Groundwater Geophysics. Springer-Verlag, Berlin., p. 489.

Kumar, D, Thiagarajan, S. and Rai, S.N., 2011. Deciphering geothermal resources in Deccan traps region using Electrical Resistivity Tomography technique. J. Geol. Soc. India, 78, 541-548.

Loke, M.H., 1997. Software: RES 2D INV. 2D interpretation for DC resistivity and IP for windows 95. Copyright by M.H. Loke. 5, Cangkat Minden Lorong 6, Minden Heights, 11700 Penang, Malaysia.

Loke, M.H., 2000. Electrical imaging surveys for environmental and engineering studies: a practical guide to 2D and 3D surveys, 61 pp.

Loke, M.H. and Barker, R.D., 1996. Rapid least-squares inversion of apparent resistivity pseudo sections by Quasi-Newton method. Geophys. Prospect., 44, 131–152.

Rai, S.N., Thiagrajan, S., Dewashish Kumar, Dubey, K.M., Rai, P.K., Ramchandran, A. and Nithya, B., 2013. Electrical Resistivity Tomography for groundwater exploration in granitic terrain- a case study from NGRI campus. Current Science, 105(10), 1410-1418.

Rai, S.N., Thiagarajn, S., Shankar, G.B.K., Shateesh Kumar, M, Venkatesam, V., Mahesh, G. and Rangarajan, R., 2015. Groundwater prospecting in Deccan traps covered Tawarja basin using Electrical Resistivity Tomography, J. Indian Geophys. Uni., 19(3) , 256-269.

Rai, S.N., Thiagarajan, S., and Dewashish Kumar, 2019. Geophysical investigation to prevent landslides in lignite mine. J. Geol. Soc. India, 93, 185-193.

Ratnakumari, Y., Rai, S.N., Thiagarajan, S. and Kumar, D., 2012. 2-D Electrical resistivity imaging for delineation of deeper aquifers in part of Chandrabhaga river basin. Curr. Sci., 102(1), 61-69.

Todd, D.K. and Mays, L.W., 2013. Ground water hydrology. 3rd Edition, Wiley India Pvt. Ltd. (Indian Edition), p. 636.

Thiagarajan, S., Rai, S.N., Kumar, D. and Manglik, A., 2018. Delineation of groundwater resources using electrical resistivity tomography. Arabian J. Geosci., 11(9), 212-228.

Wenner, F., 1912. A method of measuring earth resistivity. U.S. Bureau of Standards Bulletin 12, 469-478.

Received on: 8.1.19; Revised on: 18.1.19; Accepted on: 22.1.19

J. Ind. Geophys. Union (March 2019)
v.23, no.2, pp: 120-133

Geophysical investigation for copper and gold mineralization around Dhani-Basri and Todi ka Bas area, Dausa and Alwar districts, Rajasthan

D.C. Naskar*[1], and A.V. Kulkarni[2]

[1]Southern Region, Geological Survey of India, Bandlaguda, Hyderabad-500068
[2]Central Region, Geological Survey of India, Seminary Hills, Nagpur-440006
*Corresponding author: dcnaskar@yahoo.com

ABSTRACT

Rocks exposed in the study area, have indicated presence of isolated outcrops of quartz-sericite mica schist, amphibolite, quartzite and metasedimentary, within the Banded Gneissic Complex (BGC)/Mangalwar complex that host a number of lead, zinc and copper deposits. Today, there is a challenge before geoscientists, to discover new mineral deposits, by an exploration technique, which have low risk, consumes less time and also cost effective. Accordingly, geophysical surveys comprising SP, magnetic, IP (TD) cum resistivity, gravity and resistivity sounding have been carried out in Dhani-Basri and Todi ka Bas area, Dausa and Alwar districts of, Rajasthan, for locating base metal occurrences. IP survey has delineated several anomaly zones, where strike length varies from 400 m to 1500 m. Chargeability values of zone-I, zone-II and zone-III, are ranging from 16-22 mV/V. Zone-I supported with low SP value -100 to -200 mV, corroborate well with the Dhani-Basri known deposit. Chargeability values of zone-IV, zone-V, zone-VI and zone-VII, range from 15-24 mV/V, while peak chargeability value of zone-V is observed as 30 mV/V, over a background value of 10 mV/V. Chargeability cum resistivity pseudo-section have shown depth persistence of the inferred conductors based on the contour pattern. These chargeability zones are associated with low SP, low resistivity and moderate magnetic responses. Further, Bouguer anomaly profiles reflect a region where borehole intersected a mineralized zone. Bouguer anomaly contour map indicates a fault zone, depending on the trend of the contour that corroborate well with the regional schistosity. Gravity high closure has been observed mainly for metamorphic content below the alluvium cover. The interpreted layers by Schlumberger resistivity sounding are top soil, hard rock/fractured granite-gneiss and the Archaean basement. The SP, magnetic and gravity data have also picked up structural/lithological trend quite well. However, to strengthen the survey results, the resistivity map is compared with chargeability map; those who have intersection area between low resistivity and high chargeability (> 24 mV/V) are considered the prospective zones for base metal mineralization. Further, the mineralization is structurally controlled by a shear zone, and sulphide (chalcopyrite, pyrrhotite and pyrite) with gold are hosted in the silicified zone.

Keywords: Dhani-Basri area, Copper-gold mineralization, Integrated geophysical surveys, Hard rock/fractured granite-gneiss, Structural/lithological trend.

INTRODUCTION

India has a geological and metallogenic history, which is similar to the mineral rich shield areas of Antarctica, Australia, South Africa and South America. India's geological domains are well endowed with mineral resources; however, they are yet to be fully explored, assessed and exploited. Rajasthan is endowed with a continuous geological sequence of rocks from the oldest Archaean metamorphites, represented by Bhilwara Supergroup (Bundelkhand gneiss and the banded gneissic complex) to sub-recent, are exposed chiefly in the central plains, existing between the Aravalli and Vindhyan range (Yadav and Avadich, 2010). The sedimentary rock includes those of Aravalli Supergroup, Delhi Supergroup and Upper Vindhyan Supergroup. The south-eastern extremity of the state is occupied by a pile of basaltic flows of Deccan traps. Several mineral deposits of economic importance occur in association with the above rock units. In Rajasthan, the base metal mineralization is found to be confined to the three successive geological time domains, which are identified as the three geo-synclinal basins namely Bhilwara basin, Aravalli basin and Delhi basin (Ametha and Sharma, 2008). The area exhibits three phases of deformation, giving rise to complicated structural geometry to the lithology and mineralized zones.

Similarly, the Proterozoic Aravalli-Delhi orogenic complex hosts a large number of economically important strata bound base metal sulphide deposits. Structures associated with mineralization such as folds, faults, veins and shear zones, highlight the importance of a changing history of brittle and ductile deformation for economic mineralization. Corroborative geological, geochemical and geophysical surveys, along with borehole drilling in the Dhani-Basri and its adjoining area, have established copper and gold mineralization (GSI Pub., 2011). Drilling result indicates that borehole DBH-1 intersected a mineralized zone of 13.70 m, whereas DBH-2 intersected thin copper bearing zone, and DBH-3 has also intersected rich copper

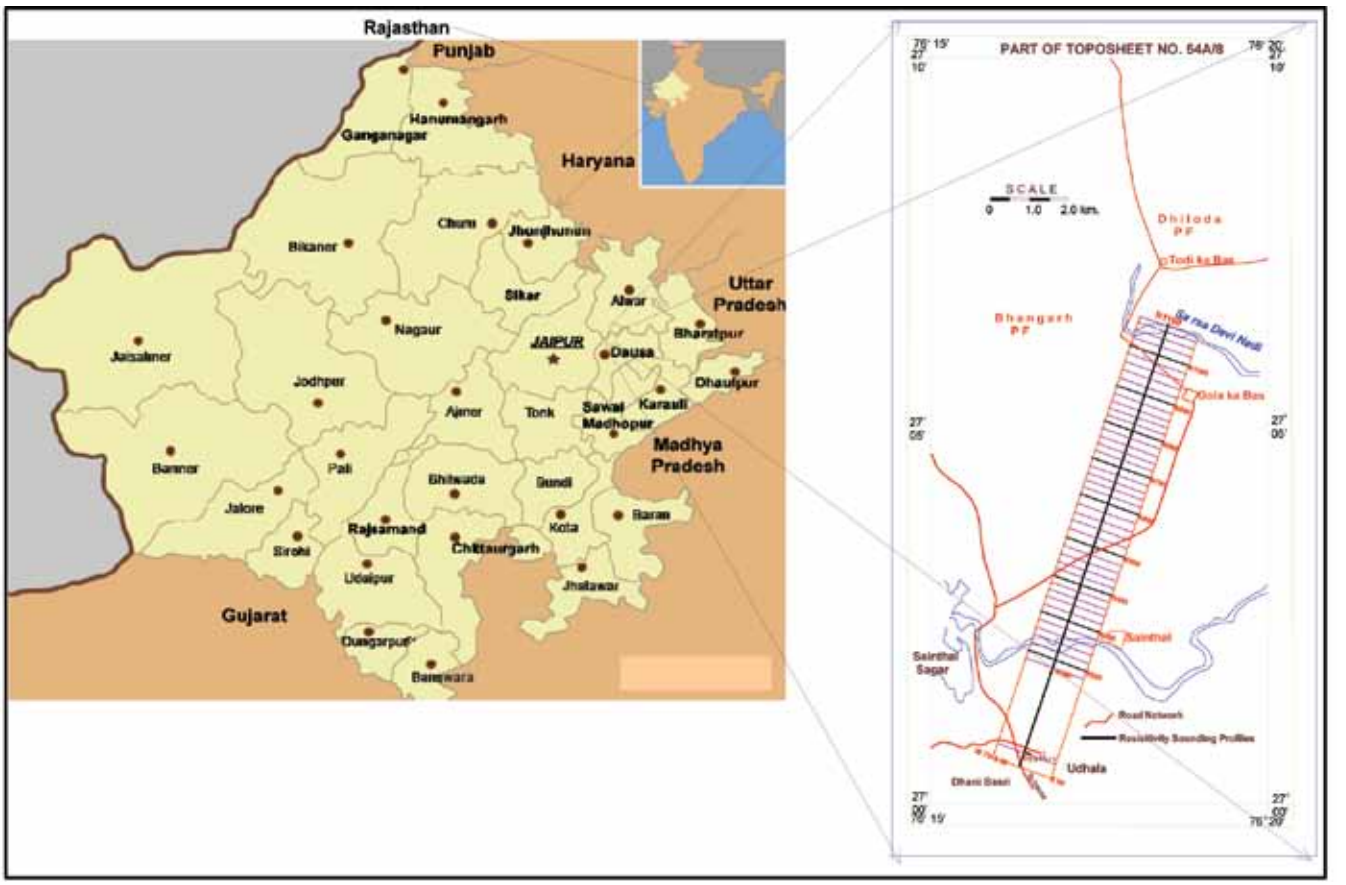

Figure 1. Location map of the study area.

mineralized zone. Due to the large study area, and the general lack of outcrop, geophysics plays a major role in mineral exploration. Mineralization occurs beneath a thick (typically 20 m) conductive cover of alluvial soil. Keeping in mind the importance of mineral exploration, integrated geophysical surveys, comprising SP, magnetic, IP (TD) cum resistivity, gravity and resistivity sounding, have been carried out in Dhani-Basri and Todi ka Bas area, Dausa and Alwar districts of Rajasthan, for delineating/assess the mineralized zones (Figure 1). An area of 17.7 sq km has been covered involving 119 lkm along 80 regular traverses and strike length 12 km.

Previous Studies

Sant et al., (1963) reported the occurrence of old working, mining dumps and slag heaps in the Gola ka Bas area. Mathew (1964) reported base metal mineralization in Dariba and Kho area by geophysical surveys. Mishra and Joshi (1967) carried out geological mapping in parts of the study area that followed the Heron's (1967) stratigraphic classification. Similarly, Sant and Sharma (1973) carried out geological mapping over Precambrian metasedimentary of Alwar and Jaipur district, while, Ravindra and Pahuja (1984) carried out mineral investigation with the help of drilling around Todi ka Bas area. Chakraborty and Gupta (1990) further carried out transect geological mapping over North Delhi Fold Belt (NDFB) and agreed with the stratigraphic classification of Sant and Sharma (1973) with minor modifications. Besides, Mukherjee et al., (1991) also made an attempt to delineate base metal mineralization in Kho Dariba area. Additionally Prasad et al., (2002) have earlier reported copper-gold mineralization in Dhani-Basri, Gola ka Bas, Kaljpuri and Andhi areas, NDFB, Dausa, Alwar and Jaipur districts, while Prasad et al., (2003) carried out geophysical surveys for exploration of base metal and associated gold mineralization in Dhani-Basri area of Dausa district. Singh et al. (2009) too carried out Geophysical surveys in Todi ka Bas area and delineated two significant anomaly zones in its central and NE part.

Apart from above mentioned investigations, Brij Kumar and Mukhopadhyay (1999) conducted systematic geological mapping for elucidation of tectono-stratigraphy and metallogeny of the Pre-Delhi basement rocks of the Dausa uplift in the northeastern Rajasthan, with special reference to its relationship of Delhi Supergroup.

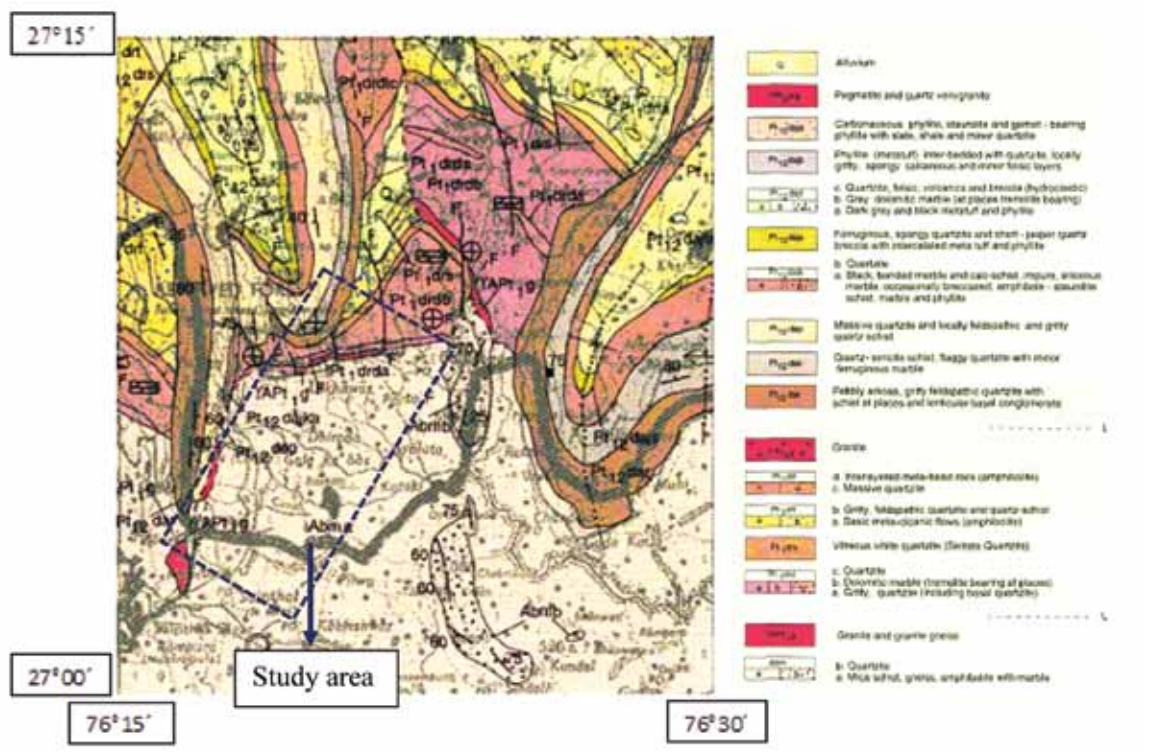

Figure 2. Geological map of the study area.

GEOLOGY OF THE STUDY AREA

Exposed rock are range in age from Archaean to Quaternary. Banded Gneissic Complex (BGC) in the study area represents the Archaean rocks, which has been reclassified as the Sandmata complex and the Mangalwar complex, belonging to Bhilwara Supergroup (Figure 2). This Supergroup also includes the Hindoli Group (erstwhile Gwalior series). The Aravalli, Delhi, Vindhyan and Marwar Supergroups, which are Archaean to Proterozoic in age, contain a number of metasedimentary belts, which are well known for base metal deposits and associated gold mineralization (Heron, 1953; Gupta et al., 1997). Dhani-Basri area is mostly associated with soil cover barring a small hillock. The rocks exposed in the area comprise mainly quartzite and mica schist. The subsurface geology suggests occurrence of thin partings and bands of amphibolite within the granite gneiss and develoement of silicified zone within the gneisses. Scanty outcrops/well dumps in the peneplained soil covered area between Dhani-Basri and Todi ka Bas, indicate presence of quartz-arenite rock. Stratigraphic succession of the study area (Gupta et al., 1997) is given as follows:

Supergroup	Group	Formation	Lithology
Delhi fold belt/Delhi Supergroup (a number of base metal deposits are located in these belts as also other minerals)	Ajabgarh Group	Kushalgarh Formation	Impure banded calc-silicate marble
	Alwar Group	Pratapgarh Formation	Fine-grained quartzite
		Kankwarhi Formation	Interbanded sequence of amphibolite and banded calc-biotite quartzite
		Rajgarh Formation	Felspathic and gritty quartzite with band of ferruginous quartzite
	Unconformity		
	Raiola Group	Tehla volcanic Serrate quartzite	Fine-grained quartzite Silicified fine-grained dull to greyish quartzite
	Unconformity		
Bhilwara Supergroup (rest on the basement rocks of the Mangalwar Complex and host a number of lead, zinc and copper deposits)	(Mangalwar) Banded gneissic complex (BGC)		Migmatite, granite- gneiss, amphibolite, quartzite

Table 1. Physical properties of the rocks

Physical properties of pyrite	
Chemical classification:	Sulphide
Luster:	Metallic
Specific gravity:	4.9 to 5.2
Chemical composition:	Iron sulphide, Fes_2
Uses:	Ore of gold.
Color:	Brass yellow often tarnished to dull brass
Magnetic susceptibility:	$k\times10^{-6}$ CGS, diamagnetic and paramagnetic property.
Resistivity:	Semiconductor, 10^{-5} to 10^{2}
Dielectric:	K=4 to 420 mean 130
Permittivity:	10<e<81
Physical properties of galena	
Chemical classification:	Sulphide
Resistivity:	Semiconductor mixed type, 6.8×10^{-6} to 17.5, and mean 2×10^{-3}
Magnetic susceptibility:	Diamagnetic/paramagnetic, K=-3 to 84
Permittivity:	18<e<205
Physical properties of Chalcopyrite	
Resistivity:	Semiconductor, 10^{-5} to 150
Magnetic Susceptibility:	Anti ferromagnetic, K=32
Permittivity:	<550
Physical properties of Malachite	
Resistivity:	Insulator, 10^{9}
Permittivity:	4<e<6
Physical properties of Graphite	
Color:	Steel grey to black
Luster:	Metallic, sometimes earthy
Specific gravity:	2.1 to 2.3
Chemical composition:	C
Physical properties of Schist	
Color:	Black, blue, brown, dark brown, green, grey silver
Luster:	Shiny
Specific gravity:	2.5 to 2.9
Density:	2.8 to 2.9 g/cm^3
Physical properties of Shale	
Luster:	Dull
Color:	Black, brown, buff, green, grey, red, yellow
Specific gravity:	2.2 to 2.8
Density:	2.4 to 2.8 g/cm^3

The regional strike of foliation in the BGC/Bhilwara and the Delhi Supergroup of rocks is dominantly NNE-SSW to NE-SW, while it is N-S and NW-SE in the Aravalli's.

MINERALIZATION

Rajasthan, endowed with a rich mineral wealth, occupies a significant position on the mineral map of the country. It is a leading state for metallic and non-metallic minerals, as it possesses about 19% of the total working mines of the country. It contains wide range of mineral resources and offers considerable potential for the future. The important metallic minerals with which the name of the state is intimately associated are, lead, zinc, copper and tungsten (GSI misc. pub., 2011). It is also richly endowed with a variety of non-metallic minerals also. Rajasthan has also enormous deposits of building stones like marble, granite, sandstone, limestone, slate etc. Besides, it is a leading producer of asbestos, soapstone/steatite, gypsum, rock phosphate, calcite, feldspar, clay etc. Presently, the State enjoys a monopoly in the production of wollastonite, emerald, jasper and semi-precious garnet. In addition, the State has good deposits of lignite in Bikaner, Nagaur and Barmer districts.

PETROGRAPHY STUDY

Mineral exploration demands study of physical properties on first hand field samples and using the data in the qualitative and quantitative analysis of the geophysical

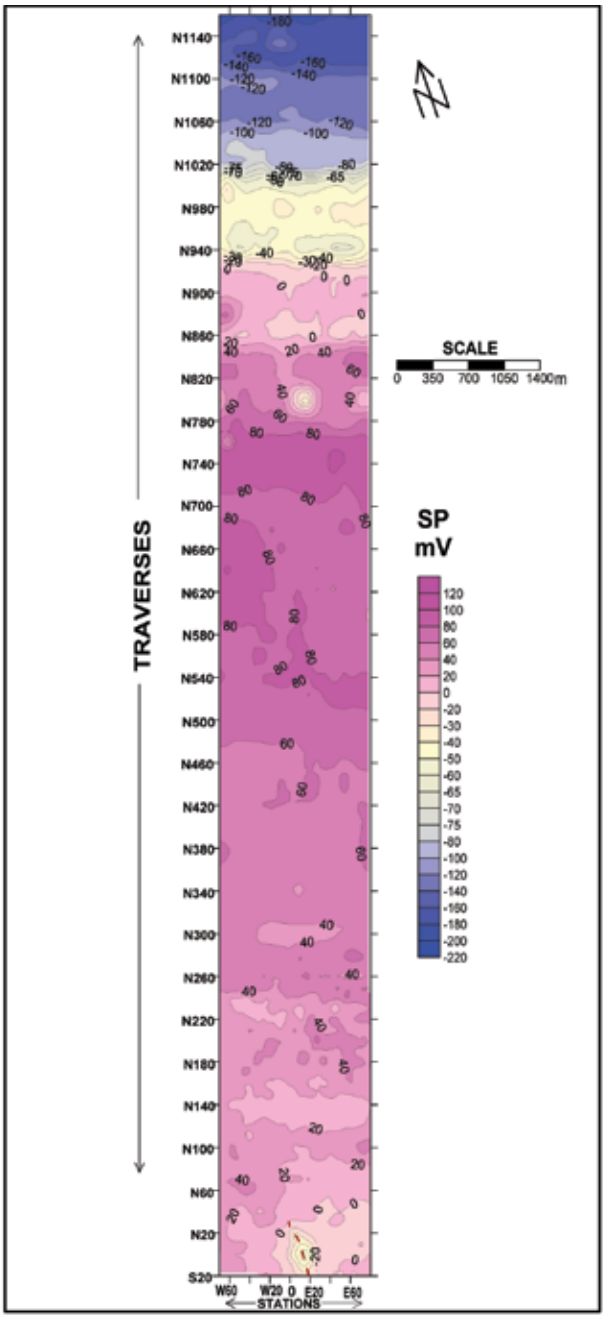

Figure 3. SP contour map north of the Dhani-Basri area, Dausa and Alwar districts, Rajasthan.

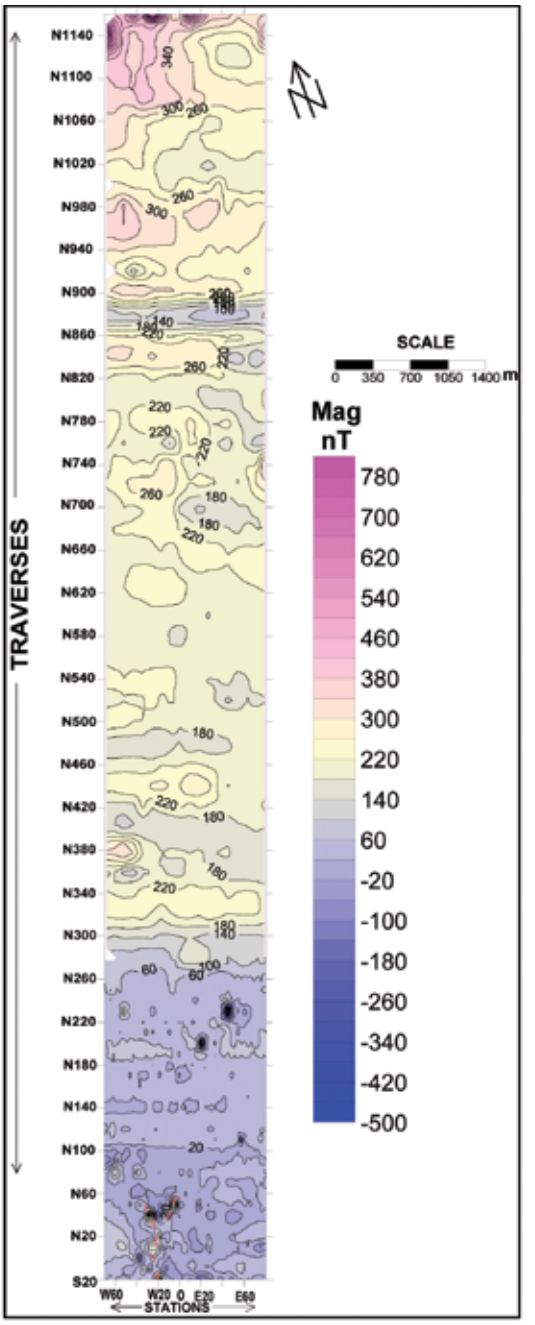

Figure 4. Magnetic (VF) contour map north of the Dhani-Basri area, Dausa and Alwar districts, Rajasthan.

anomalies. Petrographic studies of Pb-Zn ore deposits of study area have been carried out (Table-1) which is also corroborated with investigation carried out by Juned Alam et al. (2015) and Juned Alam and Siddiquie. (2015).

SURVEY LAYOUT

Geophysical surveys have been carried out with base line trending in N20°E direction. The traverses have been laid orthogonal to the base line at 200 m interval (for SP, magnetic, IP cum resistivity) and designated as N260, N280, N300, N320, …….N1140, N1160. The observation stations have been fixed at 20 m interval and designated as E20, E40,…..etc. and W20, W40…….etc. The unit of distance is kept at 10 m for traverses as well as for stations also (Figure 1).

Direct current techniques have application to a variety of mineral exploration and geoenvironmental

considerations, related to various ore deposit types. Vertical Electrical Sounding (VES) has been carried out in the study area with 1 km traverse interval designated as N280/0, N380/0,……N1080/0. Each unit is equivalent to 10 m. The wide range of earth material resistivity makes the method applicable to identification of lithology and structures that may control mineralization.

Further, gravity survey carried along stations are fixed at 40 m interval and designated as E40, E80,….etc. and W40, W80,…etc.

Results of geophysical surveys comprising SP, magnetic, IP chargeability cum resistivity, resistivity sounding and gravity, have been presented in the form of contour maps/ profile to identify the significant anomaly zones that may reveal mineralization (Babu Lal et al., 2012).

RESULTS

(i) Self Potential (SP) survey

SP values vary from +120 mV to -220 mV. An anomaly zone having peak magnitude of -60 mV almost north-south over the background value of 0 mV, is extending from N20 to S20 and open towards south indicating its extension (Figure 3). This anomaly zone is well corroborated with the main Dhani-Basri zone (marked by discontinuous line towards southern part). The closer associated with +40 mV over traverse N800 is localized and is not important for mineralization point of view. The survey has brought out the decreasing trend from N920 to N1160, which may be indicative of formational change or reflecting the combined effect of shear zone and the associated mineralization. Clear indications of SP anomaly closures of -50 mV over traverse N950 and -160 mV over traverse N1140 respectively, is obtained where mineralization is rich and shallow because this method works remarkably well due to favorable conditions, such as the shallow depth of mineralization, moderately resistive rocks, and a thin overburden.

(ii) Magnetic (vertical field) survey

The magnetic anomaly values vary from -500 nT to +780 nT. Higher values are associated with ferruginous material or amphibolites. However, there is no correlation with known Dhani-Basri main zone, since mineralization occurs within silicified zone. Survey has delineated mainly three anomaly zones, comprising of close spacing contour associated with high and low values (Figure 4). Zone I ranges from +160 nT to +280 nT in between traverse N820 and N850. Similar anomalies in Zone II range from +120 nT to +260 nT in between traverse N860 and N900. These magnetic anomalies may be due to litho–contact in subsurface rocks under soil cover or over the sheared contact controlling mineralization on the basis of linear and dense contour. The third zone extends from station E70 on traverse N680 to station W70 on traverse N720 with magnetic response of +260 nT at station W40 on traverse N720. This bi-polar anomaly may be indicative of pyrrhotite at shallow depth. Distinct magnetic highs of 260 to 780 nT in the northern portion over mica schist is indicative of ore with associated pyrrhotite. Distinct magnetic highs 260 nT to 400 nT within the sheared contact/host rock in the northern portion, is possibly controlling the mineralization. Magnetite rich rock with which sulphides are associated sometimes, are represented by discrete high closures of 220 to 300 nT.

(iii) Induced polarization (IP) survey

IP survey has been carried out in the studied area using dipole-dipole array, with a = 20 m and n = 3, where 'a' is array spacing and 'n' is represented by separation parameter between the current and potential electrode pair (Kearey et al., 2003). Dipole-dipole array is used in the field measurement by considering that even though it has low vertical resolution, it is very sensitive to deeper lateral variations, making it suitable for deeper sounding (Reynolds, 1997). Chargeability and resistivity values are measured at an interval of 20 m. The results of IP chargeability have been presented as a contour map (Figure 5), which revealed several anomaly zones that are favorable for mineralization, as discussed below depending on the high chargeability values and anomaly axes. These anomaly zones trend almost in N-S and NE-SW directions. The peak magnitude in these fair anomaly zones is varying from 18-28 mV/V. The reason for the large width of IP chargeability anomalies (20 to 30 mV/V) in the northern portion, possibly lies in the presence of sulphide minerals in the mineralized zone.

Zone I: Anomaly having peak value of 28 mV/V, trending almost N-S direction, occurs between traverses N30 and S10. The extent of this anomaly zone is about 400 m between stations E20 and W5, which falls over Dhani-Basri deposit which is supported by the low SP.

Zone II: The anomaly zone is trending in NW-SE direction, having peak magnitude of 18mV/V.

Zone III: This zone is characterized by an anomaly having peak value of 22 mV/V that occurs between traverses N160 and N200.

Zone IV: This zone is trending NW-SE direction having peak magnitude of 18 mV/V which occurs between traverses N280 and N320. The extent of the anomaly zone is about 400 m (SE of the area) between stations E10 and E80.

Zone V: This zone is trending NW-SE direction having peak magnitude of 24 mV/V that occurs between traverses N920 and N990. The extent of the anomaly zone is about 1500 m between stations E80 and W70.

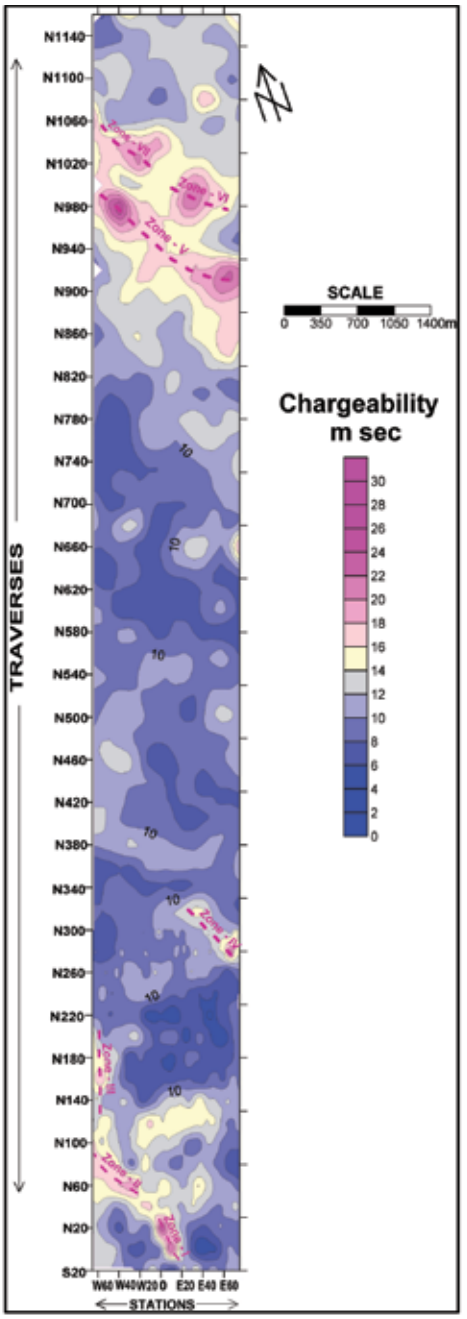

Figure 5. IP (TD) chargeability contour map (dipole-dipole array, a=20 m, n=3), north of the Dhani-Basri area, Dausa and Alwar districts, Rajasthan.

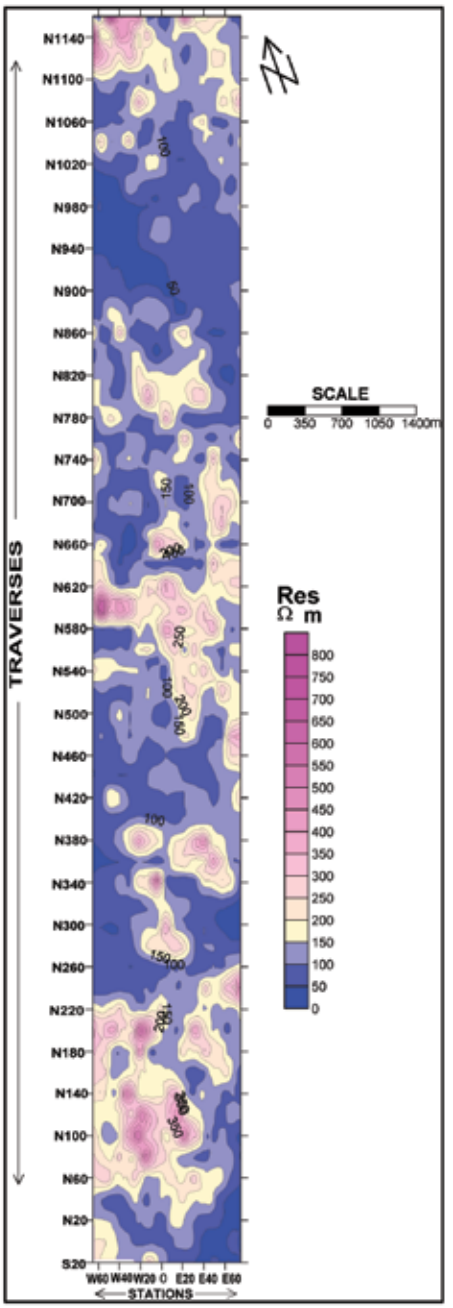

Figure 6. Apparent resistivity contour map (dipole-dipole array, a=20 m, n=3), north of the Dhani-Basri area, Dausa and Alwar districts, Rajasthan.

Zone VI: This zone has been picked up between stations E40 on traverse N980 and station W10 on traverse N1010 for a total strike length of about 500 m. The zone is characterized by peak magnitude of 22 mV/V.

Zone VII: This zone trends NE-SW direction, having peak magnitude of 18 mV/V between stations W20 on traverse N1020 and station W80 on traverse N1050, for a total strike length of 600 m.

(iv) Resistivity survey

The combined results of resistivity survey for the dipole-dipole array with a=20 m are presented in (Figure 6). The resistivity value varies from 50-850 Ohm-m. Several isolated zones of high resistivity of the order of 300-450 Ohm-m have been picked up, which may be due to the presence of hard rock beneath the surface. Resistivity survey

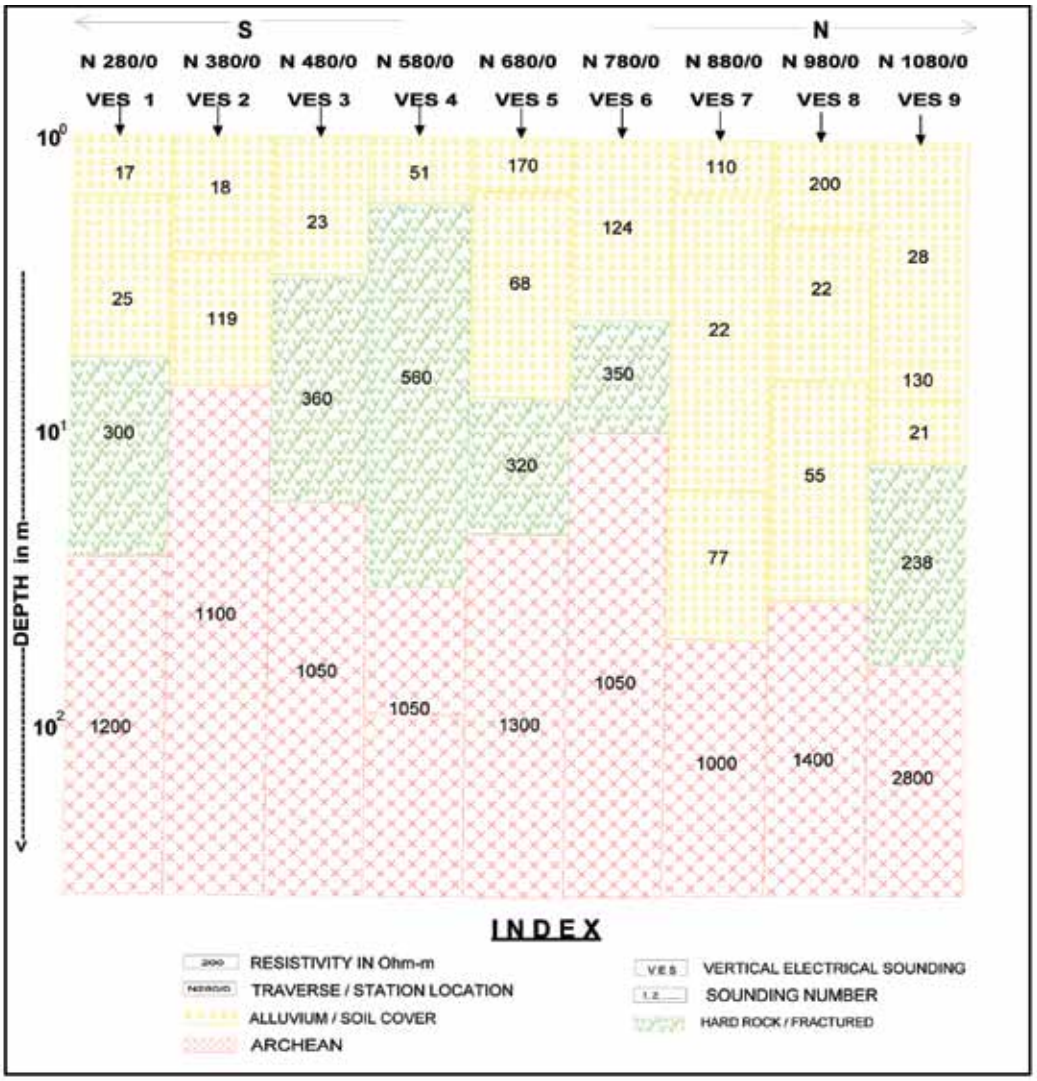

Figure 7. Geoelectric depth section north of the Dhani-Basri area, Dausa and Alwar districts, Rajasthan.

has delineated two significant low over the alluvial covered area. One extends from station E80 on traverse N870 to station W70 on traverse N1030 over a strike length of about 1500 m. This low resistivity zone is indicated near IP anomaly V, VI ad VII respectively and may be attributed to a shear zone/fault zone. Another zone extends from station E20 to E40 on traverse N320 over a strike length of about 400 m. The delineated low resistivity zone is well corroborated with IP anomaly zone IV. The mineralization gives rise to an apparent polarizability anomaly and, to a lesser extent, a resistivity anomaly. Chargeability and apparent resistivity data from the dipole-dipole array surveys must be treated with caution for several reasons.

(v) Electrical resistivity depth

Resistivity of rock is an important parameter for mapping different geological formations. It is dependent on factors like porosity, manner of the inter–connection of the pore spaces, the resistivity of the pore water and temperature. Variations of resistivity of the rocks are the main sources of electrical anomaly. The geo-electrical section, drawn based on interpreted result of 9 vertical electrical sounding (VES-1 to VES-9), have been presented in Figure 7. The interpreted vertical resistivity distribution along with inferred lithology is shown in the section for easy comprehension. The section has brought out different subsurface layers characterized by different resistivity values. The interpreted layers are soil at top followed by hard rock/fractures granite gneiss and Archaean basement. The top most layer is characterized by a resistivity value of 17-200 Ohm-m and the thickness varying from 1.65 m to 15 m, corresponds to top soil except in N880 and N980, where lateral inhomogeneities are observed. The second layer is characterized by a resistivity value of 238 Ohm-m to 560 Ohm-m and a thickness varying from 6.6 m to

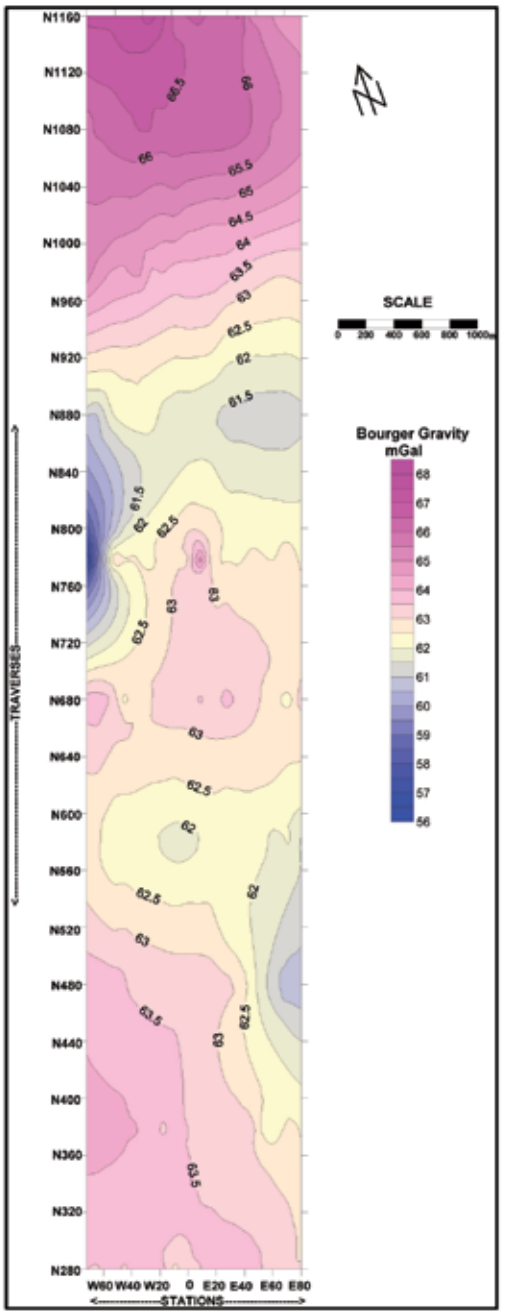

Figure 8. Bouguer gravity map north of the Dhani-Basri area, Dausa and Alwar districts, Rajasthan.

30.6 m corresponds to hard rock/fractured granite gneiss. Similarly, the third layer is characterized by a resistivity value of 1000 Ohm-m to 2800 Ohm-m and a depth varying from 7 m to 32.25 m corresponding to Archaean basement.

(vi) Gravity survey

The gravity data are reduced for elevation correction with a density factor of 2.67 g/cm^3 for the slab above mean sea level. The results of gravity survey in the form of a BA contour map, is presented in Figure 8.

A perusal of the gravity map indicates that the contour trends are predominantly E-W with amplitude of 63-65.5 mGal in the northern part of the study area from traverse N920 to N1020, which is indicative of a fault zone. This corroborates well with the regional schistosity of the area. However, towards the south, the contours are in essentially N-S and NNW-SSE directions. These alignments of the contour represent various subsurface regional features. One gravity high closure around N660 to N800 with amplitude of 64 mGal is observed. This anomaly is mainly for metamorphic content below the alluvium cover and trend

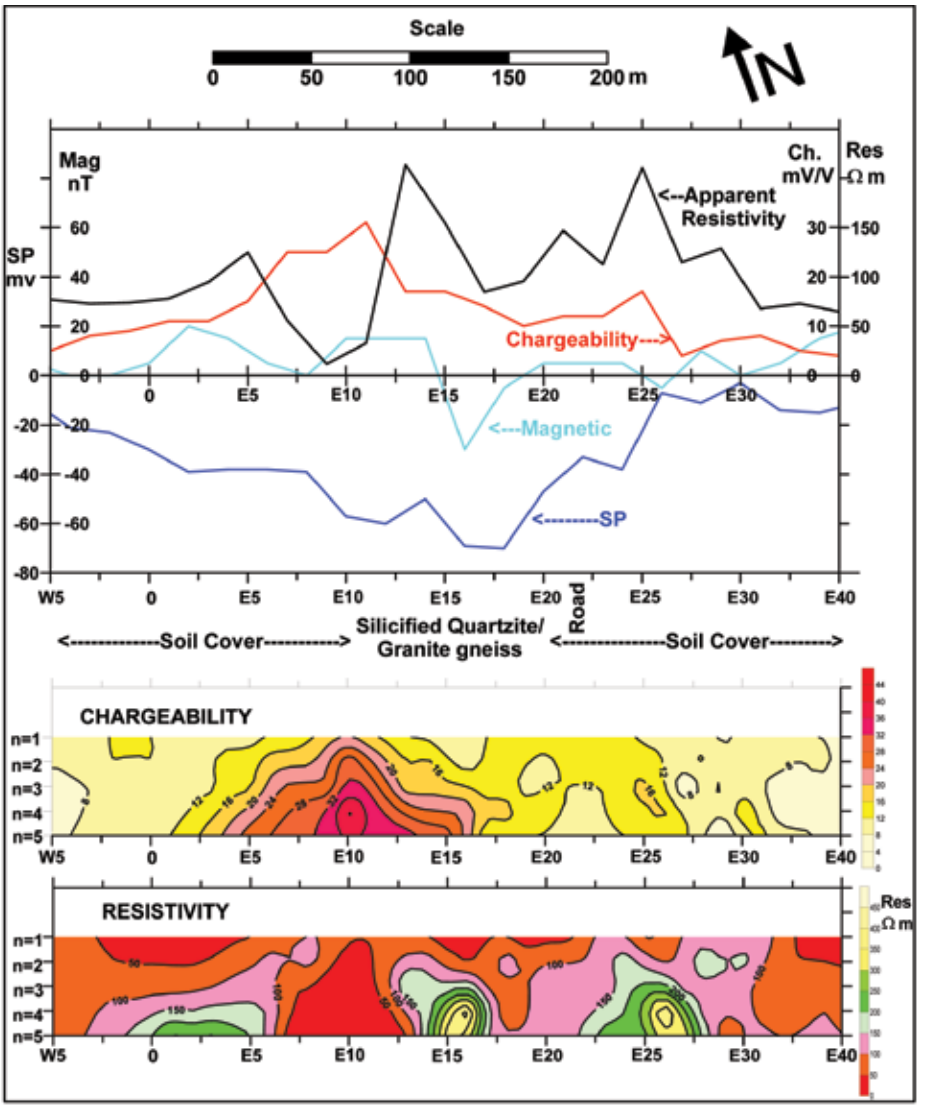

Figure 9. SP, magnetic (VF), IP (TD) chargeability, apparent resistivity profiles along with chargeability and resistivity pseudo-sections along traverse 0, north of the Dhani-Basri area, Dausa and Alwar districts, Rajasthan.

almost N-S which is well corroborated with the resistivity sounding results.

(vii) Typical profiles and IP pseudo sections

An IP cum resistivity pseudo-depth section has been prepared for the estimation of depth and depth persistence of the causative body. Dipole-dipole array with a=20 m and n=1 to 6, has been used for preparing the pseudo-depth section. The data have been plotted using Hallof's method (Hallof, 1957). Pseudo-depth section on traverses N0, N20, N160 and N980 are presented in Figures. 9, 10, 11 and 12 respectively.

Over traverse '0', the section has indicated a good anomaly zone having peak value of 36 mV/V at n=4 level, which is bounded by 16 mV/V contour in between stations E2 and E16, which corroborates well with low resistivity zone bounded by contour of 50 Ohm-m. The increase of magnitude towards downward is suggestive of depth persistence of the causative source below n=5 level. This anomaly zone is supported by low SP and feeble magnetic high zones.

Over traverse 'N20', the section has indicated a good anomaly zone having a peak value of 32 mV/V at n=4 level and is bounded by 20 mV/V contour in between stations E8 and W4, which corroborates well with the low resistivity zone bounded by contour below 100 Ohm-m. The contour of this zone is opening downward which is suggestive of depth persistence of the causative source below n=6 level. This zone is supported by low SP and feeble magnetic high zones.

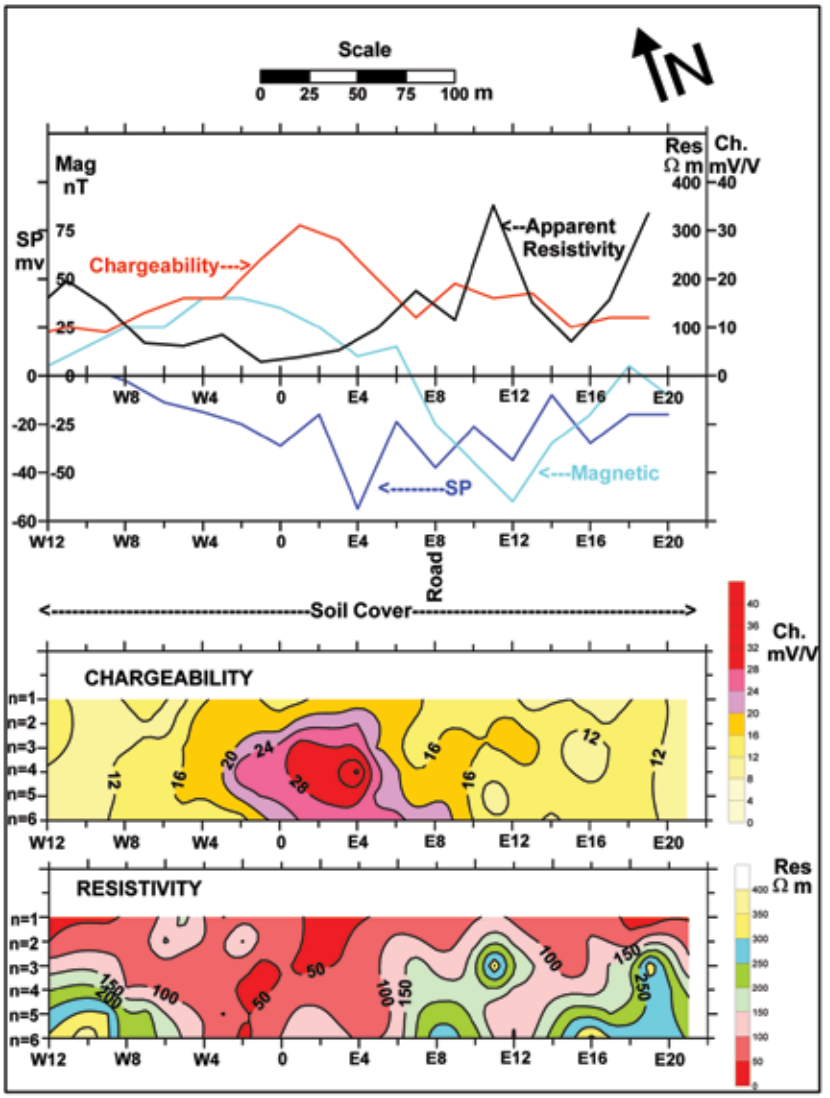

Figure 10. SP, magnetic (VF), IP (TD) chargeability, apparent resistivity profiles along with chargeability and resistivity pseudo-sections on traverse N20 north of the Dhani-Basri area, Dausa and Alwar districts, Rajasthan.

Over traverse 'N160', the section has indicated two anomaly zones, having peak value of 24 mV/V, bounded by 18 mV/V contour. One anomaly zone lying between station W52 and W56 is dipping in easterly direction, while the other zone lying between station W60 and W68 is dipping westerly. Eastern anomaly has shown two peaks of about 24 mV/V contour value, located at n=1 and n=4 levels. The contour of these both anomaly zones are opening downward which is suggestive of depth persistence of the inferred conductor below n=5 level. High chargeability in between W52 to W56 and W60 to W68 is indicative of mineralization within silicified zone associated with high resistivity anomalies.

Over traverse 'N980', the section has indicated two anomaly zones having peak value of 30 mV/V at n=5 level and bounded by 23 mV/V contour. One anomaly zone, lies between station W8 and W16 and the other, between station W42 and W50. Both of these anomalies are dipping westerly and opening towards depth is suggestive of depth persistence of the inferred conductor below n=5 level. These zones are also associated with low SP, low resistivity and moderate magnetic responses. Such integrated geophysical anomaly seems to be favorable for occurrence of sulphide mineralization. The pseudo section derived from the IP data contain anomalies that appear to be related to local facies changes, along with the evidence for the presence of mineralization.

Exploration and Development in Study Area

Four The detailed exploration activities conducted by GSI during 2011-2012, led to the estimation of the base

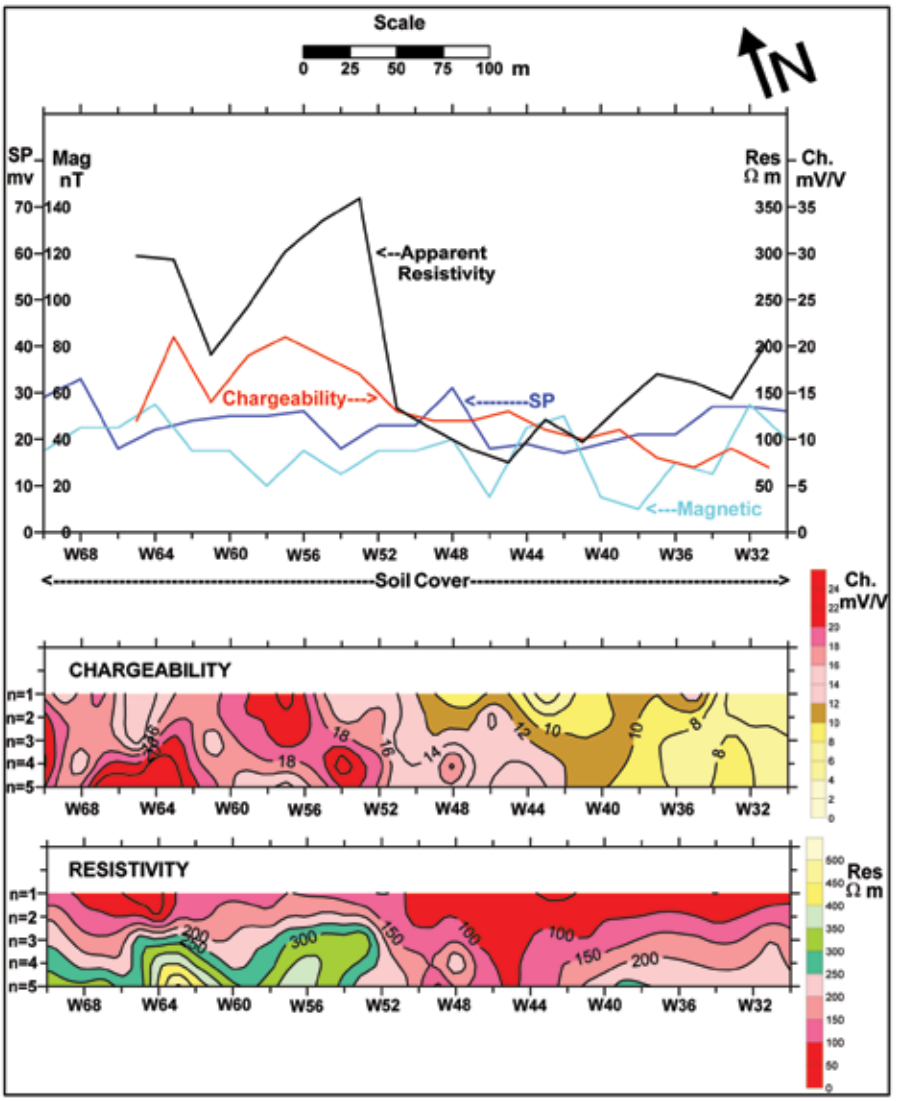

Figure 11. SP, magnetic (VF), IP (TD) chargeability, apparent resistivity profiles along with chargeability and resistivity pseudo-sections along traverse N160 north of the Dhani-Basri area, Dausa and Alwar districts, Rajasthan.

metal reserve in Mundiyawas- Khera regions of the Alwar (Rajasthan State Reviews 2014).

Four scout boreholes were drilled to test the presence of sub surface copper and associated precious metal mineralization in this block. All the four boreholes intersected sulphide mineralization, which has been established over a strike length of over 600 m in BH-1 to BH-4. Mineralization mostly occured in the form of disseminations, streaks, stringers, veinlets and fractured filled chalcopyrite, pyrrhotite, pyrite and rare specks of bornite and covellite, besides veins and specks within thin quartz and carbonate veins. The first borehole BH-1 intersected a 108.10 m thick mineralized zone with 0.29% Cu and associated silver and gold. It is a first time report of 108.10 m thick Cu mineralization from the Alwar Basin of the North Delhi Fold Belt, which includes a number of lodes aggregating to 77.65 m of 0.35% Cu (at 0.2% cut-off) and 33.8 m of 0.65% Cu (at 0.5% cut-off). Drilling in borehole BH-2, along the strike also intersected similar type of sulphide mineralization (190 m) with 0.2-0.5 % Cu (V.E.). The part analytical results of borehole BH-2 indicate a no. of lodes of 110.60 m x 0.36% Cu (at 0.2% cut-off) and 41.50 m x 0.57% Cu (at 0.5% cut-off). Borehole BH-3 was located to intersect the southern continuity of copper mineralization of BH-l and similarly, borehole BH-4 was located to intersect the northern continuity of the thick copper mineralization of BH-2, which also intersected similar type of sulphide mineralization. However, the concentration of mineralization is less as compared to borehole BH-l and BH-2.

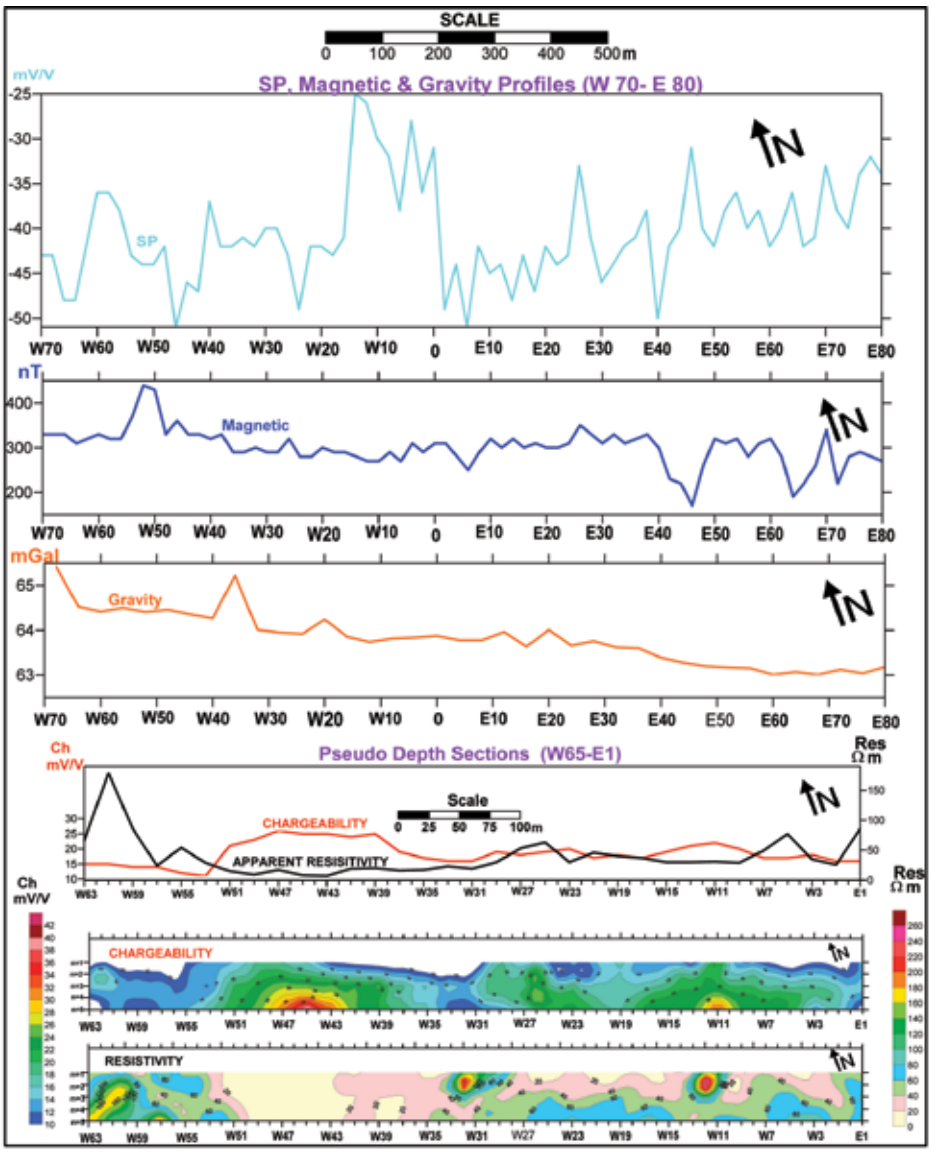

Figure 12. SP, magnetic (VF), IP (TD) chargeability, apparent resistivity, gravity profiles along with chargeability and resistivity pseudo-sections along traverse N980 north of the Dhani-Basri area, Dausa and Alwar districts, Rajasthan.

CONCLUSIONS

Geophysical surveys in the studied area have delineated seven anomaly zones, trending N-S and NW-SE directions, which are favorable for the occurrence of sulphide mineralization (Figure 5). Zone-I falling in the southern part has moderate order of anomaly and corroborates well with the proven Dhani-Basri deposit of copper-gold mineralization. The strike length of this anomaly zones vary from 400-1500 m. IP chargeability cum resistivity pseudo sections indicate depth persistence of inferred conductors. Vertical electrical sounding have also revealed the presence of three layer sequence, consisting of alluvium/soil, hard rock/fractured rock and Archaean basement. The depth of the hard rock is at 6-17 m which is underlain by highly resistive Archaean basement. High gravity values are well corroborated with high chargeability values. Besides, the magnetic, gravity and SP surveys have picked up lithological variation as well as structural features. It may be concluded that the most potential zone of possible mineralization is concentrated in the base metal sulphide deposits and the host rock for the mineralization is mostly quartzite and mica schist. Based on the present study, structural and lithological controls for base metal mineralization have been recorded. State-of-the-art modeling work□ows, can lead to a better structural insight in an already developed and explored mine settings (Vollgger et al., 2015).

Compliance with Ethical Standards

The authors declare that they have no conflict of interest and adhere to copyright norms.

REFERENCES

Ametha, S.S. and Sharma, B.B., 2008. Geology, structure and mineralization in Rajpura-Dariba-Surawa belt, Sindesar-Khurd area, Rajasmand district, Rajasthan. J. Geol. Soc. India, 72, 381-391.

Babu Lal, Naskar, D.C., Singh, R.R., Pushpraj Singh, Kulkarni, A.V., Manjeet Kumar, Ram Autar, 2012. Geophysical investigation for copper and gold mineralization, north of Dhani-Basri prospect, Dausa and Alwar districts, Rajasthan. GSI, Unpublished Progress Report.

Brij Kumar and Mukhopadhyay, 1999. A progress report on elucidation of tectono-stratigraphy and metallogeny of the Pre-Delhi basement rocks of the Dausa uplift in the north eastern Rajasthan with special reference to the relationship with volcanosedimentary cover formation of Delhi Supergroup. GSI Unpublished Progress Report.

Chakraborty, B. and Gupta, G.P., 1990. Transect geology of north Delhi fold belt. GSI, Unpublished Progress Report.

GSI, 2011. Geology and mineral resources of Rajasthan. GSI Miscellaneous Publication no. 30, part 12, 3rd Revised Edition.

Gupta, S.N., Arora, Y.K., Mathur, R.K., Iqballuddin, Prasad, B., Sahai, T.N. and Sharma, S.B., 1997. The Precambrian geology of the Aravalli region, southern Rajasthan and north-eastern Gujarat. Mem. Geol. Surv. Ind., 123, 1-262.

Hallof, P.G., 1957. On the interpretation of resistivity and induced polarization measurements. Cambridge, MIT, Ph.D. Thesis.

Heron, A.M, 1953. The geology of central Rajputana. Mem. Geol. Surv. Ind., 79, 1-389.

Heron, A.M., 1967. The geology of north eastern and adjacent district. Geo. Surv. India Memoir, 45, part-I.

Juned Alam, Siddiquie, F., and Shaif, M., 2015. Petrographic studies of Pb-Zn ore deposits of Rajpura-Dariba-Bethumni belt in district Udaipur (Rajasthan) India. Int. J. Geoscience, 6, 402-412.

Juned Alam and Siddiquie, F., 2015. Melt inclusion studies of Pb-Zn ore deposits of Rajpura-Dariba-Bethumni belt in district Udaipur (Rajasthan), India. Int. J. Geoscience, 6, 567-576.

Kearey, P., Brooks, M., and Hill, I., 2003. An introduction to geophysical exploration. Geophysical Journal International, 152(2), 506 p. Blackwell Publishing, Oxford.

Mathew, P.M., 1964. Geophysical surveys for copper ore in Dariba and Kho areas in Alwar district, Rajasthan. Int. Geol. Cong. Report of the twenty second seasons, India, part-II.

Mishra, S.P. and Joshi, S.M., 1967. Geological mapping in parts of Jaipur district, Rajasthan. GSI, Unpublished Report.

Mukherjee, A.K., Babu Lal and Murty, N.V.S., 1991. A report on the geophysical investigation for base metal in Kho-Dariba area, Alwar district, Rajasthan. GSI, Unpublished Progress Report.

Prasad, S.R., Vinod Kumar and Singh, V.N., 2002. Report on integrated geophysical surveys for copper-gold mineralization in Dhani-Basri, Kaljpuri and Andhi area, North Delhi Fold Belt, Dausa, Alwar and Jaipur districts, Rajasthan. GSI, Unpublished Progress Report.

Prasad, S.R., Babu Lal and Regar, R.L., 2003. Report on integrated geophysical surveys for copper-gold mineralization in Dhani-Basri, Kaljpuri and Andhi area, North Delhi Fold Belt, Dausa, Alwar and Jaipur districts, Rajasthan. GSI, Unpublished Progress Report.

Rajasthan State Reviews, 2014. Indian Minerals Yearbook 2012, part-I, 51st Edition. State Reviews (Rajasthan), Final release. Govt. of India, Ministry of Mines, Indian Bureau of Mines, Indira Bhavan, Civil Lines, Nagpur-440001.

Ravindra, R. and Pahuja, R.P.S., 1984. Report on the copper investigation in Todi ka Bas mineralization zone, Alwar district, Rajasthan. GSI, Unpublished Progress Report.

Reynolds, J.M., 1997. An Introduction to Applied and Environmental Geophysics", John Wiley Sons Ltd.

Sant, V.N., Sharma, S.B. and Siddiqui, M.A., 1963. Geology of Raialo-Ajabgarh-Tehla area, Alwar and Jaipur districts, Rajasthan. GSI, Unpublished Report.

Sant, V.N. and Sharma, S.B., 1973. Precambrian metasedimentary of Alwar and Jaipur district, Rajasthan and their stratigraphy sequence (abstract). Syn. Record Advances in Geology of Rajasthan in Jaipur.

Singh, R.R., Singh, S.L. and Shiv Lal, 2009. Integrated geophysical surveys for base metal and associated gold mineralization in Todi ka Bas, Alwar district, Rajasthan. GSI, Unpublished Progress Report.

Vollgger, S.A., Alexander Cruden, R., Laurent Ailleres, E. and Cowan, J., 2015. Regional dome evolution and its control on ore-grade distribution: Insights from 3D implicit modelling of the Navachab gold deposit, Namibia. Elsevier, Ore geology Reviews, 69, 268-284.

Yadav, P.K. and Avadich, P.C., 2010. Geology, structure and mineralization in Rajpura-Dariba belt, Sindesar-Khurd area, Rajasmand district, Rajasthan. J. Geol.Soc. India, 75, 731-738.

Received on: 19.11.18; Revised on: 28.12.18; Accepted on: 8.2.19

J. Ind. Geophys. Union (March 2019)
v.23, no.2, pp: 134-142

A MATLAB Based Code for gravity data Corrections

K. Satish kumar[1], Debraj Midya[2], M. Tirupathi[1*], and R.K. Tiwari[1]

[1]CSIR-National Geophysical Research Institute, Hyderabad-500007, Telangana, India

[2]Indian Institute of Technology Bombay, Mumbai, India

* Corresponding author: mtirupathi@gmail.com

ABSTRACT

An interactive MATLAB based code, designed for processing of relative ground gravity data. This interactive code is robust to compute Bouguer anomalies from relative land gravity data, acquired with reference to single standard absolute gravity base. The processed data will be viewed in the form of excel spreadsheet and graphical window. The efficacy of the code is tested on the real data set near Umred Coal field, Maharashtra and found to be feasible for handling gravity data sets for precise interpretation of the results. 1D spectral analysis of the Bouguer anomaly data shows that the depth to the basement varies from 0.5 km to 1.3 km over which Gondwana group of rocks are emplaced. Similarly, thickness of the trap is found to vary from 0.25 km to 0.6 km. The obtained results are in good agreement with the previous gravity and Magnetotelluric studies.

Keywords: MATLAB; Gravity; Bouguer anomalies; Gondwana; 1D Spectral Analysis.

INTRODUCTION

Gravity method has been invariably used in various geophysical investigations like mapping of sedimentary basins, structural features (faults, folds and lineaments), subsurface cavities, mineralised zones (Sulphide, Chromite, Iron ore, silver, gold, coal etc) and potential ground water resources. CSIR-National Geophysical Research Institute has been collecting relative gravity data sets, to address various geological problems related to mineral, oil and ground water applications (Seshunarayana et al., 2011; Pandey et al., 2014; Satish Kumar et al., 2018; Swarnapriya et al., 2017; Tirupathi et al., 2017 etc.). The acquired field gravity data provides point to point variations due to causative sources, due to earth's topography, and departure of earth shape from the sphere, atmospheric and Tidal changes. Hence, it is required to reduce these responses to obtain actual causative anomalies of the gravity sources concealed beneath the subsurface. Reduction of gravity data may play a crucial role to nullify the other responses, apart from the causative anomaly sources. Reduction of land gravity data involves drift of the gravimeter, conversion of relative gravity to absolute gravity, latitude correction, Free-air correction, Bouguer correction and terrain correction. Depending on the objective of the survey, huge gravity data sets are needed to be collected in the field. Reduction of such huge data sets is a tedious task and, in fact, need commercial softwares for processing precise Bouguer anomalies. Several researchers developed their own codes, which are available to process the gravity data e.g. CgxTool (Gabalda et al., 2003); Gravnet (Hwang et al., 2002); MCGravi (Beilin, 2006); GravProcess (Cattin et al., 2015) and pyGrav (Hector and Hinderer, 2016). In the present study, we have developed a user friendly interactive MATLAB based application "code" that can handle relative gravity data and can generate the Bouguer anomaly output along with aforesaid corrections. Particularly, user can input raw gravity data with time, latitude, longitude, elevation for a particular base gravity in the form of worksheet. User can view the output in the form of work sheet that contains the raw gravity data with latitude, longitude, elevation, drift corrected, latitude corrected, free-air corrected, Bouguer corrected and Bouguer anomaly. We tested this procedure using real field data, which is collected over the Deccan trap region of central India near Nagpur, Maharashtra. However, we have not attempted the tidal and terrain corrections in this module which can involve the input of external data sets like Digital Elevation Model (DEM). Depth to the basement and thickness of the Deccan trap are estimated through spectral analysis in aid to coal exploration using the processed data set.

BASIC STEPS FOR "CODING"

Basically, code works for land relative gravity data with reference to the single base station. For data with multiple base stations, user can subdivide the whole data set depending on occupied base stations and import the data for a single base at a time. The flow chart for this code is presented in Figure 1. To work with large datasets of any extents, a particular data format is required as the input in the form of excel spreadsheet (Table 1). User has to take care while importing the base station number i.e any alphanumeric or simple alphabetical name to mark the base station number. Otherwise, that will be considered as another station location and flow will end up with error and avoid data gap between any two rows. Further, for a particular profile, starting station number must start with zero.

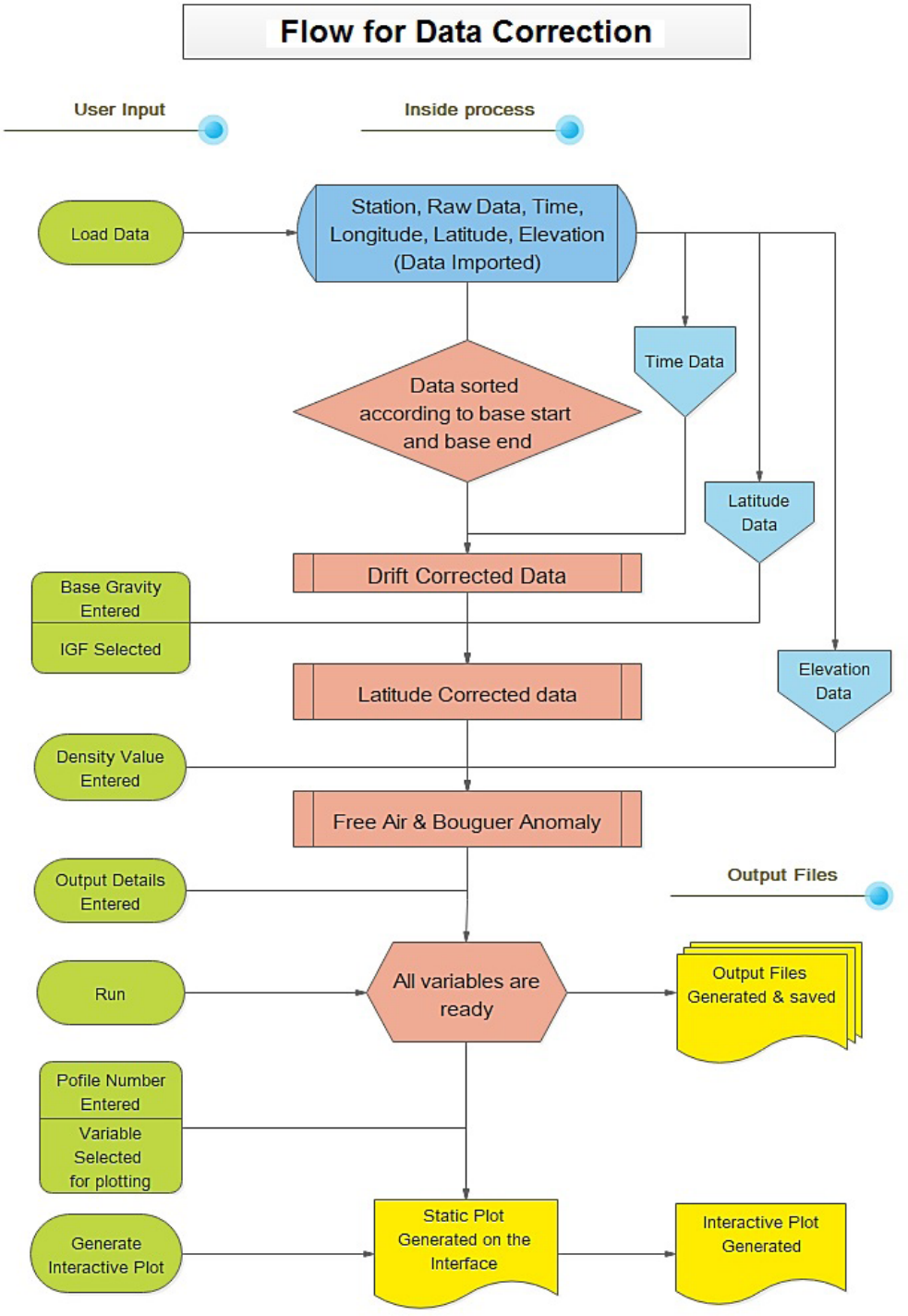

Figure 1. Flow chart for workflow for corrections.

Figure 2 shows the interactive tool panel to process the gravity data, sequential steps from 1 to 10 will be provided to execute the raw data set to calculate the Bouguer anomaly. User is required to input the density in C.G.S units.

REAL DATA ANALYSIS

To test the efficacy of code, field data of three Profile P1, P2 and P3 are considered (Figure 3) near Umred, Nagpur region, Central India which is one of the coal basins of

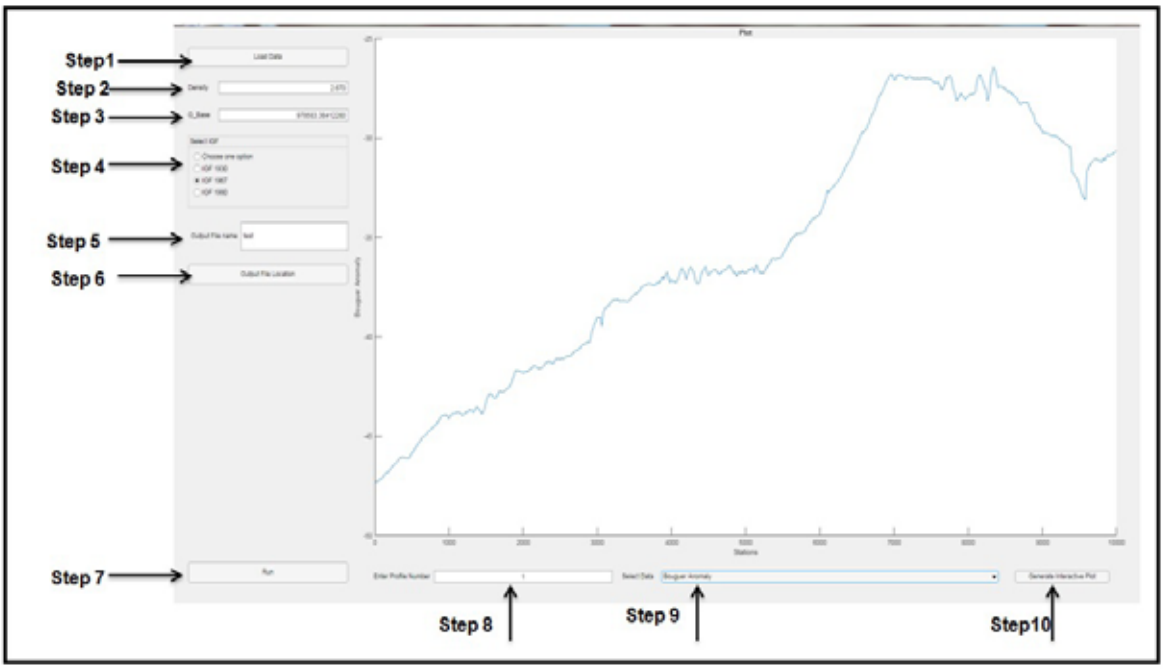

Figure 2. Interactive Window.

Table 1. Input data format for corrections.

Profile No	Station No	Raw data (mGal)	Time (HH)	Time (MM)	Time (SS. SS)	Longitude (Degree)	Latitude (Degree)	Elevation (Meter)
1	**Base 1**	**Base value**	**Hour**	**Min**	**Sec**	**Longitude**	**Latitude**	**Elevation**
1	0	Data	Hour	Min	Sec	Longitude	Latitude	Elevation
1	1	Data	Hour	Min	Sec	Longitude	Latitude	Elevation
1	**Base 1**	**Base value**	**Hour**	**Min**	**Sec**	**Longitude**	**Latitude**	**Elevation**
1	**Base 1**	**Base value**	**Hour**	**Min**	**Sec**	**Longitude**	**Latitude**	**Elevation**
1	3	Data	Hour	Min	Sec	Longitude	Latitude	Elevation
1	4	Data	Hour	Min	Sec	Longitude	Latitude	Elevation
1	**Base 1**	**Base value**	**Hour**	**Min**	**Sec**	**Longitude**	**Latitude**	**Elevation**
2	**Base 1**	**Base value**	**Hour**	**Min**	**Sec**	**Longitude**	**Latitude**	**Elevation**
2	0	Data	Hour	Min	Sec	Longitude	Latitude	Elevation
2	1	Data	Hour	Min	Sec	Longitude	Latitude	Elevation
2	2	Data	Hour	Min	Sec	Longitude	Latitude	Elevation
2	**Base 1**	**Base value**	**Hour**	**Min**	**Sec**	**Longitude**	**Latitude**	**Elevation**

India (De et al., 1982; Rama Krishna et al., 1999a, 1999b). The study area is capped by alluvium and some patches of exposed Deccan basaltic rocks, which are underlain by a Gondwana group of rocks (Naskar and Saha, 2015). Gravity data has been collected along three profiles P1, P2, and P3 with lengths of 10 km, 2.6 km and 9.5 km respectively across the regional strike of the study area (Figure 3). Gravity data was collected with a sample interval of 20 m. The data have been acquired using CG-5 gravimeter with an accuracy of ± 1μGal. Coordinates (longitude and latitude) and elevation of the station is recorded using Trimble Geo XT handheld model global positioning system (GPS) receiver. Differential correction was also applied to the coordinate data using the base station data.

Bouguer anomalies are computed using present code for the profiles P1, P2, and P3 and discussed in the following sections and also demonstrated output of applied corrections (drift, latitude, free air, Bouguer and Bouguer anomaly) to the field relative gravity data. Hence, user can easily find the errors in each stage of processing. Further, 1D spectral analysis has been carried out for the Bouguer anomalies of P1 to P3 to understand the depth to the basement and thickness of Deccan trap.

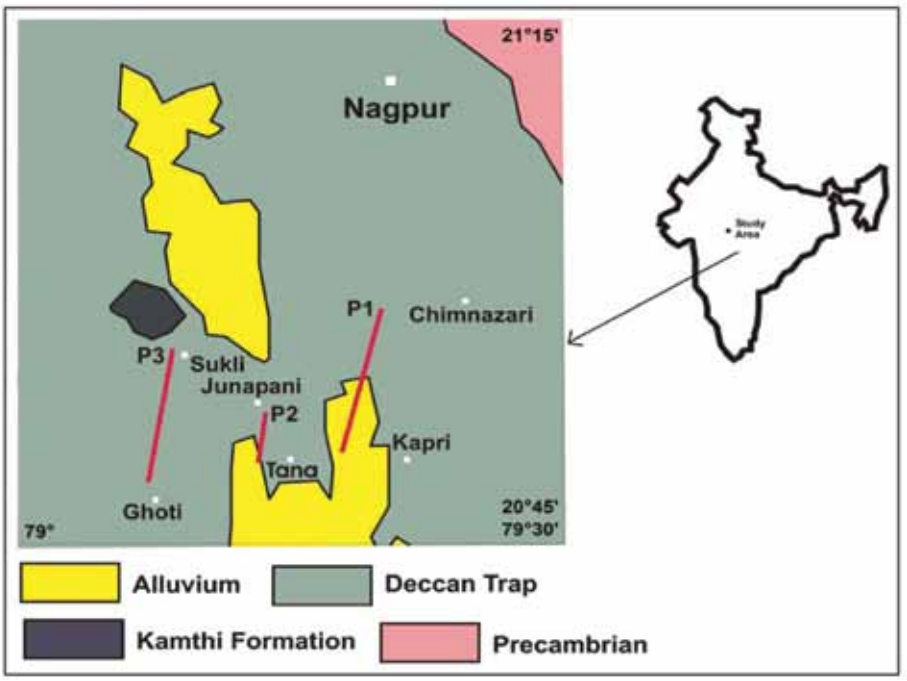

Figure 3. Location of Profile P1, P2, and P3 (after Naskar and Saha, 2015; Satish Kumar et. al., 2018)

Profile P1

The SSW-NNE trending Profile- P1 starts from west of Kapri village and ends near Chimnazari village with a length of 10 Km (Figure 3). Alluvium, basalts are occupied in SSW and NNE part respectively.The Bouguer gravity anomaly varies from -39 mGal to -18 mGal from SSW and NNE of the profile (Figure 4a). The nature of the gravity anomaly which is increasing from SSW to NNE of the profile may represent increasing thickness of the basaltic layer from Kapri to Chimanzari village. Further, a sharp gravity gradient is also observed between 0.6 km and 0.7 km, which might be a contact zone. 1D spectral analysis (Spector and Bhattacharyya, 1966; Bhattacharyya, 1966; Spector and Grant, 1970; Naidu, 1970; Hahn et al., 1976; Mishra and Tiwar,1966; Prabhakara Prasad et.al., 2013; Satish Kumar et al., 2014; Satish Kumar et al., 2015; Tirupathi et al., 2017; Satish Kumar et al., 2018; Pandey et al., 2018) was performed for Bouguer anomaly profile P1 (Figure 4b) and also P2 and P3, to estimate depth to the basement and thickness of the trap. The 1D amplitude spectra of Bouguer anomaly shows two discernible segments with different slopes (Figure 4b). The depth is computed from slope of each segment by using the formula:

$$\text{Depth} = 1/4\pi \times (\Delta E/\Delta N)$$

Where $\Delta E/\Delta N$ is the slope of each segment, ΔE is the log energy and ΔN is the wave number increment. The depth computed from slopes of two straight line segments are 1.25 Km and 0.25 Km, which may represents depth to the basement and thickness of the Deccan trap respectively.

Profile P2

Gravity data along Profile P2 is collected from Tana to Junapani villages, covering a length of about 2.6 km (Figure 3). The Bouguer anomalies vary from -37 mGal to -44 mGal from SSW to NNE. The nature of the Bouguer anomaly, increasing from SSW to NNE, might represent the increase in basaltic thickness from Tana village to Junapani (Figure 5a). 1D amplitude spectrum of Bouguer anomaly shows one straight line segment (Figure 5b). The estimated depth from the slope of the segment is 0.5 km and it is attributed to thickness of the basaltic layer, underlain by Gondwana group of rocks. Due to limited extended of profile length, depth to the basement could not be resolved from the amplitude spectrum.

Profile P3

Profile P3 is starts from Ghoti village and ends at Sukli village and has a length of about 9.5 Km (Figure 3). The entire profile is covered by basaltic layer. The gravity anomaly varies from -67 mGal to -57mGal from SSW to NNE, with amplitude of 10 mGals (Figure 6a). The nature of the Bouguer anomaly increase from SSW to NNE, might represent the increase in basaltic thickness from Ghoti village to Sukli village. 1D amplitude spectrum of Bouguer anomaly shows two straight line segments (Figure 6b). The estimated depths from the slope of the segments are 1.2 km and 0.6 km and it is attributed to depth to the thickness of the basaltic layer underlain by Gondwana group of rocks respectively.

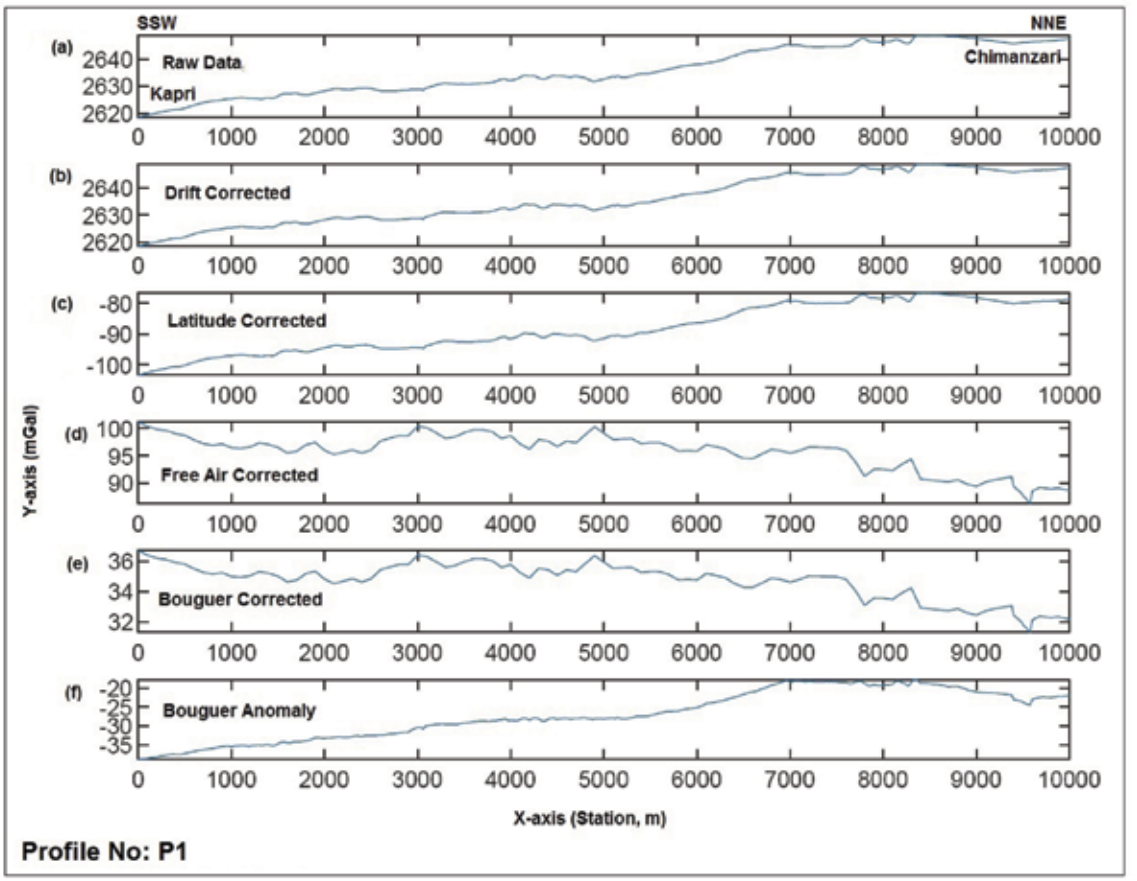

Figure 4a. Plot of (a) raw gravity data, (b) drift corrected, (c) Latitude corrected, (d) Free-air corrected, (e) Bouguer corrected and (f) Bouguer anomaly along profile P1

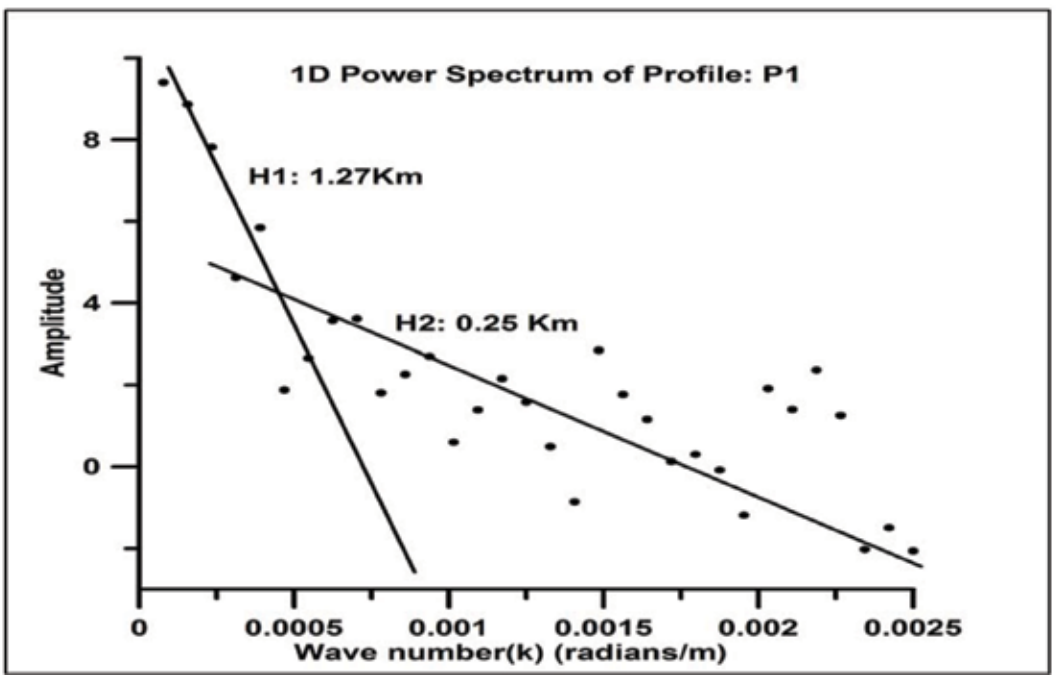

Figure 4b. Amplitude Spectrum of Profile P1

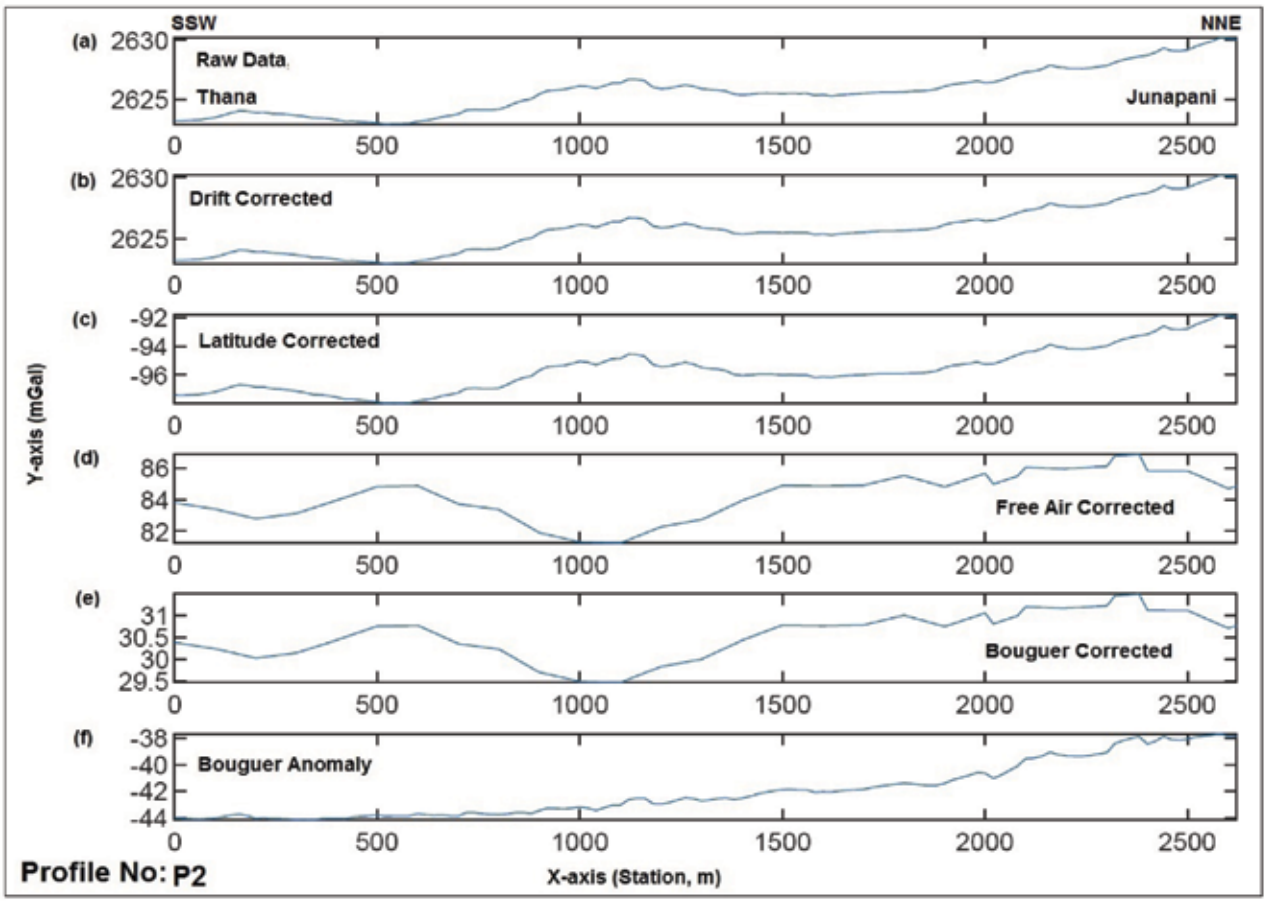

Figure 5a. Plot of a) raw gravity data, b) drift corrected, c) Latitude corrected, d) Free-air corrected, e) Bouguer corrected and f) Bouguer anomaly of profile P2

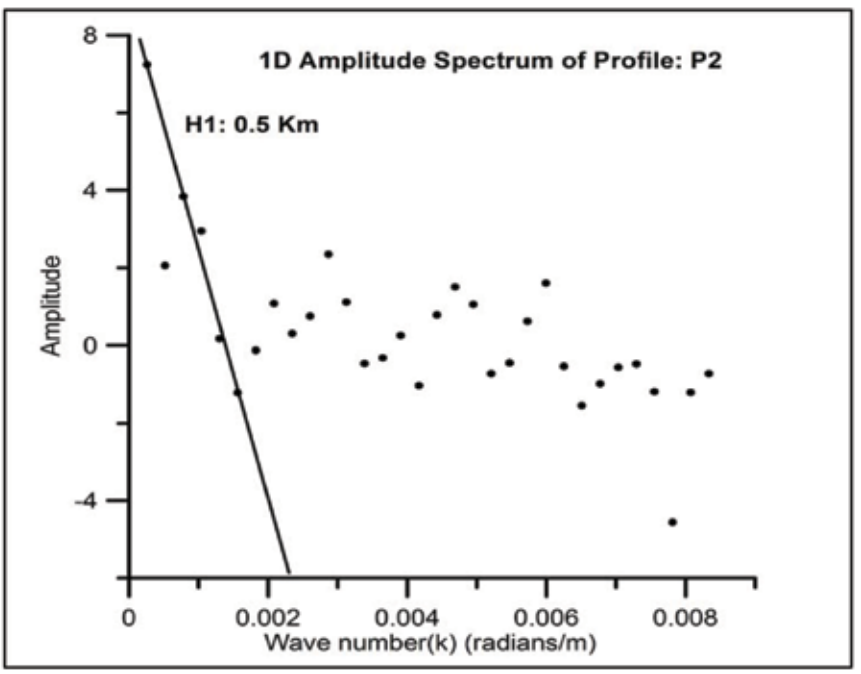

Figure 5b. Amplitude Spectrum of Profile P2

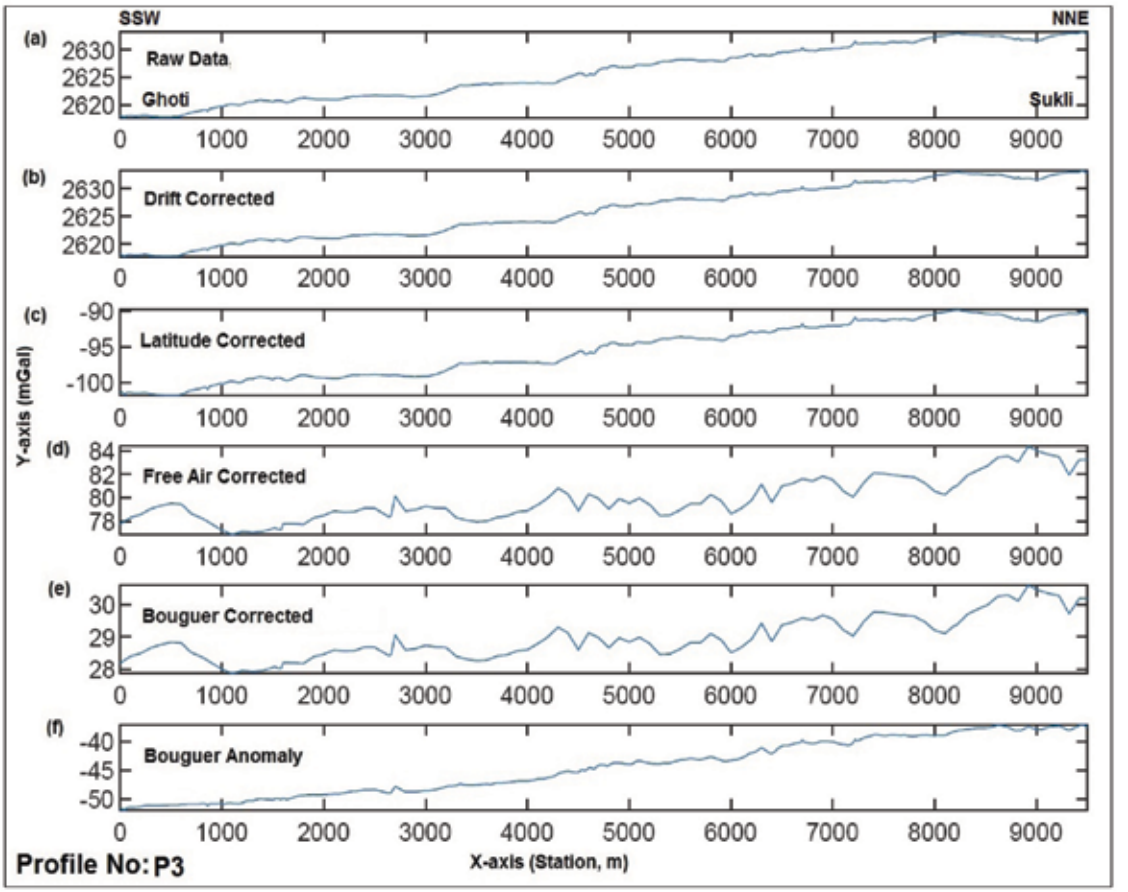

Figure 6a. Plot of (a) raw gravity data, (b) drift corrected, (c) Latitude corrected, (d) Free-air corrected, (e) Bouguer corrected and (f) Bouguer anomaly along profile P3

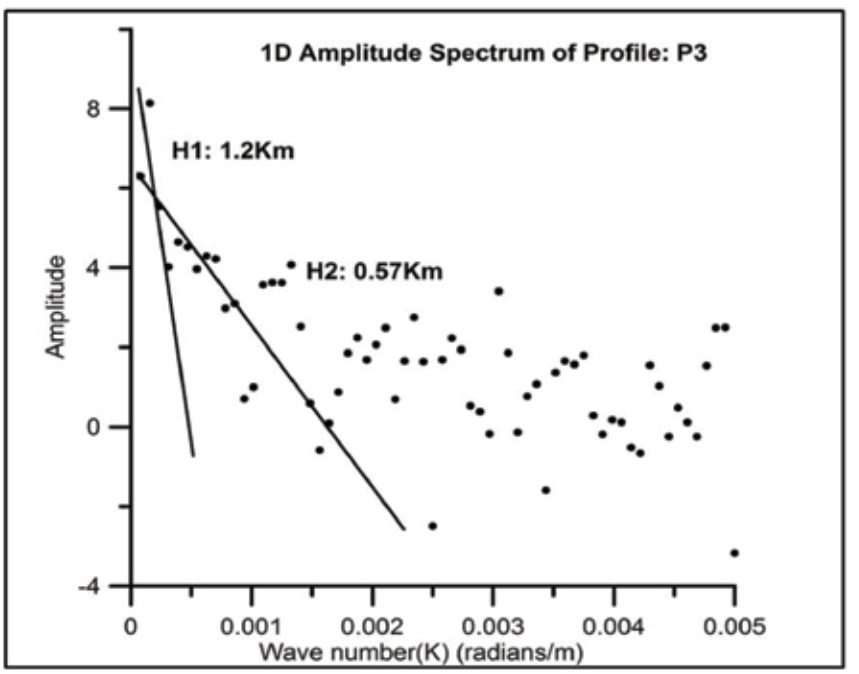

Figure 6b. Amplitude Spectrum of Profile P3

It is inferred from the spectral analysis that the depth to the basement varies from 0.5 Km to 1.3 in the study area. The shallowest basement is observed at profile P2, where as deepest part is observed at P1 and P3. The obtained results are good agreement with the results of lithological (Raja Rao, 1982), Magnetotelluric (Jitendra Kumar et al., 2004) and Gravity (Satish Kumar et al., 2018) studies.

CONCLUSIONS

The developed code is useful for processing of land relative gravity data. The efficacy of the code is tested on the real data set near Umred Coal field, Maharashtra and found to be feasible for handling gravity data sets for precise interpretation of the results.

ACKNOWLEDGEMENTS

The authors gratefully acknowledge the CSIR-NGRI GEOMET Project. The authors are also grateful to Dr.V.M.Tiwari, Director of NGRI for granting permission to publish this paper. Dr R. K. Tiwari especially thanks the Department of Atomic Energy for Raja Rama Fellowship. The authors would also like to extend their gratitude to the Directorate of Geology and Mining, Government of Maharashtra, Nagpur, for permission to conduct research in the study area and sharing their knowledge during the data acquisition. Thanks also to the staff of the Engineering Geophysics group for their help during field data acquisition and during various stages of this work. Thank to the Mr. Kalyan Netti for help to completion of the manuscript. Mr. Debraj Midya grateful to Prof. M.Radhakrishna and Prof. T.N.Singh from IIT Bombay for giving permission to work at NGRI. NGRI Library Ref.No: NGRI/Lib/2018/Pub-66.

CODE AVAILABILITY

The "code" and user guide is available on request from the author. To get the file for installing within MATLAB® environment, go to the following link:
https://drive.google.com/open?id=1TL8fXJdv1eyandsa5crRSYEnRgWiAYKO
or
https://drive.google.com/drive/folders/1TL8fXJdv1eyandsa5crRSYEnRgWiAYKO?usp=sharing

Compliance with Ethical Standards

The authors declare that they have no conflict of interest and adhere to copyright norms. Before references subsection.

REFERENCES

Beilin, J., 2006. Apport de la gravimétrie absolue à la réalisation de la composante gravimétrique du Réseau Géodésique Français. Inst. Géogr. Natl., Paris, France.

Bhattacharya, B.K., 1966. Continuous spectrum of the total magnetic field anomaly due to rectangular prismatic body. Geophysics, 31, 97-121.

Cattin, R., Mazzotti, S. and Baratin, L.M., 2015. GravProcess: an easy to use MATLAB software to process campaign gravity data and evaluate the associated un- certainties. Comput. Geosci., 81, 20–27. http://dx.doi.org/10.1016/j.cageo.2015.04.005.

De, S., Ghosh, D. and Rao, K.J., 1982, Report on geophysical investigations for delineating Gondwana below traps in Umred trough inNWextension for Wardha valley coal field, Nagpur district, Maharashtra: Unpublished Report, Geological Survey of India.

Gabalda, G., Bonvalot, S. and Hipkin, R., 2003. CG3TOOL: an interactive computer program to process Scintrex CG-3/3 Mgravity data for high-resolution applications. Comput. Geosci., 29(2), 155–171. http://dx.doi.org/10.1016/S0098-3004 (02)00114-0.

Hahn, A., Kind, F.G. and Mishra, D.C., 1976. Depth estimation of magnetic sources by means of Fourier amplitude spectra. Geophys. Prosp., 24, 287–308

Hwang, C., Wang, C.G. and Lee, L.H., 2002. Adjustment of relative gravity measurements using weighted and datum free constraints. Comput. Geosci., 28(9), 1005–1015. http://dx.doi.org/10.1016/S0098-3004 (02)00005-5.

Jitendra Kumar., Singh, P., Dutta, D., 2004. Infra Trapean modelling of deccan syneclise. 5th Conference and Exposition on Petroleum Geophysics, Hyderabad-2004, India, 65-68.

Mishra, D.C. and Tiwari, R.K., 1981. Spectral study of the Bouguer anomaly map of a Rift Valley and adjacent areas in Central India. PAGEOPH, 119, 1051-1062.

Naidu, P.S., 1970. Statistical structure of aeromagnetic field. Geophysics, 35(2), 279- 292.

Naskar, D. C. and Saha, D. K., 2015. Geophysical investigations for delineation of Gondwana sediments below Deccan trap beyond the western limit of Wardha Valley coalfields, Yeotmal and Wardha districts, Maharashtra: a comprehensive analysis of case studies: J. Indian Geophys. Union, 19, 433–446.

Pandey, O.P., Chandrakala, K., Vasanthi, A. and Satish Kumar, K., 2018. Seismically imaged shallow and deep crustal structure and potential field anomalies across the Eastern Dharwar Craton, south Indian shield: Possible geodynamical implications. J. Asian Earth Sci., 157, 302–316.

Pandey, O.P., Srivastava, R.P., Vedanti,N., Dutta, S. and Dimri, V.P., 2014. Anomalous crustal and lithospheric mantle

structure of southern part of the Vindhyan basin and its geodynamic implications. J. Asian Earth Sci., 91, 316–328. http://dx.doi.org/10.1016/j.jseaes.2013.11.015.

Prabhakara Prasad, P., Satish Kumar, K., Seshunarayana, T. and Rama Rao, Ch., 2013. New approach for interpretation of scattered ground magnetic data in a part of Delhi Fold Belt-NW Indian shield. Arab. J. Geosci. DOI 10.1007/s12517-013-0926-1.

Rama Krishna, T.S., Ramarao, M.S.V., Bhaskar Rao, K.V.S. and Punekar, D.V., 1999a.Geophysics of the Mahrashtra Gondwana: GSI special publication, 47.

Rama Krishna, T.S., Ramarao, M.S.V., Bhaskar Rao, K.V.S. and Punekar, D.V., 1999b. Geophysics of the Mahrashtra Gondwana: GSI special publication, 49.

Raja Rao, C., 1982. Coalfields of India: Geol. Survey of India, Bulletin Series A, no. 45.

Satish Kumar, K., Kishore, R.K., Parveen Begum., Seshu, D. and Rama Rao, Ch., 2014. Estimation of depth extent of Gangam-Peruru complex of Eastern Dharwar Craton (EDC) from aeromagnetic data. Arab. J. Geosci., DOI 10.1007/s12517-014-1383-1.

Satish Kumar, K., Kishore, R.K., Raj Kumar, R., Seshu, D., Pradeep Kumar, V. and Parveen Begum., 2015. Aeromagnetic Analysis to Locate Potential Ground Water Zone - A Case Study from South Indian Shield. J. Ind. Geophys. Un., 19(2), 160-166.

Satish Kumar, K., Rajesh, R. and Tiwari, R.K., 2018. Regional and residual gravity anomaly separation using the singular spectrum analysis-based low pass filtering: a case study from Nagpur, Maharashtra, India. Exploration Geophys., 49, 398-408. http://dx.doi.org/10.1071/EG16115.

Satish Kumar, K., Srinivas, K.N.S.S.S., Pradeep Kumar, V., Prabhakara Prasad, P. and Seshunarayana, T., 2018. Magnetic mapping of banded iron formation of Sandur Schist belt, Dharwar Craton, India. J. Geo. Soc. India, 91, 174-180.

Seshunarayana, T., Rajendra Prasad, B, Prasad, A.S.S.S.R.S. and Mysaiah, D., 2011. Subsurface Structure Derived from Detailed Gravity and Magnetic Investigations along the Pala-Maneri Traverse of the Main Central Thrust, NW Himalaya. J. Geol. Soc. India, 77, 213-218.

Spector, A. and Bhattacharyya, B.K., 1966. Energy density spectrum and auto correction function of anomalies due to simple magnetic models. Geophys. Prosp., 14, 242–272.

Spector, A. and Grant, F.S., 1970. Statistical models for interpreting aeromagnetic data. Geophysics, 35(2), 293–302.

Swarnpriya Chowdaria., Bijendra Singha., Nageswara Rao, B., Niraj Kumara., Singh, A.P. and Chandrasekhara, D.V., 2017. Structural Mapping Based on Potential Field and Remote Sensing Data, South Rewa Gondwana Basin, India. J. Earth Syst. Sci, 126(84). Indian Acad. Sci., DOI 10.1007/s12040-017-0857-4.

Tirupathi, M., Satish Kumar, K., Laxmaiah, B., Bansal, A.R. and Tiwari, R.K., 2017. Gravity and magnetic investigation along Rewa - Shahdol Basin Central India: Spectral Analysis Results. Socity of Exploration Geophysicsts, 12th Biennial International Conference Exhibition 17thto 19th November 2017.

Received on: 31.8.18; Revised on: 7.1.19; Accepted on: 8.2.19

J. Ind. Geophys. Union (March 2019)
v.23, no.2, pp: 143-151

Rapid Visual Screening of RC frame buildings in 2001 Bhuj earthquake affected Rambaug area of Ahmedabad, Gujarat

Russi Modi* and Kapil Mohan

Institute of Seismological Research, Next to Petroleum University, Raisan-382007, Gandhinagar, Gujarat.
*Corresponding author: modirussi017@gmail.com

ABSTRACT

The buildings in Ahmedabad experienced heavy damage in the 2001 Bhuj earthquake, which exposed the deficiencies in their design and construction practices. The enhanced seismicity in the region warrants assessment of seismic vulnerability to aid engineers in urban development. The current study attempts to assess the vulnerability of RC frame buildings using Rapid Visual Screening (RVS) in the Rambaug area (Ahmedabad) where the collapses of a similar type of buildings were observed due to 2001 Bhuj earthquake. The RVS of 100 RC frame buildings was conducted. The performance score of the surveyed building ranges from 20 to 125. The parameters such as soft storey and overhang are found in most of the surveyed buildings, which make the buildings vulnerable to earthquake. The vulnerability here is defined as a relative measure based on the obtained performance score of the considered buildings. Most of the buildings lay in the performance score range of 43-84, which indicates moderate vulnerability of these buildings due to earthquake occurrence.

Keywords: Earthquake, Vulnerability assessment, Rapid visual screening.

INTRODUCTION

In recent times, a number of damaging earthquakes have been experienced in our country that include Bhuj earthquake (2001), North Andaman (2002), North Kashmir (2005) and Sikkim earthquake (2006), which demonstrated the high seismic hazard leading to huge loss of life and economy.. Rampant construction, coupled with improper implementation or planning in urban areas, led to substantial losses during 2001 earthquake while putting the safety of the people at stake. The occurrence of many other damaging earthquakes following the 2001 Bhuj earthquake has put further seismic safety as a big concern to the seismologist as well as the government. The estimated losses according to the Gujarat government was Rs. 10,000 crores and death figure were 13,805 in Gujarat during the 2001 Bhuj earthquake. (Mishra, 2012).

In fact, the city of Ahmedabad, a major city located 250 km from the epicenter, has also suffered huge losses in terms of life and property in the 2001 Bhuj earthquake. It is highlighted by Mishra (2012) that 80 buildings that collapsed in Ahmedabad were mostly of more than 3 storeys and were constructed within the last thirty years. Ahmedabad being the fastest growing city in Gujarat, where the population is on the rise and the infrastructural development is continuous past earthquake experiences suggests that buildings in the city are vulnerable to future earthquakes, highlighting the need to assess the seismic vulnerability of buildings in Ahmedabad.

SEISMIC VULNERABILITY

Seismic vulnerability of a building is highly dependent on the structural properties and soil type. Seismic vulnerability assessment is a two-step procedure, (i) preliminary analysis, and (ii) detailed analysis. In the preliminary analysis, rapid visual screening and collection of structural drawings are to be done. In the detailed analysis, linear or nonlinear analysis of the buildings needs to be performed based on collected structural drawings.

Rapid Visual Screening (RVS) was developed by the Applied Technology Council (ATC) and was first published by the Federal Emergency Management Agency (FEMA) in 1988. This method uses to screen buildings based on visually observable vulnerability parameters of the building. Based on these observed vulnerability parameters, expected performance score of the building to be calculated which indicates its adequacy against earthquakes. RVS does not require the screener to perform any structural calculations but only needs to identify the type of building and its attributes that affect the performance of the structure against seismic forces. Dutta et al., (2016) have carried out the damage survey for the RBI properties in Patna after Gorkha (M 7.8) earthquake (April 25, 2015). It puts forward an attempt to validate a RVS method for non-engineered structures and highlights the need and the importance of such quick assessment technique that will be helpful in assessing the vulnerability of large region and mitigation process in an event of earthquake.

Table 1. Considered vulnerability parameters in different vulnerability assessment method for RC structure.

Vulnerability assessment method	FEMA, 2015	Sucuoglu et al., 2003	Jain et al., 2010	Arya, 2000	Srikanth et al., 2010
Soft storey	Y	Y	Y	N.G.	Y
Heavy overhang	Y	Y	N	N.G.	Y
Short column	Y	Y	Y	N.G.	Y
Pounding possibility	Y	Y	N	N.G.	Y
Age of the structure	Y	N	N	N.G.	N.G.
Building height	Y	Y	Y	N.G.	Y
Maintenance	Y	N	Y	N	Y
Apparent quality	Y	Y	Y	N	Y
Re-entrant corner	Y	N	Y	N.G.	Y
Basement	N. G.	N	Y	N	Y
Soil type	Y	Y	Y	N.G.	Y
Topographic effect	Y	Y	N	N	Y
Vertical Irregularity	Y	-	-	N.G.	Y
Plan irregularity	Y	-	-	N.G.	Y

*Y: Yes; N: No; N.G.: Not graded

Different RVS methods available among several countries are USA (FEMA, 2015), Canada (NRCC, 1993), New Zealand (NZSEE, 2006), Japan (JBDPA, 2001), and Turkish RVS (Sucuoglu et al., 2007). The researchers (Nanda and Majhi, 2013) have done a brief review and comparison of some of the RVS methods among several countries.

FEMA recently revised its RVS method in 2015 (FEMA, 2015), which is much detailed and consistent with the current building typologies in the US. It addresses the problem of the negative scoring observed in the earlier version (FEMA, 2002). The score in the RVS form have been derived using capacity spectrum method, but since they were derived for US building typologies and considering their soil conditions, this method cannot be directly applied to other regions and would require calibration to adopt the same in different regions as suggested by the available literature.

Jain et al., (2010) proposed an RVS method for RC-frame buildings using statistical analysis of post-earthquake damage data of 2001 Bhuj earthquake. A mean error of 20% in accurately predicting damage category was observed for the 1000 bootstrap samples considered for comparison between Expected Performance Score and Observed Performance Score but this method was based on limited data from damages in one Indian city and for one building typology. Further research on the same was recommended. A RVS procedure was proposed by Chanu and Nanda (2018) based on the Multivariable regression analysis performed on damage data of RC buildings during Manipur (M 6.7) earthquake (January 4 2016). Further, Arya (2000), proposed RVS Method for RC and Masonry structures, utilizing the damageability-grading system. It considers various building typologies and relevant vulnerability parameters. However, for grading of the structures, the vulnerability parameters show no influence on the final grade, as the grading is based on the observed damage of past earthquake for the considered building type and the seismic zone in which the building lies. This, in turn, may not be enough to accurately predict the vulnerability of the structure due to the earthquake.

Sucuoglu et al., (2003) attempted to evaluate several selected parameters simultaneously to obtain a performance score for each building rather than a group of buildings as done in FEMA and other methods for 3-6 storey substandard concrete buildings. This score separates each building from the other buildings in the inventory in risk classification. Only 4 parameters were considered for vulnerability classification in the revised version (Sucuoglu et al., 2007) namely, the number of stories, the presence of a soft storey, the presence of heavy overhangs, and apparent building quality. Other parameters were dropped from the revised version, as they were not found to be significantly affecting the performance of the buildings in their study area. Srikanth et al., (2010) also proposed another RVS method which has been used in Gandhidham and Adipur cities, Kachchh, Gujarat in 2010 and a slightly modified version was used to survey buildings of Himachal Pradesh (Kumar et al., 2017). They have used Jain et al., (2010) and the Turkish method as a reference to develop the base score and score modifiers. Some additional vulnerability parameters were added, and their scores may be based on engineering judgment, as the basis of these scores is not explained in detail in the available literature. A tabulated format for comparison between different vulnerability assessment methods is given in table 1.

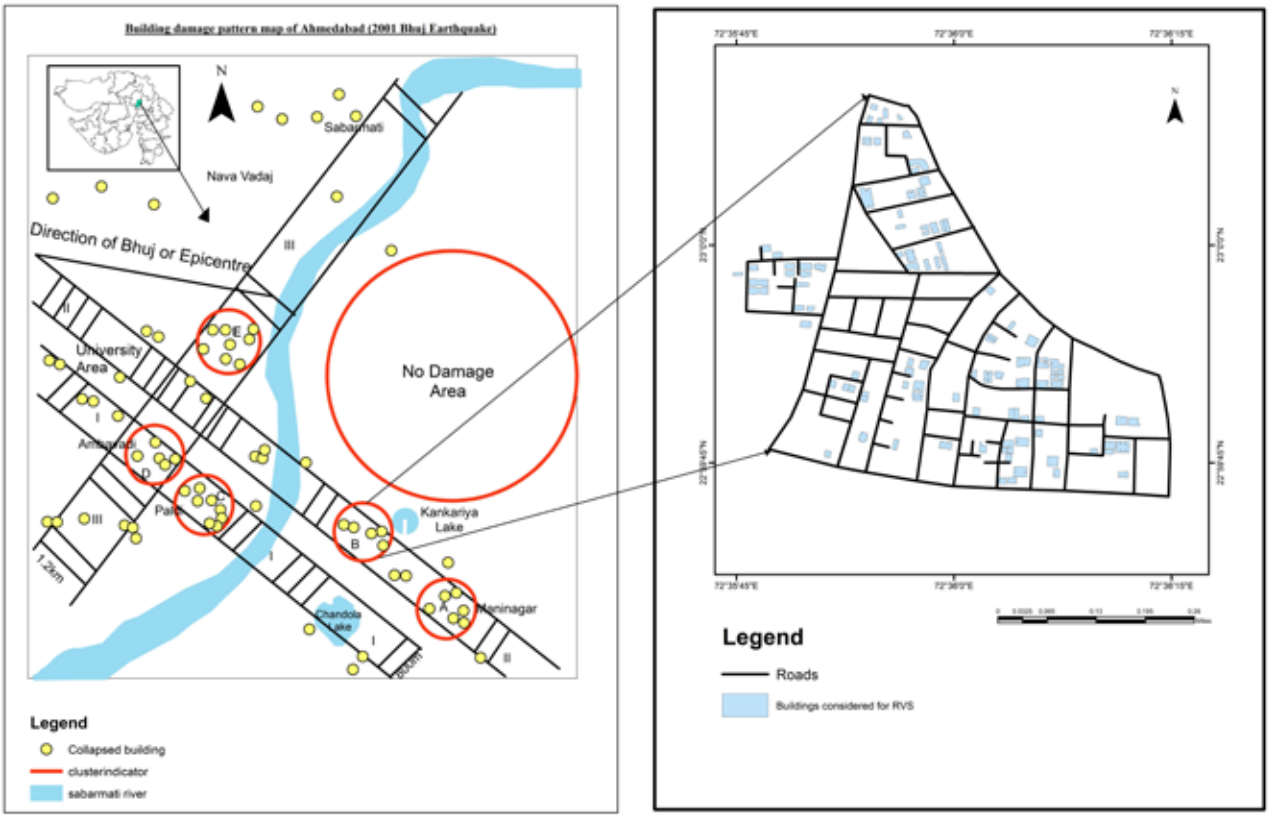

Figure 1. Location of Study area.

STUDY AREA

Based on the effects of 2001 Bhuj earthquake on the different types of buildings in Ahmedabad city, Jain et al., (2002) reported that 2 out of approximately 1500 RC frame buildings (of around 10 stories) and ~130 buildings out of approximately 25000 RC frame buildings (5 stories) had collapsed in Ahmedabad. Figure 1 shows the building collapse pattern map of Ahmedabad city during the 2001 Bhuj earthquake (Bhandari and Sharma, 2001). In their map, a group of collapsed buildings in close proximity has been encircled indicating areas of heavy damage in the city. Previous studies (Ghosh, 2001 and Mathur et al., 2005) have indicated that the area surrounding Kankariya Lake has shown the presence of soft soil condition, which may have contributed to the building damages in the area as observed in cluster "B" near Kankariya Lake (Figure 1). From available literature and with the help of local residents, 18 buildings that collapsed in the South zone of Ahmedabad during the 2001 Bhuj earthquake, were located on the ground. A cluster of six buildings was found in Rambaug area of Maninagar, which nearly aligns with cluster B shown in Figure 1a. Hence, the buildings in the Rambaug area has been considered for the RVS.

Determination of soil type is a major factor in the data collection form. The soil type for the study area is determined based on Mathur et al., (2005) that the area falls in zone D, which is the most hazardous zone having the Standard penetration N-value less than 10 and had suffered maximum damage during 2001 Bhuj earthquake. Hence based on the standard penetration N-value soil type 3 was considered as per IS 1893 Part I, (2016).

METHODOLOGY

Randomly selected 100 RC frame buildings of Rambaug area are considered for this study because similar RC frame buildings had collapsed and suffered heavy damage in the 2001 Bhuj earthquake. RVS on all selected 100 buildings has been carried out based on the form proposed by Srikanth et al., (2010). The RVS form Performa is shown in Figure 2. Information about the building identity such as the building type, address, use, number of stories and if required photographs are gathered during the walk down survey for RVS.

The base score is evaluated based on the number of stories and seismic zone. The vulnerability score is evaluated based on the presence of vulnerability parameters

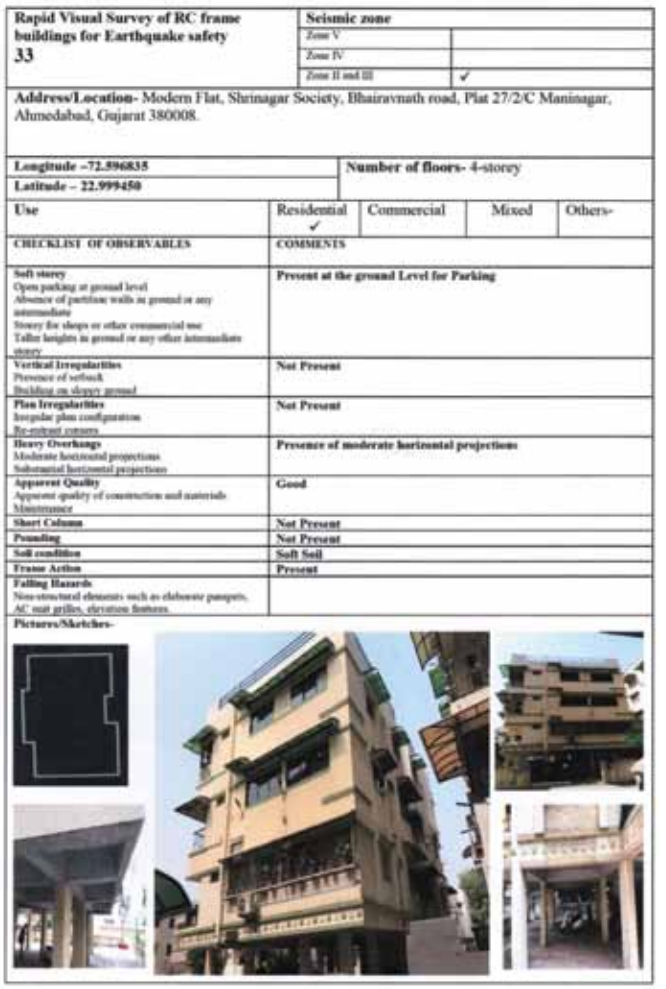

Rapid Visual Survey of RC frame buildings for Earthquake safety 33	Seismic zone	
	Zone V	
	Zone IV	
	Zone II and III	✓

Address/Location- Modern Flat, Shrinagar Society, Bhairavnath road, Plat 27/2/C Maninagar, Ahmedabad, Gujarat 380008.

Longitude –72.596835	**Number of floors-** 4-storey
Latitude – 22.999450	

Use	Residential ✓	Commercial	Mixed	Others-

CHECKLIST OF OBSERVABLES	COMMENTS
Soft storey Open parking at ground level Absence of partition walls at ground or any intermediate Storey for shops or other commercial use Taller heights in ground or any other intermediate storey	**Present at the ground Level for Parking**
Vertical Irregularities Presence of setback Building on sloppy ground	**Not Present**
Plan Irregularities Irregular plan configuration Re-entrant corners	**Not Present**
Heavy Overhangs Moderate horizontal projections Substantial horizontal projections	**Presence of moderate horizontal projections**
Apparent Quality Apparent quality of construction and materials Maintenance	**Good**
Short Column	**Not Present**
Pounding	**Not Present**
Soil condition	**Soft Soil**
Frame Action	**Present**
Falling Hazards Non-structural elements such as elaborate parapets, AC unit grilles, elevation features	

Pictures/Sketches-

(a)

RAPID VISUAL SCREENING OF EARTHQUAKE SAFETY — **CALCULATION SHEET RC FRAME**

Falling hazards identifier 'F'		Stories	Seismic Zone V	Seismic Zone IV	Seismic Zone II-III	Base Score
Marquees/headings roof signs		1 or 2	100	130	150	
AC units/grillwork	✓	3	90	120	140	
Elaborate parapets		4	75	100	120	120
Heavy elevation features		5	65	85	100	
Heavy canopies		>5	60	80	90	
Substantial balconies						
Heavy cladding						
Structural glazing						

Vulnerability Score (VS)						Vulnerability Score Modifier (VSM)	VS×VSM
NUMBER OF STOREYS	1or2	3	4	5	>5		
Soft storey	0	-15	-20	-25	-30	Absent =0 Present=1	-20
Vertical irregularities, setbacks, building on slopes	-10	-10	-10	-10	-10	Absent =0 Present=1	0
Plan irregularities	-5	-5	-5	-5	-5	None=0 Moderate=1 Extreme=2	0
Heavy overhangs	-5	-10	-10	-15	-15	Absent =0 Present=1	-10
Apparent quality	-5	-10	-10	-15	-15	Good=0 Moderate=1 Poor=2	0
Short columns	-2	-5	-5	-5	-5	Absent = 0 Present=1	0
Poundings	0	-2	-3	-3	-3	Absent = 0 Unaligned floors= 2 Poor apparent quality of adjacent building = 2	0
Soil conditions	10	10	10	10	10	Medium = 0 Hard =1 Soft = -1	-10
Frame action	10	10	10	10	10	Absent = 0 Present =1 Not sure = 0	10
Basement – Full or Partial	0	3	4	5	5	Absent = 0 Present =1	0
						∑ (VSMXVS) =	-30
						Performance Score = Base Score - ∑ (VSMXVS) =	90

(b)

Figure 2. RVS form for RC frame buildings.

in building like frame action, pounding effect, structural irregularity, short columns, apparent quality, basement and heavy overhang present in the building. The base score, vulnerability score, and the vulnerability score modifiers have been calculated in order to get the performance score for the building. The formula for the evaluation of performance score for the present vulnerability assessment is based on the methodology proposed by Srikanth et al. (2010).

$$PS = (BS) + \Sigma [(VSM) \times (VS)] \quad \ldots (1)$$

Where Vulnerability Score Modifier (VSM) is multiplied to Vulnerability Score (VS) to obtain the actual modifier, which is then added to the Base Score (BS) in order to obtain the Performance Score (PS) of the building.

The data analysis for obtained performance scores of the 100 buildings in the region from RVS is done using a Gaussian (Normal) distribution method (Srikanth et al., 2010). This method is used for the statistical analysis of data sets. A normal distribution in a variate X with mean μ and variance σ^2 is a statistic distribution with probability density function is given as:

$$f(x) = \frac{1}{\sigma\sqrt{2\pi}} e^{-\frac{(x-\mu)}{2\sigma^2}} \quad \ldots (2)$$

Generally, a cumulative probability refers to the probability that the value of a random variable falls within a specified range. Frequently, cumulative probabilities refer to the probability that a random variable is less than or equal to a specified value. The cumulative Distribution function, which gives the probability that a variate will assume a value $\leq x$, is then

$$f(x) = \int_{-\infty}^{x} P(x)dx = \frac{1}{\sigma\sqrt{2\pi}} \int_{-\infty}^{x} e^{-\frac{(x-\mu)}{2\sigma^2}} dx \quad \ldots (3)$$

From this statistical analysis, the obtained performance scores of the buildings are distributed approximately normal. It helps to represent the probability that the obtained performance score is less than or equal to the

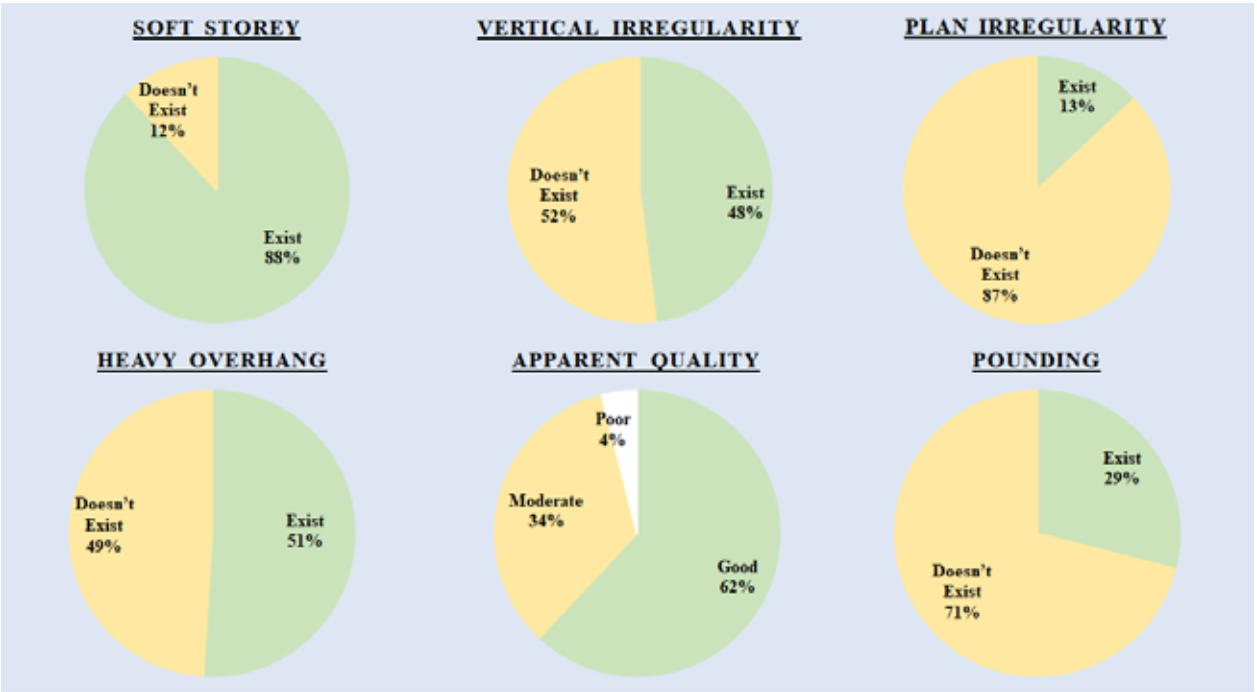

Figure 3. Distribution of various vulnerability parameters present in surveyed buildings.

specified value under the curve and to decide the cut-off range for the low, medium and high scores. Based on the obtained scores and its distribution, buildings were selected for further detailed evaluation.

RESULT AND DISCUSSION

The Performance score of the building depends on the base score and the vulnerability score. The Base score in the RVS form for a building depends on the seismic zone where it lies in, and the number of storeys. For 100 surveyed buildings, the number of storeys ranges from 2 to 6, which consists of 67 buildings having 5 storeys. 89 buildings out of 100 were the residential type. Figure 3 shows the distribution of the vulnerability parameters observed in buildings during the survey.

From RVS, it was observed that soft storey was present in 88 buildings, which are a significant number considering the fact that Murty et al., (2002) have reported the presence of this factor was also found in almost all of collapsed RC frame buildings of Ahmedabad during 2001 Bhuj earthquake. Figure 4 shows the presence of open ground storey which was observed in one of the flat/apartment type residential building to facilitate the vehicle parking. A surveyed building is shown in Figure 5 of G+4 storey has half of the ground storey left open which is used for the vehicle parking and another half of the ground storey used for the residence. Thus making the building partially open/soft storey. As also seen in Figure 5 the floor level of the left and the right portion of the building are not in the same level, therefore, several irregularities can be observed both along the height as well as in the plan.

It is also reported (Murty et al., 2002) that the buildings with the poor quality of construction, horizontal irregularities (e.g., those with re-entrant corners such as L-shape plans) and those with vertical irregularities (e.g., vertical setbacks in structures), were common in the affected area. 48 surveyed buildings had vertical irregularities in the form of vertical setbacks. Figure 6(a) shows the presence of setback observed in the building at the time of the survey (approximate measurements taken using the google earth). Plan irregularities observed in the surveyed buildings in the form of the re-entrant corners. The pounding effect found to be existing in the 29-screened buildings. Figure 6(b) shows the location of pounding seen in a building, where the roof of the shorter building may pound at the mid-height of the columns in the taller building, which might be dangerous and can lead to storey collapse. Overhang found to exist in 51 buildings. Figure 6(c) shows the presence of overhang. Its presence will not lead to the collapse of the buildings but it might contribute to the building damage. Buildings also observed with the issue of poor quality of construction and maintenance, which may require moderate repairs. Figure 6(d) shows the building with poor construction quality. Presence of these vulnerability parameters can affect the performance of the buildings in an event of an earthquake if not properly designed for. Some surveyed buildings had suffered heavy damages in the 2001 earthquake. The carried out retrofitting works such as jacketing of column

Figure 4. Soft storey

Figure 5. Partial soft storey

and beam, wall thickening and adding of infill walls (RC/ Brick filling) were observed in the survey. Figure 6(e) shows the retrofitting work column jacketing observed in a screened building.

Based on the performance scores and Gaussian Normal distribution, a conclusion can be drawn that higher the performance score lesser the vulnerability of the building to earthquake when compared to buildings having the low-performance score. Figure 7 shows the Gaussian distribution of the obtained scores for the surveyed buildings. The performance scores for the surveyed RC frame buildings in the study area are predominantly ranging from 20 to 125. The buildings in the middle range (43-84) of performance score are large in number. However, there are some low-performance score buildings, which are potentially vulnerable to future earthquakes. The total number of buildings surveyed are 100 with mean and the standard deviation scores as 63.41 and 61.5 respectively. Hence, these scores are helpful in selecting buildings with a higher vulnerability for detailed evaluation. Building Vulnerability map is shown in Figure 8, it represents the building state based on the obtained RVS scores and applied statistical method. Here the building damage states like no damage, slight damage, moderate damage, severe damage, and collapse state are classified based on the μ-3σ, μ-2σ, μ-σ, μ, μ+σ, μ+2σ, and μ+3σ.

Figure 6. ((a) Vertical setback, (b) Possible location of occurrence of Pounding, (c) Overhang in form of jutting out balconies, (d) Poor quality of construction (e) Retrofitting through Column jacketing and steel I beam).

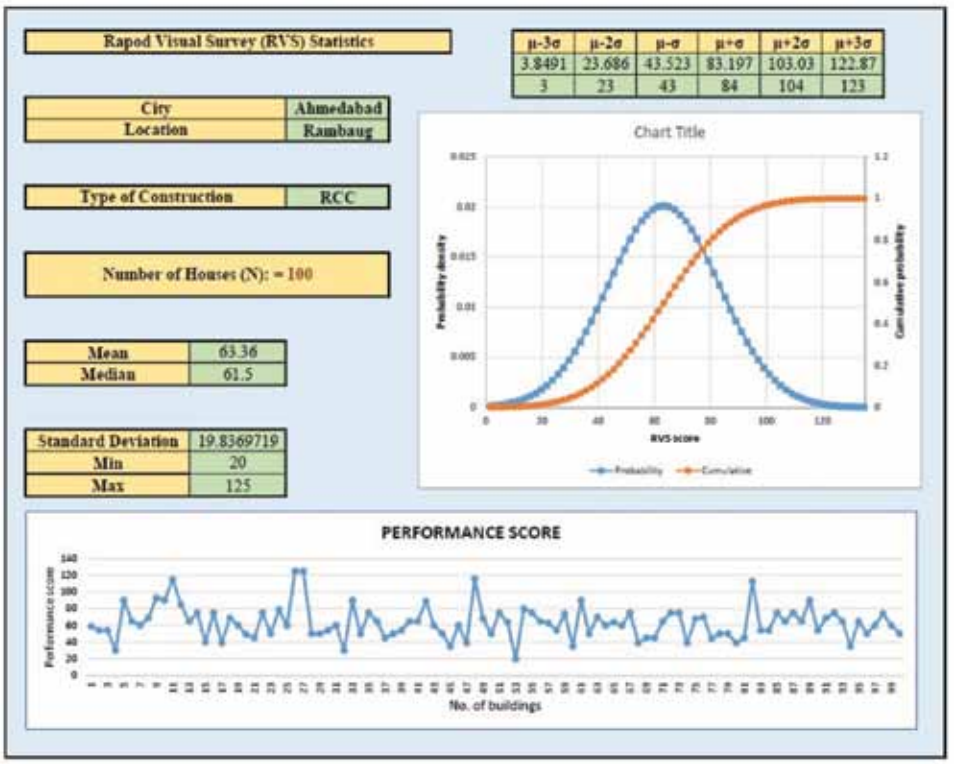

Figure 7. Gaussian distribution for surveyed buildings.

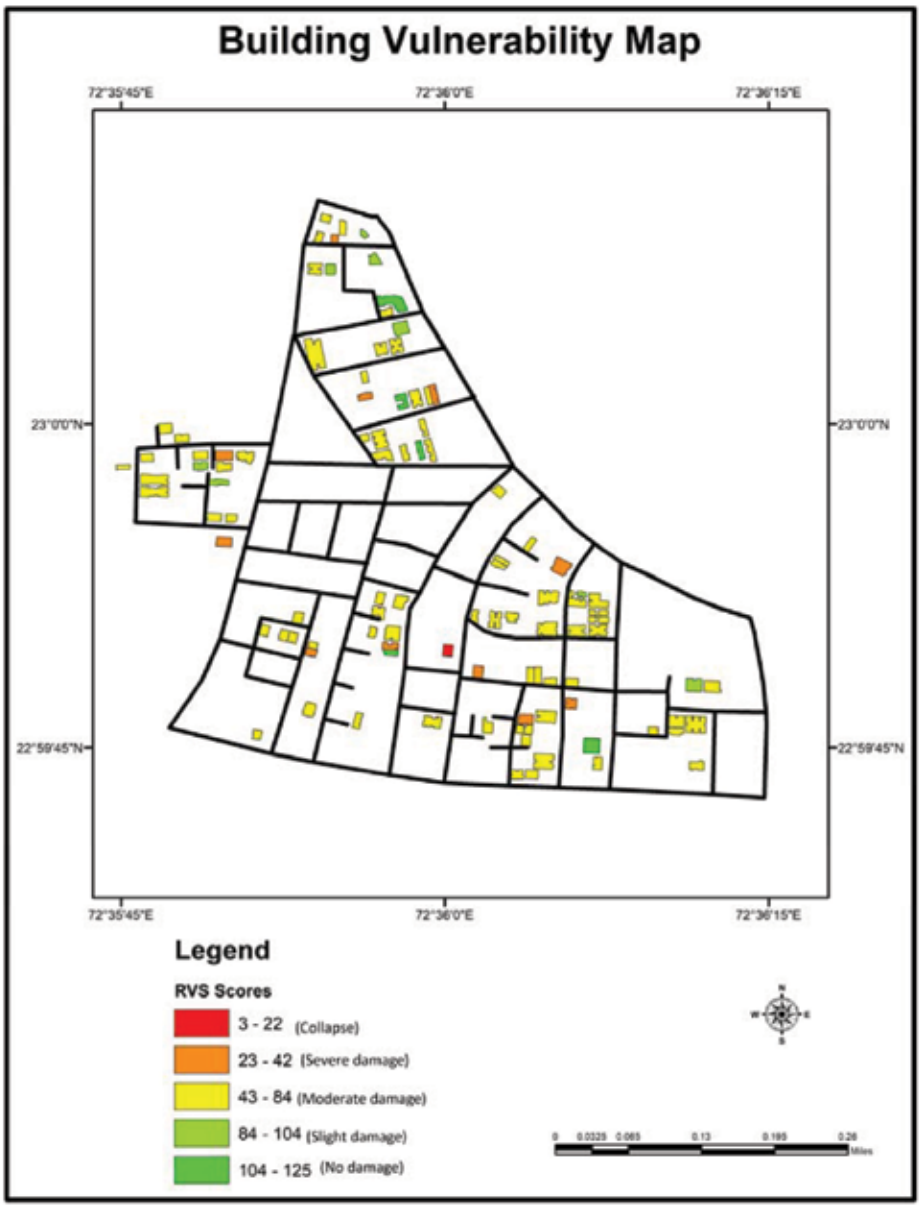

Figure 8. Building Vulnerability map

CONCLUSION

This study focuses on using RVS process in the Rambaug area of Ahmedabad where significant damage occurred during the 2001 Bhuj Earthquake. Total 100 RC frame type buildings were surveyed. The parameters considered for calculating RVS score are soft storey, vertical irregularity, plan irregularity, pounding, overhang, apparent quality, soil condition and short column. The collected data is analyzed, and each building is given a performance score based on its structural conditions. The area has soft soil conditions, which can have catastrophic effects on vulnerable buildings in this area. The past earthquakes have revealed that the presence of the soft storey, heavy overhang, vertical irregularity, re-entrant corner and pounding effect in the buildings led to collapse/substantial damage. The result indicated that soft storey (88%), heavy overhang (51%), vertical irregularity (48%) and pounding effect (29%) were mostly observed which is alarming. The 38 surveyed buildings were observed with the moderate apparent quality in terms of maintenance as some of the buildings are approximately more than 16-18 years old. The presence of considered vulnerability parameters warrants a detailed evaluation of the selected building to quantify the vulnerability level for the study area. It is observed that the RVS scores range from 20 to 125. For the estimation

of building state/condition, a statistical method using the RVS score is used. Most buildings lie in the middle score range (43-84); however, there are also low RVS score buildings ranging from 3 to 23, which are vulnerable to future earthquake. The buildings with score less than or equal to 63 need to be analyzed in detail.

This type of work will help in distinguishing seismically vulnerable buildings for developing disaster mitigation programs. It can also help in predicting or estimating the damage that can happen due to an earthquake. Lives can be saved if we can predict the damage better by taking precautionary measures well in advance.

ACKNOWLEDGMENT

Authors are thankful to Director General and Director, Institute of Seismological Research for their permission to publish this research work.

Compliance with Ethical Standards

The authors declare that they have no conflict of interest and adhere to copyright norms.

REFERENCES

Arya, A.S., 2000. Rapid visual screening of RCC Buildings. Disaster Risk Management–Document Series.

Bhandari, N. and Sharma, B.K., 2001. Damage pattern due to January, 2001 Bhuj earthquake, India: Importance of site amplification and interference of shear waves, in: 2001 International Conference on Seismic Hazard with particular reference to Bhuj Earthquake, 26, 19-21.

Chanu, N.M. and Nanda, R.P., 2018. A Proposed Rapid Visual Screening Procedure for Developing Countries. Int. J. Geotech. Earthq. Eng., 9, 38–45. https://doi.org/10.4018/IJGEE.2018070103

Dutta, S.C., Nayak, S., Acharjee, G., Panda, S.K. and Das, P.K., 2016. Gorkha (Nepal) earthquake of April 25, 2015: Actual damage, retrofitting measures and prediction by RVS for a few typical structures. Soil Dyn. Earthq. Eng., 89, 171–184. https://doi.org/10.1016/j.soildyn.2016.08.010

FEMA, 2002. Rapid Visual Screening of Buildings for Potential Seismic Hazards: A Handbook, Edition 2. Federal Emergency Management Agency Report, FEMA. P.154.

FEMA, 2015. Rapid Visual Screening of Buildings for Potential Seismic Hazards: A Handbook, Third Edition. Federal Emergency Management Agency Report, FEMA. P.154.

Ghosh, S.K., 2001. Observations from the Bhuj earthquake of January 26, Pci Journal 46(2), 34-42.

IS 1893 Part I, 2016. Indian Standard Criteria for Earthquake Resistant Design of Structures (6th Rev.), Bureau of Indian Standards, New Delhi, India.

Jain, S.K., Murty, C., Jaiswal, A., Shah, D., Mehta, V.V., Shah, R. and Desai, N.S., 2002. Postearthquake handling of buildings. Earthq. Spectra 18, 297–317. https://doi.org/10.1193/1.2803917.

JBDPA, 2001. Seismic evaluation and retrofit. The Japan Building Disaster Prevention Association, Tokyo.

Jain, S.K., Mitra, K., Kumar, M. and Shah, M., 2010. A proposed rapid visual screening procedure for seismic evaluation of RC-frame buildings in India. Earthq. Spectra, 26, 709-729. https://doi.org/10.1193/1.3456711

Kumar, S.A., Rajaram, C., Mishra, S., Kumar, R.P. and Karnath, A., 2017. Rapid visual screening of different housing typologies in Himachal Pradesh, India. Nat. Hazards, 85, 1851–1875. https://doi.org/10.1007/s11069-016-2668-3

Mathur, A.K., Saxena, A.K., Surendra Prasad, Fulzele, D.N., Singh V.N. and Regar, R.L., 2005. Seismic hazard and risk microzonation of Ahmedabad City, Gujarat. Report No. NSEL-008 Geological Survey of India (GSI), 75.

Mishra, P.K., 2012. The Kutch earthquake, 2001: recollections, lessons, and insights, National Institute of Disaster Management, New Delhi.

Murty, C., Goel, R.K., Goyal, A., Jain, S.K., Sinha, R., Rai, D.C., Arlekar, J.N. and Metzger, R., 2002. Reinforced concrete structures. Earthq. Spectra, 18, 149–185. https://doi.org/10.1193/1.2803911

Nanda, R. and Majhi, D., 2013. Review on Rapid Seismic Vulnerability Assessment for Bulk of Buildings. J. Inst. Eng. India Ser. A, 94, 187–197. https://doi.org/10.1007/s40030-013-0048-5

NRCC, 1993. Manual for screening of buildings for seismic investigation. Institute for Research in Construction, National Research Council Canada. Ottawa, Canada.

NZSEE, 2006. Assessment and improvement of the structural performance of buildings in earthquakes, New Zealand Society for Earthquake Engineering (NZSEE), Wellington, New Zealand.

Srikanth, T., Kumar, R.P., Singh, A.P., Rastogi, B.K. and Kumar, S., 2010. Earthquake vulnerability assessment of existing buildings in Gandhidham and Adipur Cities, Kachchh, Gujarat (India). Eur. J. Sci. Res., 41, 336–353.

Sucuoglu, H. and Yazgan, U., 2003. Simple survey procedures for seismic risk assessment in urban building stocks, in: Seismic assessment and rehabilitation of existing buildings. Springer, 97–118. https://doi.org/10.1007/978-94-010-0021-5_7

Sucuoglu, H., Yazgan, U. and Yakut, A., 2007. A screening procedure for seismic risk assessment in urban building stocks. Earthq. Spectra, 23, 441–458. https://doi.org/10.1193/1.2720931

Received on: 17.10.18; Revised on: 16.1.19; Accepted on: 22.1.19

J. Ind. Geophys. Union (March 2019)
v.23, no.2, pp: 152-163

Onset of southwest monsoon- A study of the precursors in South Indian Ocean

Onkari Prasad[1]*, K. Prasad[2] and O. P. Singh[3]

[1]43, Ritu Apartments, A-4 Paschim Vihar, New Delhi-110063
[2]D-104, Seema Apartments, Sector 11, Dwarka, New Delhi-110085
[3]B44, First Floor, Parshvnath Paradise, Mohan Nagar, Ghaziabad (U.P.)-201007
*Corresponding author: prasadonkari123@yahoo.in

ABSTRACT
Satellite observed cloud data from the Indian Ocean region are now available for more than 50 years. An analysis of the cloud data for a period of 16 years (1972-1989 except 1978 and 1981), had shown that precursors to monsoon develop as different features in the activity of South Indian Ocean Convergence Zone (SIOCZ) (Eq.-20ºS and 40-100ºE). This had formed the basis for proposing SIOCZ model of long range forecast of rainfall over India, during the southwest monsoon period. Cloud data from 1990 onwards were used for preparing forecast on the real time basis and to further improve the model. The model has since produced reasonably good forecast of monsoon rainfall for India as a whole and also for individual meteorological subdivisions (numbering 36) for a period of 29 years (1990-2018), and in the districts of Tamilnadu for 14 years (2005-18), Himachal Pradesh for 11 years (2008-18), Andhra Pradesh and Telanagana for 4 years (2015-18) and Maharashtra and Goa for 3 years (2016-18). This has confirmed close relationship between the precursors as identified in cloud data, and the activity of southwest monsoon over India. In some of the years, the precursor did change during the season. Change in the rainfall scenario, resulting due to the change in the precursor, is included in the forecast update/updates. The relationship between precursors and onset of monsoon over Kerala has been further studied using satellite observed cloud data for a period of 50 years (1969-2018). It has been shown that (i) onset of monsoon over Kerala is related to the development of precursor, as a feature in the activity of SIOCZ, (ii) there is no one to one relationship between the date of onset and the performance of monsoon, and (iii) a close relationship between the precursors and the activity of monsoon during the season, has resulted in providing a reliable information on the performance of monsoon.

Key words: Southwest monsoon, Satellite observed cloud data, South Indian Ocean Convergence Zone, Rainfall.

INTRODUCTION

Southwest Monsoon (SWM) sets in over south Andaman Sea, Andaman and Nicobar Islands and parts of southeast Bay of Bengal by 20th May. It takes another 10 days for SWM to arrive over Kerala. The term onset generally refers to the first arrival of monsoon over Kerala and the term 'monsoon has advanced' is used to indicate its arrival over other regions of India. Utilizing daily mean rainfall from dense rain gauge networks in Kerala, for the period 1901-1980, Ananthakrishnan and Soman (1988) had shown that the mean onset date for south Kerala is 30th May and it is 1st June for north Kerala. Kerala extends from lat. 8º 15′ N to lat. 12º 50′ N. The dividing line between north and south Kerala is around Lat. 10º N.

Joseph et al. (1994) have given a critical review of the literature on the onset of monsoon over Kerala. Joseph et al. (2003) have also discussed the conditions leading to onset of monsoon over Kerala and the associated Monsoon Hadley Cell. The date of onset of monsoon over Kerala is determined by India Meteorological Department (IMD). Determining the date of onset is based on rainfall, wind field and Outgoing Longwave Radiation (OLR) data. If after 10th May, 60% of the 14 stations, viz., Minicoy, Amini, Thiruvananthapuram, Punalur, Kollam, Allapuza, Kottayam, Kochi, Thrissur, Kozhikode, Thalassery, Kannur, Kudulu and Mangluru report rainfall of 2.5 mm or more for two consecutive days, the onset over Kerala is declared on the 2nd day, provided that (i) the depth of the westerlies are maintained up to 600 hPa level in the box, between equator & 10ºN and long. 55-80ºE and the zonal wind speed over the area bounded by lat. 5-10ºN and long. 70-80ºE are of the order 15-20 Kts at 925 hPa level. The source of wind data can be, analyzed wind/satellite derived wind from the Regional Specialized Meteorological Centre (RSMC) New Delhi, and (ii) INSAT derived OLR value which should be below 200 watts/square meter in the box bounded by lat. 5-10ºN and long.70-75ºE. Prior to the availability of winds/cloud motion vectors and OLR data, determining the date of onset was based on the rainfall data alone and the stations chosen for the purpose were, Colombo (Sri Lanka), Minicoy, Trivendrum (now Thiruvananthapuram), Alleppey, Cochin, Kozhikode and Mangalore (now Mangaluru) (Ananthakrishnan, et al., 1967). The normal date of

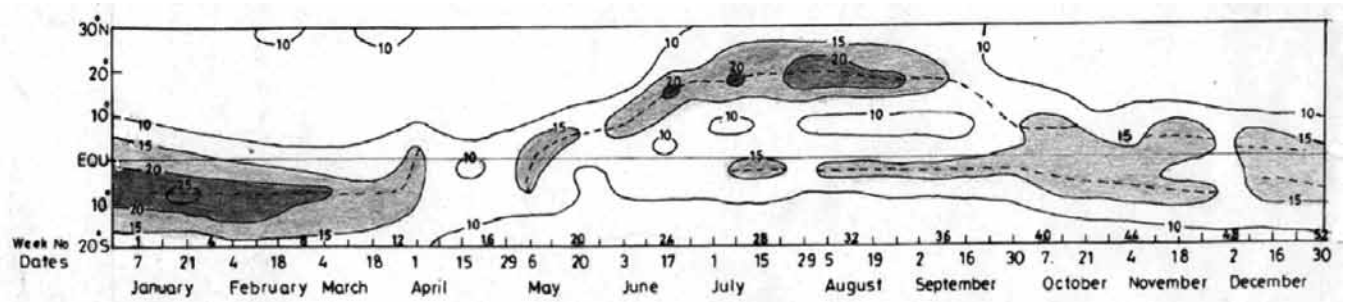

Figure 1. Long period zonal weekly mean cloudiness over the region bounded by Lat. 20°S-30°N and Long. 40-100°E. The contours have been drawn for 10%, 15%, 20% and 25% area covered by cloudiness. Areas covered by 15% cloudiness and more have been shaded. [Period: (i) January-May 1972-2012. There were some missing data in 1972, 1978 and 1979, (ii) June-December 1983-2005]

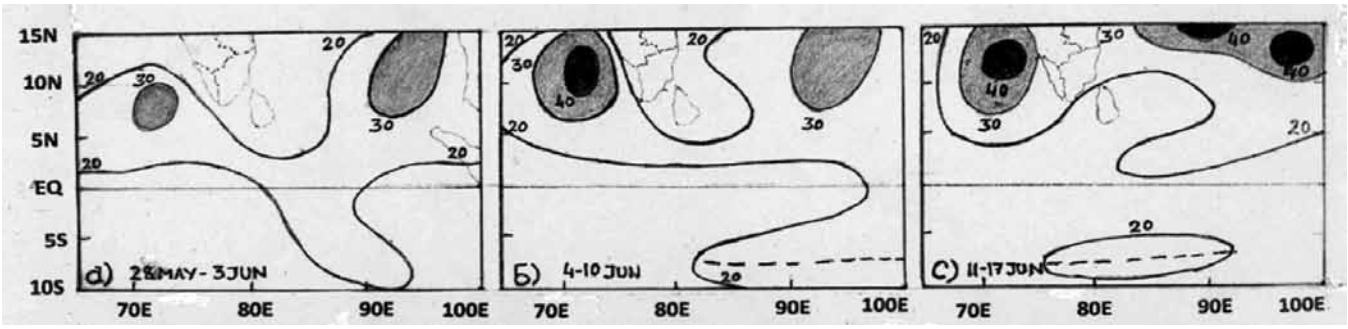

Figure 2. Long period weekly mean cloudiness during the weeks ending on 3rd, 10th and 17th June. Contours have been drawn at 20%, 30%, 40%, and 60%. Areas covered by 30% cloudiness and more have been shaded. [Period: Figure 2(a):1973-2012. Data for 1978 were missing. Figure 2(b) and 2(c): 1983-2005]

onset of monsoon over Kerala is 1st June and the Standard Deviation (S.D.) in the date of onset over Kerala is 8 days. In this study, we have used data on the dates of onset of monsoon over Kerala as determined by IMD.

Cross Equatorial Flow

Establishment of Cross Equatorial Flow (CEF) in north Indian Seas (Arabian Sea and the Bay of Bengal), is the single most important factor in onset and advance of monsoon. Both, development of deep layer westerlies and low values of OLR, are associated with the development of CEF in east Arabian Sea. Year to year variation in the date of onset is, therefore, related to variation in development of CEF. Existence of an east-west oriented Maximum Cloud Zone (MCZ) in satellite observed cloudiness in the near equatorial regions of oceans, is a visible manifestation of the existence of Inter-Tropical Convergence Zone (ITCZ). The term South Indian Ocean Convergence Zone (SIOCZ) refers to Indian Ocean (IO) part of ITCZ. SIOCZ generally develops between Long. 40-100°E and between equator and 5°S during monsoon months. In an extreme case, it could move southward up to 15°S. Its location and intensity is closely related with the activity of SWM over India. Figure 1, prepared using long period cloud data from the region bounded by Lat. 20°S-30°N and Long. 40-100°E, shows the location and northward propagation of MCZs developing in SIOCZ. An E-W oriented MCZ in the zone of SIOCZ could be seen in South Indian Ocean (SIO) during the period January-March only. There is a reduction in convection during April and, in general, northward movement of the MCZ begins in May. However, there are year- to-year variations in it. Figure 2 shows the development and movement of MCZ over the region bounded by Lat. 10°S-15°N and Long. 65-100°E in the weekly mean cloud data. Two well known features associated with the onset of monsoon, i.e., development of convection and formation of an 'Onset vortex' at the leading edge of the monsoon current in east Arabian Sea, are also seen in cloud data. Development of an 'Onset vortex' is seen as a circular cloud mass in east Arabian Sea. One of the aims of the present study is to examine the relationship between the features developing in the activity of SIOCZ during pre-monsoon months and the date of onset of southwest monsoon over Kerala.

Long range forecasting

Long range forecasting of monsoon rainfall has remained an important aspect of weather forecasting in India because of the challenges in foreshadowing extreme seasons (excess/drought) and preparing forecast for individual

subdivisions (numbering 36) and their clusters of districts/ districts. SIOCZ model (Gupta and Prasad, 1992, 1993; Onkari Prasad, 1993; Onkari Prasad et al., 2010b; Onkari Prasad and Singh, 2012; Onkari Prasad et. al., 2014) had been providing subdivision-wise long range forecast of SWM rainfall since 1990. District level Long Range Forecast (LRF) of seasonal rainfall are being provided for Tamilnadu for the past 14 years (2005-18) (Onkari Prasad, et al.,2010a), Himachal Pradesh for the past 11 years (2008-18), Andhra Pradesh and Telangana for the past 5 years (2014-18), Maharashtra and Goa for the past 3 years (2016-18) (Onkari Prasad, et al.,2016). This model has several advantages over other models: (i) the model is simple and requires only one data, i.e., satellite observed cloud/OLR from IO region, (ii) it is robust as it has produced reasonably good forecast for the past 29 years, (iii) this model alone could foreshadow the droughts in 2002, 2004 and 2009 and severe rainfall deficiency during June-July of 1992 and 2012, (iv) forecasts from the model were reasonably good for India as a whole, as well as in meteorological subdivisions and the districts of the six states as mentioned above. Recognition of the precursors, in the activity of SIOCZ, is the main feature of the model. Further, the identification of the precursors in cloud field had been reasonably good in each year during the past 50 year period (1969-2018).

DATA AND ANALYTICAL METHOD

Date of onset of SWM for a period of 50 years (1969-2018) (Table 1) and the estimates of satellite observed cloud data for the same period, are used in the present study. Visible cloud imagery from NOAA series of polar orbiting satellites for the period 1972-1983 and INSAT/METEOSAT- Indian Ocean Data Collection (METEOSAT- IODC) satellites for the remaining period had been used to obtain daily estimate of clouds (0%, 10%, 20%,.., 80%, 100%) in each 5° lat. x 5° long. boxes over the region bounded by Lat. 20°S-30°N and Long. 40-100°E. Using daily data, Weekly Mean Cloudiness (WMC) in each box has been worked out. Zonal Weekly Mean Cloudiness (ZWMC) has been prepared for each 5° lat. belt between 20°S and 30°N over the region bounded by Long. 40-100°E. WMC and ZWMC data for the period January-May 1973-2012 and June-December 1983-2005 have been used to obtain their long period mean. It may be mentioned here that digital cloud imagery data are not available regularly from any satellite, polar orbiting or geostationary. The cloud data for the period 1972-89 had been used for developing SIOCZ model for LRF of monsoon rainfall (Gupta and Onkari Prasad, 1992, 1993; Onkari Prasad,1993). Data for the period 1990-2018 have been used for issuing real time forecast and further improvement in the model (Onkari Prasad, et al., 2010b, Onkari Prasad and Singh, 2012, Onkari Prasad, et al., 2014). The information on the precursors, developing in the activity of SIOCZ, as identified in cloud data, are now available for a period of 47 years (1972-2018). Spectral analysis of daily digital cloud data from NOAA series of polar orbiting satellites for the years 1966-73 by Yasunari (1980) had shown a dominant mode of 30 to 40 days, a feature related to development of a normal SWM, in all the other years, except 1972 when the dominant periodicity was 60 days. Yasunari (1980) also composed the time-latitude cross sections of band-pass filtered cloudiness over the longitudinal sector of 70-90°E for the years 1966-73. A northward propagation of cloudiness was seen in all the years. It has been indirectly inferred that a precursor for development of a normal monsoon was present in the cloud data for the pre-monsoon months in the years 1969-71. The precursors identified for development of Excess (E)/Active(A)/Normal(N)/Weak(W)/Deficient(D) monsoon (Table 1) form another set of data used in the study.

It follows from Table 1 that onset had taken place either around the normal date or within 1 S.D. in the date of onset in 43 (86%) years. Onset was early in 5(10%) years and delayed in 2(4%) years only. Development and northward movement of MCZs and precursors identified in the activity of SIOCZ during E/A/N/W/D monsoon during the period of study are discussed below.

Early onset of SWM

Early onset of SWM in 1972

1972 was a severe drought year and ISMR was 26% below normal. The % departure of weekly rainfall over Kerala during the weeks ending on 3rd, 10th and 17th May 1972 was -11%, 100% and 559% respectively. Temporary onset of monsoon had been indicated over Kerala on 13th May. The % departure of rainfall over Kerala during the weeks ending on 14th, 21st and 28th June was -96%, -64% and 2% respectively. A regular onset had been declared on 18th June. The increase in rainfall was more marked during the first spell, as compared to the second. We have, therefore, included 1972 in the years of early onset.

Figure 3 shows time-latitude cross section of ZWMC during the period 1st April- 30th June 1972. The main feature was the appearance of a 7 week period between the development of two active spells of SIOCZ- a feature recognized as a precursor to development of a severe all India drought in the new approach to long range forecasting of monsoon rainfall in India based on SIOCZ model (Gupta and Onkari Prasad, 1992; Onkari Prasad and Singh, 2012). A MCZ had developed during the week beginning on 14th April in the 5° lat. belt of 10-15° S. It had moved northward up to 20°N by the week ending on 19th May. The next MCZ in the zone of SIOCZ developed during the week ending on 16th June. It moved up to 15°N during the week ending on

Table 1. Year, date of onset of SWM, precursor to development of an Excess(E)/Active(A) /Normal(N)/Weak(W)/Deficient(D) monsoon and % departure of Indian Summer Monsoon Rainfall (ISMR) from its long period average (100%) during the period 1969-2018

Year	Date of onset	Pre-cursor	% departure of ISMR	Year	Date of onset	Pre-cursor	% departure of ISMR	Year	Date of onset	Pre-cursor	% departure of ISMR
1969	16May	N	1	1986	4June	D	-13	2003	8June	A	5
1970	24May	N	12	1987	2June	D	-18	2004	18May	D	-14
1971	31May	N	4	1988	26May	E	18	2005	5June	D	-1
1972	13May	D	-26	1989	3June	N	1	2006	26May	N	0
1973	19May	N	6	1990	19May	A	6	2007	28May	N	5
1974	25May	D	-15	1991	2June	W	-9	2008	31May	N	-2
1975	31May	E	12	1992	5June	D	-8	2009	23May	D	-23
1976	30May	N	0	1993	28May	N	0	2010	31May	N	2
1977	30May	N	4	1994	28May	A	10	2011	29May	N	-5
1978	28May	A	7	1995	8June	N	0	2012	5June	D	-8
1979	11June	D	-21	1996	3June	N	3	2013	1June	A	6
1980	1June	N	0	1997	9June	N	2	2014	6June	D	-12
1981	31May	N	4	1998	2June	N	6	2015	5June	D	-15
1982	28May	D	-14	1999	25May	A	-4	2016	8June	D	-3
1983	12June	A	13	2000	1June	W	-8	2017	30May	W	-5
1984	31May	W	-4	2001	23May	W	-9	2018	28May	N@	-9
1985	28May	W	-8	2002	29May	D	-19				

Excess (E) : ISMR >10%, Active (A): 10 - 5%, Normal (N): 4 - -4%, Weak(W): -5 - -10%, Deficient (D): < -10%. @ Forecast was downgraded to 'W' monsoon on 11th July 2018. In 1972, an early onset on 13th May had been termed as temporary onset. Regular onset had been declared on 18th June.

23rd June. The period between the developments of these two MCZs was 7 weeks. As mentioned above, spectral analysis of daily digital cloud data of the years 1966-73 (Yasunari, 1980), had shown a dominant mode of about 60 days in 1972. Yasunari (1980) had also composed time-latitude cross sections of band-pass filtered cloudiness over the longitudinal sector of 70-90°E for the years 1966-73. A northward propagation of cloudiness, similar to other years, i.e., 1966-71 and 1973, was also seen in 1972, but the dominant periodicity was at about 60 days.

Figure 4 shows WMC during the weeks ending on 12th, 19th and 26th May 1972, associated with the development and movement of the MCZ in May. Similarly, Figure 5 shows WMC during the weeks ending on 16th, 23rd and 30th June 1972, associated with the development and movement of the MCZ in June. But for its early arrival over Kerala, development, northward movement and the northern limit to which the MCZ had reached during May was very similar to that of the MCZ which had developed in June. The difference was only in the reduction of cloudiness in the Arabian Sea and quick movement of cloudiness northward in the Bay of Bengal during the week ending on 26th May. An important observation has been that a period of 7-8 weeks between the developments of the two MCZs was a precursor to development of a severe drought in 1972.

Early onset of SWM in 1918

The earliest onset of SWM on record, was in the year 1918, when SWM had set in over Kerala on 11th May (Ananthakrishnan, et al., 1967). 1918 was also a severe drought year, like 1972. The rainfall for the country as a whole was 25% below normal and comparable to that in 1972 (26% below normal). Thus, there is a similarity between onset as well as the performance of monsoon in 1972 and 1918. As cloud data were not available for 1918, weekly rainfall of 3 southern most subdivisions of India, namely, Bay Islands, Madras (Tamilnadu), and Malabar (Kerala) during pre-monsoon months of 1918 (Figure 6), had been examined by Gupta and Onkari Prasad (1992), in a manner similar to that used by Joseph and Pillai (1988), for the occurrence of a period of 7-8 week in rainfall during the pre-monsoon months of 1918. A significant increase in the rainfall is seen during the week ending on 21st March over Malabar and in all the 3 subdivisions in the subsequent week. The second significant increase in the weekly rainfall over Malabar was recorded during the week ending on 9th May. The period between the two spells of increased rainfall comes out to be 7 weeks. The onset of monsoon over Malabar had been declared on 11th May. Similarly, after the onset, the subsequent significant increase in weekly rainfall occurred during the week ending on 4th July, i.e., after a

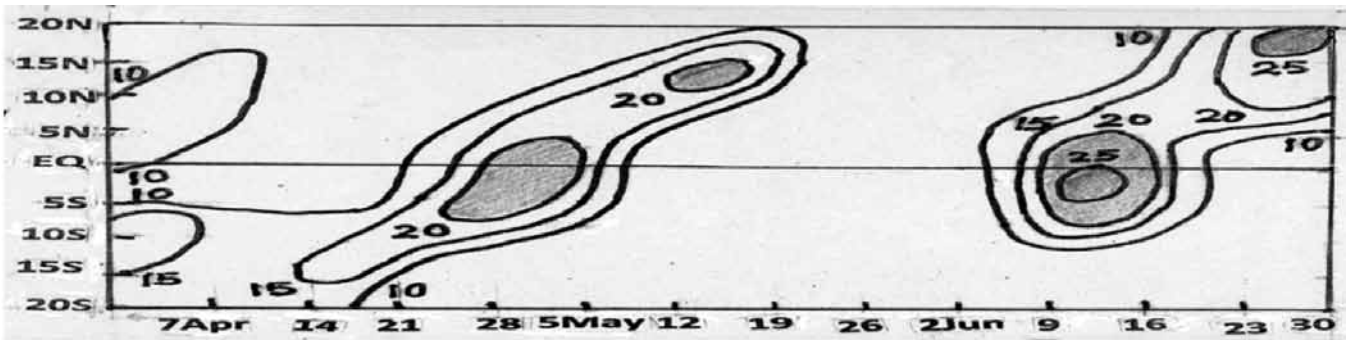

Figure 3. Time-latitude cross section of zonal weekly mean cloudiness from the week ending on 7th April - the week ending on 30th June 1972 over the region bounded by 20°S-20°N and 40°-100°E. Areas covered by the contours of 20% or more cloudiness have been shaded

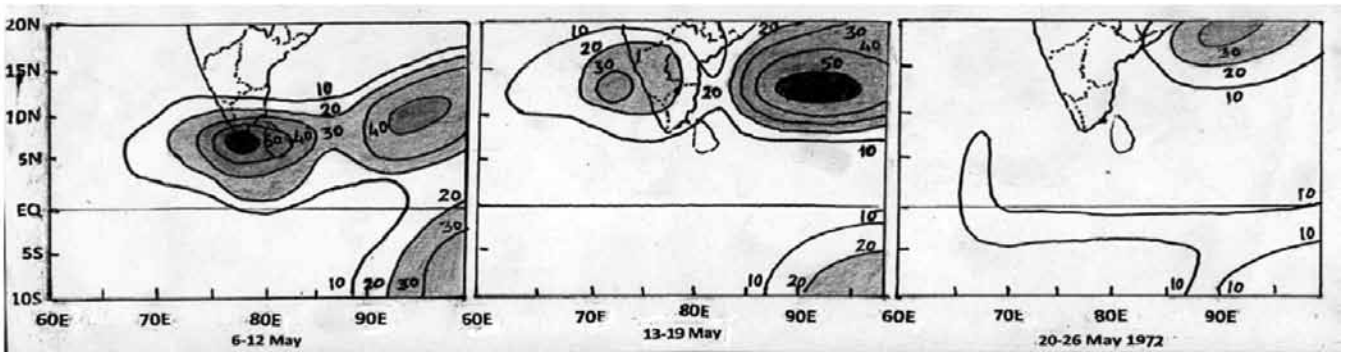

Figure 4. Weekly mean cloudiness during the weeks ending on 12th, 19th and 26th May 1972

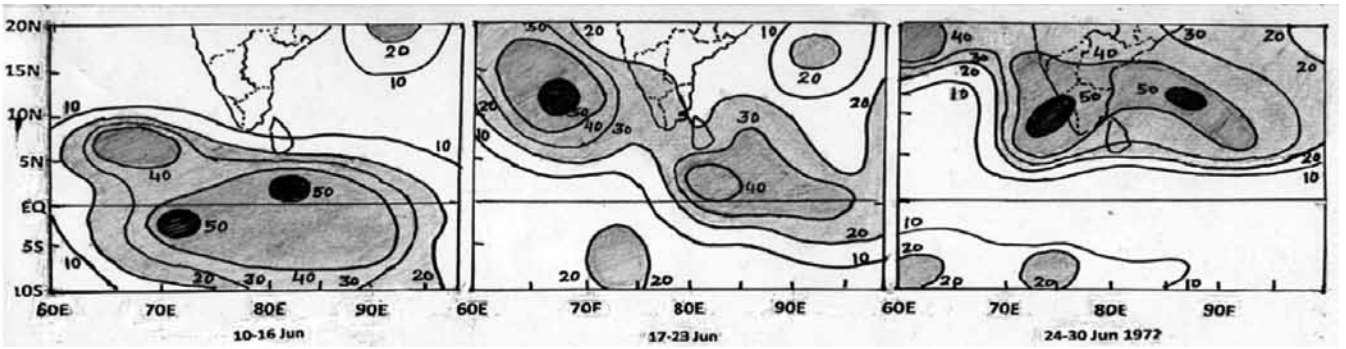

Figure 5. Same as Figure 4 but for the weeks ending on 16th, 23rd and 30th June 1972

period of 8 weeks. The fourth significant increase in rainfall over Malabar was recorded during the week ending on 22nd August. Here again the period between the rainfall peaks comes out to be 7 weeks. This confirms the occurrence of a period of 7-8 week in rainfall over Malabar during 1918 SWM. Appearance of a period of 7-8 weeks in the development of MCZs in 1972/rainfall peaks in 1918 was a precursor to development of a drought with deficiency of rainfall, of the order of 25% below normal.

Early onset of SWM in 1973

In 1973, the onset of SWM had taken place on 19th May, i.e., 12 days before the normal date. Rainfall, for India as a whole, was 6% above normal. The ZWMC for the period 4th March -27th May 1973, are shown in Figure 7 and WMC for the weeks ending on 12th, 19th and 26th May in Figure 8. Development of MCZs with a tendency to move northward was the characteristic feature in the cloud field during the period March-May 1973. The period between the MCZs, which had developed during April-May, was 4 weeks. Cloudiness extended from east Arabian Sea to the Bay of Bengal across Kerala and Tamilnadu during the week ending on 12th May. After onset, cloudiness did not move northward during the subsequent week. A period of 4 weeks in the development of MCZs in the zone of SIOCZ and their northward movement was a precursor to development of an active monsoon in 1973.

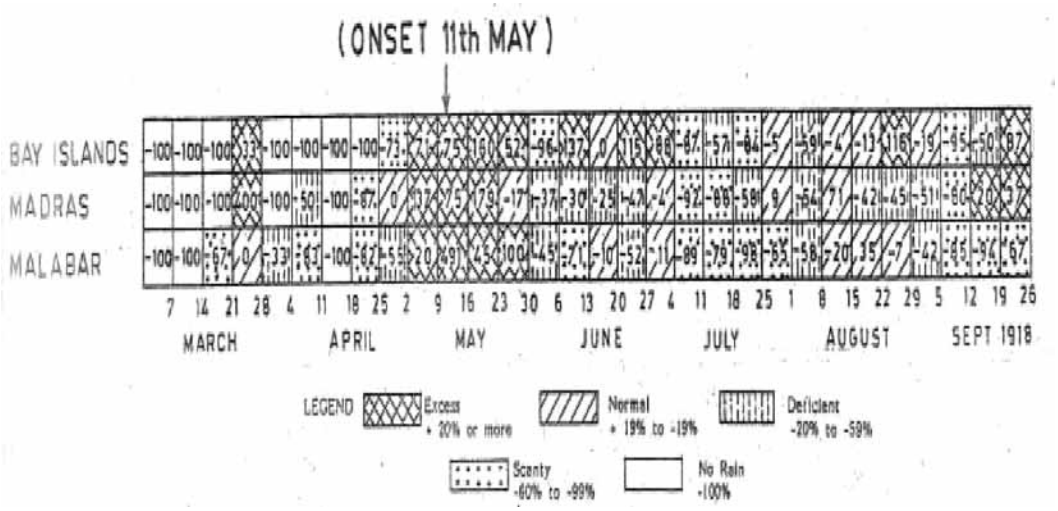

Figure 6. Percentage departure of weekly rainfall from normal.

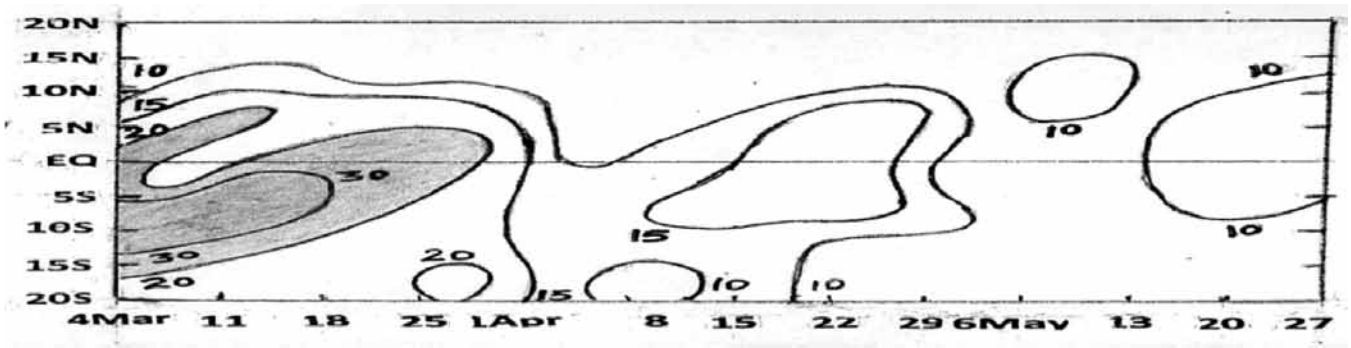

Figure 7. Same as Figure 3 but from the weeks ending 11th March- week ending on 27th May 1973.

Early onset of SWM in 1990

SWM had set in over Kerala on 19th May, i.e., 12 days in advance, in 1990. The ZWMC for the period from the week beginning on 7th April to -week beginning 30th June 1990 are shown in Figure 9 and WMC during the weeks ending on 12th , 19th and 26th May in Figure 10. Four MCZs had developed during the weeks ending on 7th April, 12th May, 9th June and 30th June. The average period between them comes out to be 3 weeks. The second MCZ, which developed to the south of equator during the week ending on 12th May, was quite active, convection associated with it weakened to the south of equator, it developed to the north of equator and had reached up to Kerala coast during the subsequent week (Figure 10). Onset had been declared on 19th May. Appearance of an average period of 3 weeks in the development of MCZs and progressive northward movement of the second MCZ was a precursor to development of an active monsoon during 1990.

Early onset of SWM in 2004

Southwest monsoon had set in over Kerala on 18th May 2004, i.e., 13 days in advance. ZWMC for the period from the week ending on 7th April- the week ending on 30th June, are shown in Figure 11 and WMC for the weeks ending on 12th ,19th and 26th May in Figure 12. Out of the four MCZs which had developed in the zone of SIOCZ during April-June, only two of them which had developed during the week ending on 7th April and 16th June were prominent. The other two were short lived and did not show movement. The MCZ which developed during the week ending on 7th April weakened slightly during the next week. It continued to move northward. However, the northward movement was sluggish. The MCZ could reach 5° lat. belt of 10-15° N by the week ending on 12th May. Onset of 2004 monsoon had been declared on 18th May. Development of a period of about 8 weeks between the two prominent MCZs, Sluggish northward movement of one of the prominent MCZ, development of another 2 short lived MCZs, were the features identified in the activity of SIOCZ. Collectively, a precursor to development of a weak monsoon had been inferred in 2004.

Normal onset of SWM

Out of 43 years when onset was either on the normal date or within 1 S.D. in the dates of onset, the precursor

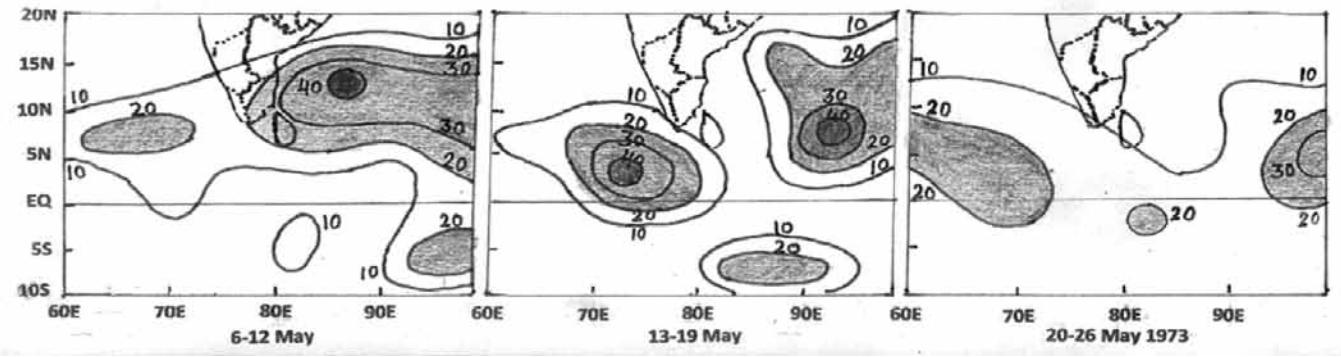

Figure 8. Same as Figure 4 but for the weeks ending on 12th, 19th and 26th May 1973.

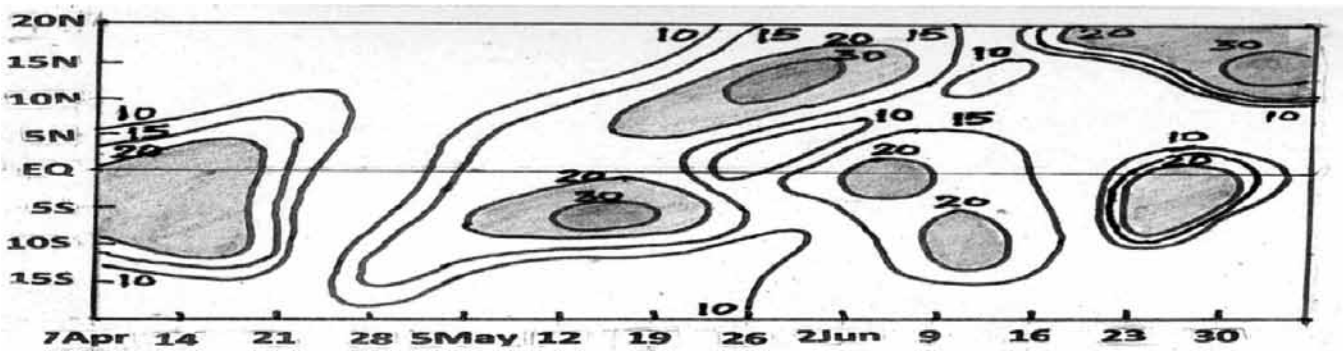

Figure 9. Same as Figure 3 but from the week beginning from 7th April-week beginning on 30th June 1990.

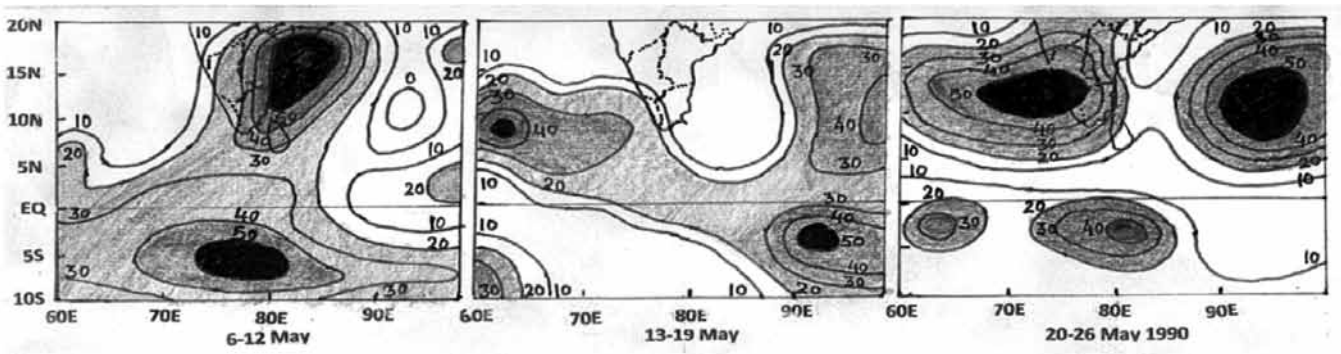

Figure 10. Same as Figure 4 but for the weeks ending on 12th, 19th and 26th May 1990.

for development of a normal/active monsoon was present in 25(50%) years. Thus in the majority of the years of normal onset, India had received normal rainfall. During 2 years, i.e., 1975 and 1988, the precursors were for excess monsoon and the realized rainfall, for country as a whole, was also in excess category. During 6 years (1984, 1985, 1991, 2000, 2001 and 2017), the precursors were for weak monsoon. The realized rainfall was in below normal category in 5 years and it was in normal category, but on the lower side of normal, in 1 year, i.e., 1984. In the remaining 10 years of normal onset (1974, 1982, 1986, 1992, 2005, 2009, 2012, 2014, 2015 and 2016), the precursors were for deficient rainfall. The realized rainfall was in deficient category in 7 years, in below normal category in 2 years (1992 and 2012) and in normal category in one year (2005). Intra-seasonal changes were responsible for improvement in rainfall during the years 1992, 2005, 2012 and 2016. Intra-seasonal changes are not limited only to some of the years and these changes are not exclusively dependent on the activity of SIOCZ. This aspect becomes clear from the discussions, presented below, on intra-seasonal changes during the years 1992,2005,2012,2016 and 2018.In the normal onset year of 2018, the precursor was for a normal monsoon. However, a feature in the activity of SIOCZ, relating to development of a weak monsoon had just appeared in May. Intra-seasonal changes and their impact on rainfall in these 5 years have earlier been studied by Onkari Prasad, et al. (2014, 2018) and

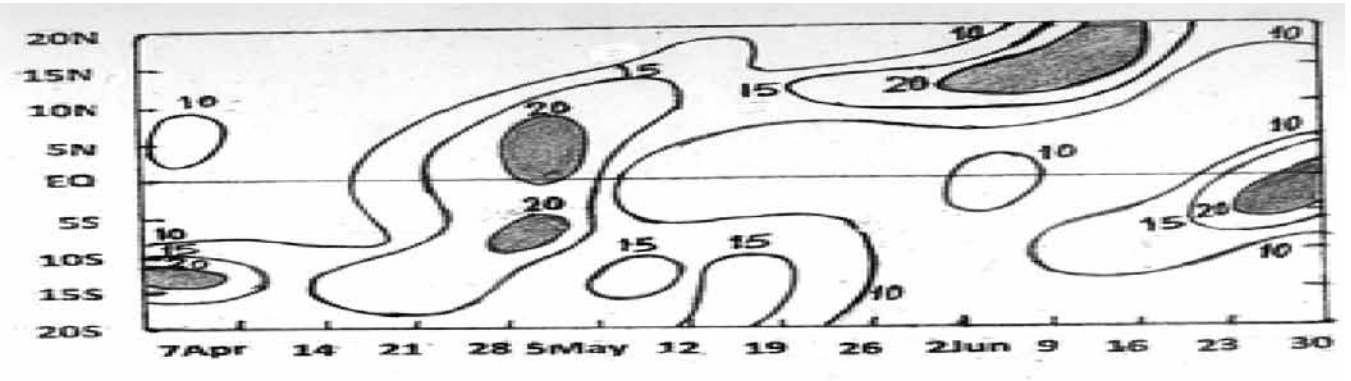

Figure 11. Same as Figure 3 but from the week ending on 7th April- the week ending on 30th June 2004.

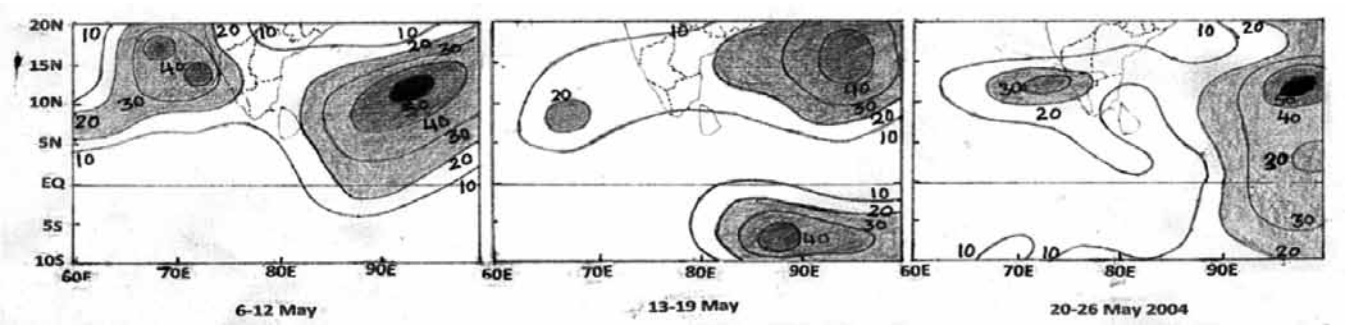

Figure 12. Same as Figure 4 but for the weeks ending on 12th, 19th & 26th May 2004

the results are briefly summarized below. Due to lack of space, the figures showing ZWMC during April-June and northward propagation of the MCZs during three weeks, i.e., week before the onset, during the week of onset and the week subsequent to the week of onset, could not be reproduced for normal onset years. Development of a MCZ in the zone of SIOCZ at an interval of 4-6 weeks and its northward propagation up to 10° N lat. or further north in the east Arabian Sea around the normal date of onset, or within one S.D. in the date of onset, was common to most of the years of normal onset.

The precursor identified for 1992 SWM was that for a severe drought with 16% below normal rainfall for country as a whole and as per the improved version of SIOCZ model (Onkari Prasad and Singh,2012; Onkari Prasad, et al., 2014), the forecast rainfall was 11% below normal, i.e., in deficient category. Severe drought conditions prevailed over India during the first half of the season: The weekly cumulative rainfall, for India as a whole, was below normal by 20% till the end of July. Thus, the rainfall during the first half of the season was well captured by SIOCZ model. Monsoon trough strengthened during the second half of the season and rainfall situation improved. Rainfall was 8% below normal at the end of the season. The intra-seasonal changes occurred in association with the ongoing changes in the Equatorial Indo-Pacific region: El- Nino of 1991-92, which had been at its peak during December 1991-February 1992, started weakening and ENSO-neutral conditions returned from July and continued till the end of the season. The intra-seasonal changes in the activity of SIOCZ and improvement in rainfall scenario over India began in August and continued in September also.

The forecast for 2005 SWM was 14% below normal rainfall and with the improved version of the model, it was 9% below normal. The realized rainfall was 1 % below normal. The precursor identified for 2005 SWM was that for a moderate drought/weak monsoon (Onkari Prasad, et al., 2014). The precursor, for a moderate drought/ weak monsoon, continued throughout the season. The cumulative rainfall for India as a whole was 8% below normal up to 7th September. However, the rainfall which occurred during the next 2 weeks, in association with the development and movement of the Bay of Bengal cyclonic storm of 17-21 September 2005, was able to reduce the deficiency from 8% to 1%. The cyclone initially moved across central India and then re-curved to north giving heavy rainfall in a number of subdivisions, where rainfall was deficient. The strengthening of monsoon circulation was related to the ongoing changes over the Equatorial Indo-Pacific region: demise of EL-Nino of 2004 and setting in of ENSO-neutral conditions from July 2005 onwards.

The precursor identified for 2012 SWM was that for a severe drought with 20% below normal rainfall (Onkari Prasad, et al., 2014). 2012 SWM displayed features of a severe drought during June and July. Rainfall was 28% below normal in June and 27 subdivisions, out of 36, had

received deficient/scanty rainfall. No low pressure area formed in June and such a situation had not occurred during the past 31 year period of 1981-2011 (IMD, 2012). July rainfall was 13% below normal. Monsoon circulation strengthened during August and this situation continued up to the middle of September. A part of the deficiency was made up and the realized rainfall was 8% below normal by the end of the season. La Nina of 2011 had continued up to the three monthly period of February-March-April of 2012. SST anomalies became zero during the three months period of June-July-August and 0.3°C during July-August-September 2012. So, the improvement in rainfall could not be attributed to the ongoing changes in Equatorial Indo-Pacific region. The improvement resulted due to the changes in the activity of SIOCZ: SIOCZ remained generally active during the second half of 2012 monsoon, but in the latitude belt of 15-20°S, i.e., in its southern most location during the season. This coincided with the strengthening of monsoon trough. As per the inverse relationship between monsoon trough and SIOCZ, strengthening of monsoon trough was not expected during the second half of 2012 SWM also. The inverse relationship between monsoon trough and SIOCZ was nearly ineffective in the reduction of rainfall over India during the second half of the season. Monsoon trough remained active and quasi-stationary in its normal location for a period of one and a half month, i.e., during August-first half of September 2012. SIOCZ is most effective in weakening the monsoon trough and, thereby, in reduction of rainfall over India when it is active in its normal location during the season, i.e., between equator-5°S lat. Though active, but being located between 15-20° *S* lat., SIOCZ could not weaken the monsoon trough. The improvement in rainfall during the second half of 2012 SWM had, therefore, resulted due to the extreme southern most location (15-20° S) of an active SIOCZ.

The precursor identified for 2016 SWM was that for a deficient monsoon with 14% below normal rainfall for India as a whole (Onkari Prasad, et al., 2018a). Except for the month of July when rainfall, for country as a whole, was above normal by 7%, rainfall was below normal by 11%, 9% and 3% in June, August and September respectively. Severe drought like conditions prevailed over north India and south peninsula in August and over NW India and south peninsula in September. For the season as a whole, rainfall was 6% above normal over central India, but it was below normal in NW India, NE India and south peninsula by 5%, 8% and 11% respectively. Seasonal rainfall for country as a whole was 3% below normal. Intra-seasonal changes were responsible for improvement in rainfall: A mid season transition from ENSO neutral-to-La Nina had taken place during 2016 monsoon. La Nina conditions prevailing during August-September had been found to be generally associated with an active monsoon conditions over India. But this did not happen in 2016. Changes in the activity of SIOCZ were more closely related to the distribution of rainfall over India during the second half of 2016 SWM than the mid-season transition from El Nino-ENSO Neutral-La Nina conditions in Equatorial East Pacific. Beginning from 2013, forecast updates are being issued to take into account the changes in monsoon circulation system and thereby in rainfall, resulting due to intra-seasonal change as seen in the appearance of a new feature in the activity of SIOCZ. The improvement in rainfall had been captured in the update issued on 1 Aug 2016, wherein, the forecast had been upgraded to a normal monsoon (100% of long period average) (Onkari Prasad, et al., 2018a).

Based on OLR and cloud data up to March 2018, the main feature identified for 2018 SWM was that for development of a normal monsoon and accordingly, the qualitative long range forecast for seasonal rainfall for India as a whole, issued on 11th April 2018 (Onkari Prasad, et al., 2018b) was for a normal monsoon. The quantitative forecast issued on 5th June (Onkari Prasad, et al., 2018b) was also that for a normal monsoon with 2% above normal ISMR. But, a precursor, relating to development of a weak monsoon, appeared in May. A mention of this had been made in the quantitative forecast issued on 5th June. The precursor relating to weak monsoon repeated during June and during the first week of July also. Accordingly, the forecast was downgraded to a weak monsoon with 7% below normal rainfall for country as a whole, in the update issued on 11th July (Onkari Prasad, et al., 2018b). The realized rainfall for country as a whole for 2018 SWM was 9% below normal. It follows from the above discussions that the identification of the precursors was satisfactory in 1992, 2005, 2012, 2016 and 2018. The intra-seasonal changes in monsoon circulation system and the corresponding changes in rainfall scenario in 2016 and 2018 had been captured in the update.

Delayed onset of SWM

Delayed onset of SWM in 1979

1979 was a severe drought year with 21% below normal rainfall for country as a whole. Onset over Kerala had been delayed by 11 days. The ZWMC for the period April-June 1979 are shown in Figure 13. Onset occurred during the northward propagation of the MCZ which had developed over the equator during the week ending on 3rd June. Initially, the MCZ remained confined to the areas between 5° lat. on either side of the equator. Northward propagation began only during the week ending on 10th June. Onset took place on 11th June. The MCZ which had developed during the last week of May remained practically stationary and close to equator. This caused delay in onset of monsoon in

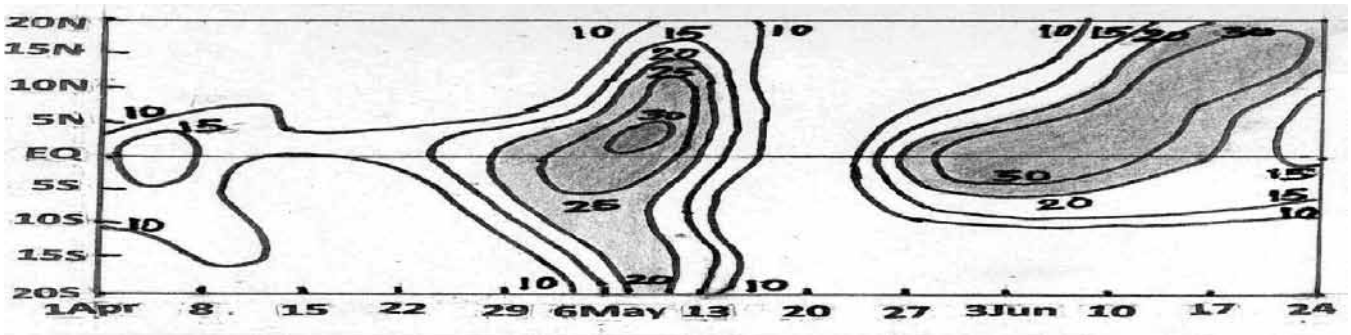

Figure 13. Same as Figure 3 but from the week ending 8th April- week ending 24th June 1979

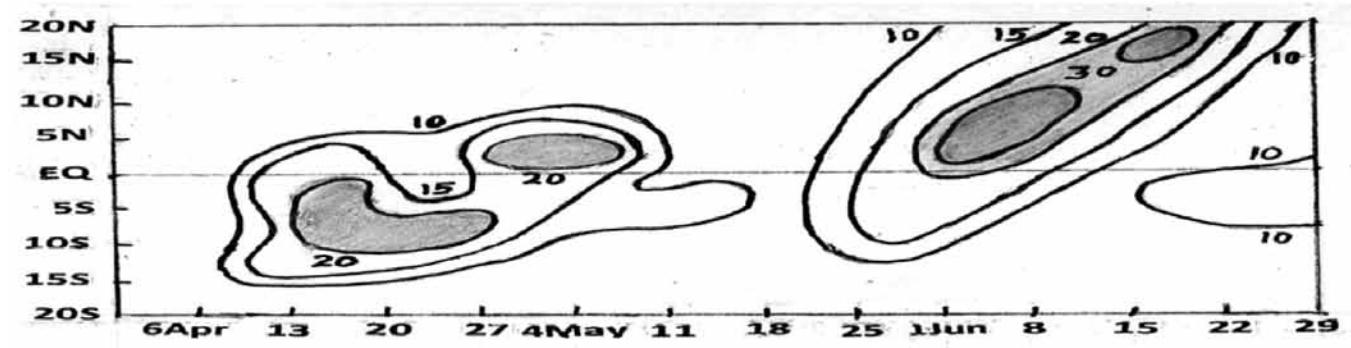

Figure 14. Same as Figure 3 but from the week ending on 6th April- the week ending on 29th June 1983

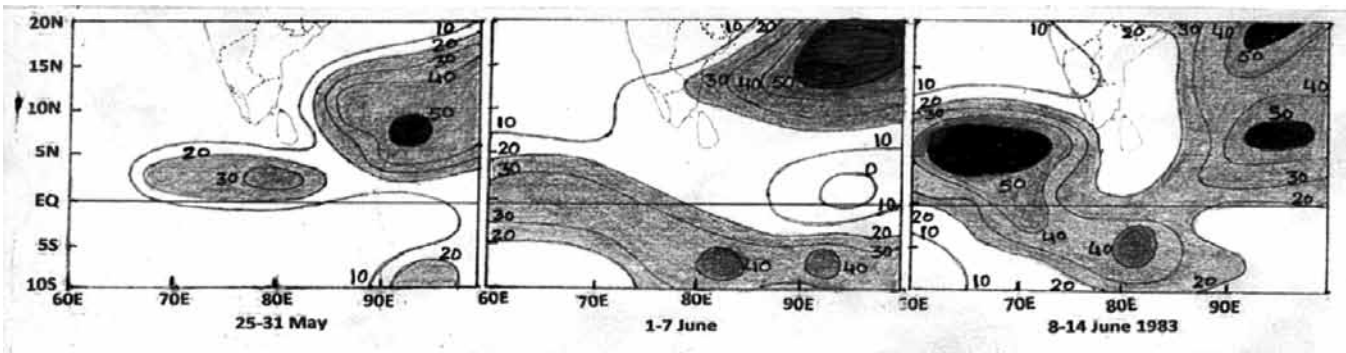

Figure 15. Same as Figure 4 but for the weeks ending on 31st May, 7th and 14th June 1983.

1979. The WMC data are not available for the year 1979 and hence the figure showing week by week propagation of the MCZ could not be included here.

The MCZs which had developed in the beginning and at the end of April, had a tendency to move towards north as well as towards south of equator. This was more clearly seen in the MCZ which had started developing over the equator during the last week of April. Movement of MCZs on either side of the equator was a precursor for likely development of a weak monsoon/drought during 1979.

Delayed onset of SWM in 1983

SWM had set in over Kerala on 13th June in 1983. 1983 was an excess monsoon year with 13% above normal rainfall for India as a whole. ZWMC for the period 6th April- 29th June 1983 are shown in Figure 14. The WMC during the weeks ending on 31st May, 7th June and 14th June 1983 are shown in Figure 15. The MCZ had reached up to 15°N in the Bay of Bengal and up to 5° N in the east Arabian Sea by the week ending on 31st May. The MCZ to the north of equator was expected to move northward and reach Kerala coast during the next few days. However, during the subsequent week, i.e. during the week ending on 7th June, there was considerable reduction in the cloudiness in east Arabian Sea. The MCZ was now seen between 5°N-5°S over the areas in the sector 60-70° E, giving an impression as if the MCZ had shifted southwards. In fact, the northward moving MCZ had weakened and a fresh MCZ had developed close to equator but south of it. This

MCZ extended further eastward and it was seen between 5-15°S east of 80°E, where it was more marked. The MCZ was not confined to SIO alone, but it extended over south West Pacific also. This situation changed in the subsequent week. The MCZ in the sector 55-80°E moved northward and reached up to 10°N in east Arabia Sea. Onset of SWM was declared on 13th June. It is interesting to note that the development of an active spell of SIOCZ for one week did not repeat till the end of 1983 monsoon season. Development of SIOCZ during 1-7 June 1983 had caused considerable weakening of the convergence zone to the north of equator and hence a delay in the onset of monsoon over Kerala. The MCZ which developed in the zone of SIOCZ during the week ending on 13th April (Figure 14) remained active for the next 4 weeks and moved northward up to 5° N lat.. This feature in the activity of SIOCZ was an indication of development of CEF in Arabian Sea and its sustenance for 4 weeks in continuation. Establishment of CEF in Arabian Sea in the beginning of Apr and its sustenance for 4 weeks in continuation was a precursor to development of an active-to-excess SWM during 1983.

CONCLUSIONS

There is a remarkable consistency in the date of onset of southwest monsoon over Kerala. During the period of 50 years (1969-2018), onset had taken place either around or within 1 S.D. in the dates of onset, in 86% years. Onset was early in 10% years and it was delayed in 4% years only. Development of a MCZ in the zone of SIOCZ during pre-monsoon months with a period of 4-6 weeks and its progressive northward movement up to about 10° N or further north in the east the Arabian Sea is common to most of the years of normal onset.

Development of a MCZ at the end of April/beginning of May and its uninterrupted northward movement results in early onset. Development of a MCZ over the equator during the last week of May and its slow movement northward results in delay in onset, as was the case in 1979. Delay in onset may also result due to development of an active spell of SIOCZ during the first week of June as was the case in 1983.

Large intra-seasonal changes take place in southwest monsoon in some of the years, due to either development of new features in the activity of SIOCZ or changes in sea surface temperature over equatorial Indo-Pacific region. Monitoring of development of new features helps in issuing forecast update. Experience of issuing update for the past few years has shown that the updates were able to capture the changes in rainfall scenario over India.

Development of a MCZ in the zone of SIOCZ is linked to the development of a slow northeastward propagating mode, which originates in west IO and travels eastward. Inter-annual and intra-seasonal changes in this mode are linked to SST distribution over SIO. Further studies, using long period weekly mean cloud/OLR and weekly mean SST anomaly from SIO are required for understanding the mechanism of development of MCZs and the period between them.

ACKNOWLEDGEMENT

The data on the date of onset of southwest monsoon over Kerala were supplied by the Office of Climate Research and Services, IMD, Pune. The authors are thankful to the anonymous reviewers and Editor JIGU, whose comments helped in improving the manuscript.

Compliance with Ethical Standards

The authors declare that they have no conflict of interest and adhere to copyright norms.

REFERENCES

Ananthakrishnan, R., Acharya, U.R. and Ramanathan, A.R., 1967. IMD, FMU Report No.1, November 1967, 'On the criteria for declaring the onset of southwest monsoon over Kerala', p.19.

Ananthakrishnan, R. and Somon, M.K., 1988. The onset of southwest monsoon over Kerala: 1901-1980, J. Climatology, 8, 283-296.

Gupta, G.R. and Onkari Prasad, 1992. Role of southern hemispheric equatorial trough in long range forecasting, Jalvigyan Sameeksha, VII, 83-97.

Gupta, G.R. and Onkari Prasaed, 1993. Southern hemispheric equatorial Trough model of long range forecast of monthly rainfall during southwest monsoon, J. Indian Association of Hydrologists, Hydrology J., 16, 49-76.

IMD, 2012, End of season report on 2012 southwest monsoon.

Joseph, P.V. and Pillai, P.V., 1988. 40 day mode of equatorial trough for long range forecasting of Indian summer monsoon onset, Curr. Sci., 57, 951-954.

Joseph, P.V., Eishcheid, J.K. and Pyle, R.J., 1994. Inter annual variability of the onset of the Indian summer monsoon and its association with atmospheric features, El-Nino and seas surface temperature anomalies, J. Climate, 7, 81-105.

Joseph, P.V., Sooraj, K.P. and Rajan, C.K., 2003, Conditions leading to monsoon onset over Kerala and associated Hadley Cell, Mausam, 54(1), 155-164.

Onkari Prasad, 1993. Performance of Southern Hemispheric Equatorial Trough model of sub-division-wise long range forecast of rainfall during southwest and northeast monsoons, Proceedings of TROPMET Symposium-1993, held at New Delhi, 17-19 March 1993.

Onkari Prasad, Singh, O.P. and Subramanian, S.K., 2010a. Seasonal forecast of southwest monsoon rainfall- District level, J. Ind. Geophys. Un., 14, 93-113.

Onkari Prasad, Singh, O.P. and S. Prasad, 2010b, South Indian Ocean Convergence Zone model: A new approach to seasonal forecasting of monsoon rainfall in India Part I:South Indian Ocean Convergence Zone and its role in the development of Indian summer monsoon, J. Ind. Geophys. Un., 14(4), 233-248.

Onkari Prasad and Singh, O.P., 2012. South Indian Ocean Convergence Zone model: A new approach to seasonal forecasting of monsoon rainfall in India Part II: Forecast for India as a whole, J. Ind. Geophys. Un., 16(1), 1-10.

Onkari Prasad, Singh, O.P. and K. Prasad, 2014. South Indian Ocean Convergence Zone model: A new approach to seasonal forecasting of monsoon rainfall in India Part VI: Merits of the model and limitations in seasonal forecasting of rainfall in India, J. Ind. Geophys. Un.,18(3), 363-386.

Onkari Prasad, Singh, O.P. and K. Prasad, 2016. Long range forecast of rainfall during southwest monsoon in the states of Maharashtra and Goa, J. Ind. Geophys. Un., 20(6), 586-595.

Onkari Prasad, Singh, O.P. and K. Prasad, 2018a, 2016 southwest monsoon and its long range forecast, J. Ind. Geophys. Un., 22(1), 90-100.

Onkari Prasad, Singh, O.P. and Prasad, K., 2018b. Long range forecast of rainfall during 2018 southwest monsoon based on South Indian Ocean Convergence Zone model issued on 11th April and 5th June and update issued on 11th July 2018 submitted to IMD and user agencies of Govt. of India.

Yasunari, T., 1980. A quasi-stationary appearance of 30 to 40 day period in the cloudiness fluctuations during the summer monsoon over India, J. Met. Soc. Japan, Ser. II, 58, 225-229.

Received on: 1.10.18; Revised on: 17.1.19; Accepted on: 10.2.19

J. Ind. Geophys. Union (March 2019)
v.23, no.2, pp: 164-172

A case study on pre- and post-monsoon seabed topography using bathymetry near Kalingapatnam, Srikakulam District, Andhra Pradesh (India)

S. Balasingh John Samuel[1]*, Y.Srinivas[1], and R. Subramanian[2]

[1]Centre for GeoTechnology, Manonmaniam Sundaranar University, Tirunelveli-627012, India
[2] Institute of Remote Sensing, Anna University, Guindy Campus, Chennai-600025, India
*Corresponding author: geophysingh@gmail.com

ABSTRACT

A study of seabed topography is important to understand the landforms under sea water, which has various oceanographic applications like navigation safety, nautical charts, water volume computation, seabed sediment computation, pollution control, sediment transport, under water engineering, harbour and docks construction etc. Bathymetry is one of the tools to delineate seabed topography using echo sounding principle. In this study, bathymetric survey was carried out at near-shore areas by covering about 10 km distance along the coast and into the sea up to 20 m contour at 100 m line spacing, during pre- and post-monsoon seasons. The survey area was spitted into three zones and data was collected using dual frequency echo-sounder, which was processed and presented in Chart Datum, based on tides measured at every 10 minutes interval during survey period, using vale-port tide gauge at river Vamsadhara. The results demonstrate that the water depth is increasing gradually towards seaward and structuring gentle slope from seashore. The depth contours are running parallel to the coast during both seasons. The seabed profiles show that the seabed experienced erosion and deposition at river mouth and also in the northern side of study area. The overall seabed topography suggests that this region is suitable for coastal development activities in the southern part, where the seabed has adequate natural depth and lesser sediment migration.

Key Words: Pre- and post- monsoon bathymetry, Sediment deposition, Sediment volume computation, Near-shore sediment deposition, Monsoon, Kalingapatnam

INTRODUCTION

Kalingapatnam is a village in Srikakulam district of Andhra Pradesh situated in eastern part of India. It is located in Gara mandal of Srikakulam revenue division and falls in geographical coordinates 18.3387° N and 84.1211° E. It has one of the major beach sand deposits in the state. Kalingapatnam is the place where river Vamsadhara enters into Bay of Bengal. The nearest port and fishing harbour is Visakhapatnam, which is located 110 km south from Gopalpur (Figure 1). The seabed topography has been studied through bathymetric survey carried out in two different seasons, covering approximately 40 sq. km off Kalingapatnam coast, using single beam, dual frequency echo sounder. Bathymetry is the key tool to understand depth profiles and to measure/monitor/quantify the sediment distribution/movement in water-bodies (Richard et al., 2000). The total study area has been divided into three zones in order to study in detail (Figure 2). Acoustic depth sounding was first used in 1930s but until the 1950s or 1960s, it did not replace reliance on lead line method. Depending on applications and depths, a variety of acoustic depth systems are used throughout the hydrographic survey industries, these include single beam acoustic system, multiple transducer channel sweep systems, and multi-beam sweep systems. (Lavery et al., 2010; Sathishkumar et al., 2013; Manik et al., 2014; Mohamed et al., 2016). The Echo-sounding systems measure the elapsed time that an acoustic pulse takes to travel from a transducer to seabed and back (Figure 3). The travel time (t) of the acoustic pulse depends on the velocity (v) of propagation in the water column. The corrected depth (d)/seabed can be computed by the measured travel time of the pulse for known sound velocity:

$$d = ½^{\star} (v \cdot t)$$

Where, d is corrected depth, v is average velocity of sound in the water column, t is measured elapsed time from transducer to seabed and back to transducer.

Bathymetric study is commonly used in pre-dredge, post-dredge monitoring, navigation, pipeline laying projects, jetty/wharf/breakwater/seawall constructions, shoreline changes/monitoring, to calculate de-silting quantity, channel design etc., (Fröhle and Kohlhase, 2004; Thompson et al., 2015; Yaacob et al., 2017). In view of this, bathymetric investigation has been carried out to study the feasibility of developing coastal infrastructure through analysis of seabed topographic contours, vertical depth profiles and volume of sediment accumulation, between pre- and post- monsoons for the above mentioned three zones (Smith and Marks, 2014).

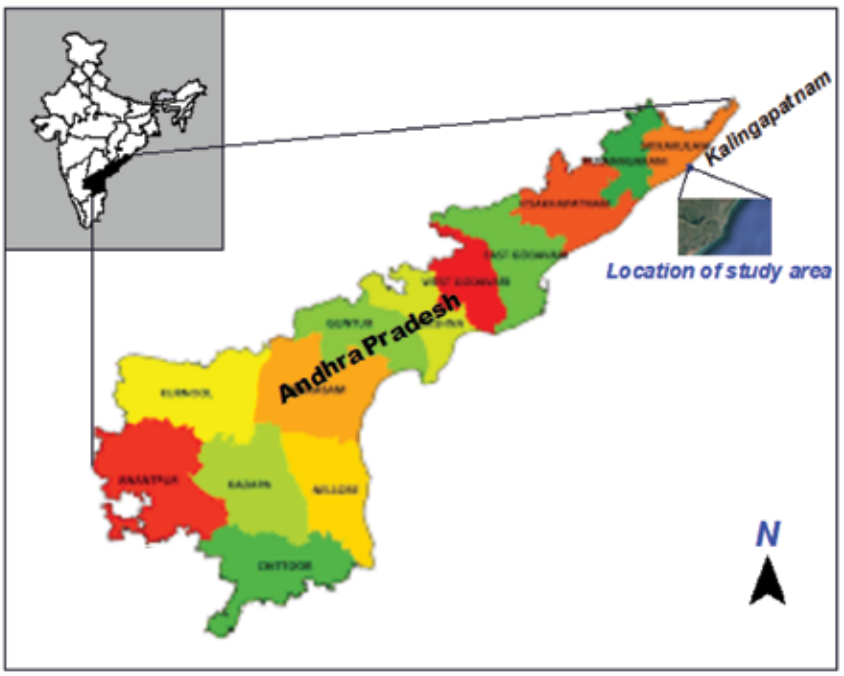

Figure 1. Location map of the studied region.

Figure 2. Satellite imagery showing zone 1, zone 2 and zone 3 of the studied region.

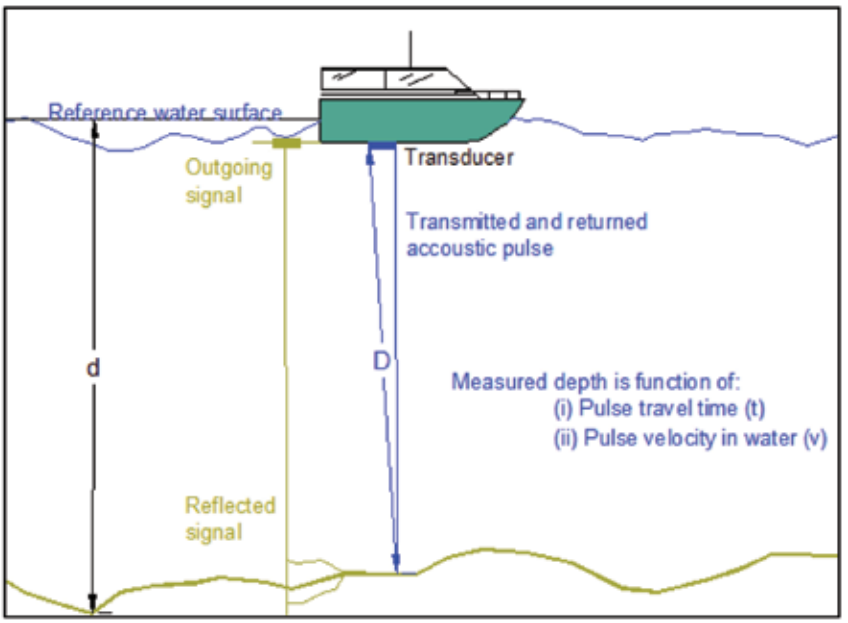

Figure 3. Schematic diagram showing principles of echo sounder.

METHODOLOGY

Data Acquisition

The bathymetry data acquisition was carried out using Teledyne Odom Echo-trac CV 100 and Trimble SPS 351 DGPS systems. The Echo-sounder and DGPS system were installed onboard and operated in accordance with the manufacturer's instructions. The transducer was installed rigidly to a strut at star-board side on fishing boat. The transducer shoe was immersed 1 m below water surface not to experience turbulence and aeration, when the vessel steams at survey speed. Prior to commencing survey works, the echo-sounder was calibrated against a bar check. The technical specification of echo-sounder used are: resolution- 0.01m / 0.1 ft; accuracy- ± 0.1% of measured depth for 200kHz, Depth range- 0.2 – 200 m for 200 kHz, 0.5 – 1500 m for 33 kHz; sound velocity- 1370–1700 m/s.

The bathymetry survey lines were planned perpendicular to the coast and data was acquired on dual frequency mode at low band-33 kHz and high band-210 kHz (Figure 4). The water depths of 5 m and above were surveyed using 40 feet fishing trawler, arranged from Visakhapatnam fishing harbour. The near shore area and inside river Vamsadhara, wherever the depths are less than 5m, were surveyed using small FRP boat set from Kalingapatnam village (Lyzenga, 1985). The water depth in the wave breaking zone up to 0.7m from low water line was measured by Sokkia Total-station during early morning hours, whenever the sea was calm without heavy waves (Figure 5). The vessel used for survey was equipped with TRIMBLE SPS 351 Beacon Receiver for precise dynamic positioning to give the real time position. The DGPS Beacon Transmitter operated from Dolphin's nose by Department of Lighthouse and Navigation was taken as reference station for horizontal positioning corrections. The transmitting frequency of this reference Beacon transmitter is 295 kHz. The DGPS system was setup to operate on UTM North Grid, Zone 45, WGS-1984 ellipsoid coordinate. The GTS bench mark located in the light-house, Kalingapatnam, has been used as vertical reference for this study and to measure the tides in order to reduce the soundings into Chart Datum. The tide measurement was carried out during survey period at every 10 minutes at river Vamsadhara, using Valeport Automatic Tide gauge. The measured water levels were connected to Bench Mark through fly leveling method by digital Auto-level and reduced to Chart Datum.

Data Analysis:

The survey points were closely observed and invalid points were removed if any abnormal position or depths in the raw data are seen. At each line intersection, depths were checked carefully to ensure that they are within the allowable limits. The corrections and offsets were checked carefully and applied on processed data. The data taken from total station was brought into same horizontal and vertical datum applied on bathymetry and both the data sets were combined together. The corrected soundings and near-shore spot levels were sorted and exported as XYZ file format. Though there are many algorithms for gridding, the Kriging algorithm is used in this process which is one of the more flexible and accurate gridding methods; typically this algorithm is recommended when gridding the data (Kader et al., 2013). Kriging is one of the most used techniques in geo-statistics field for interpolation in which

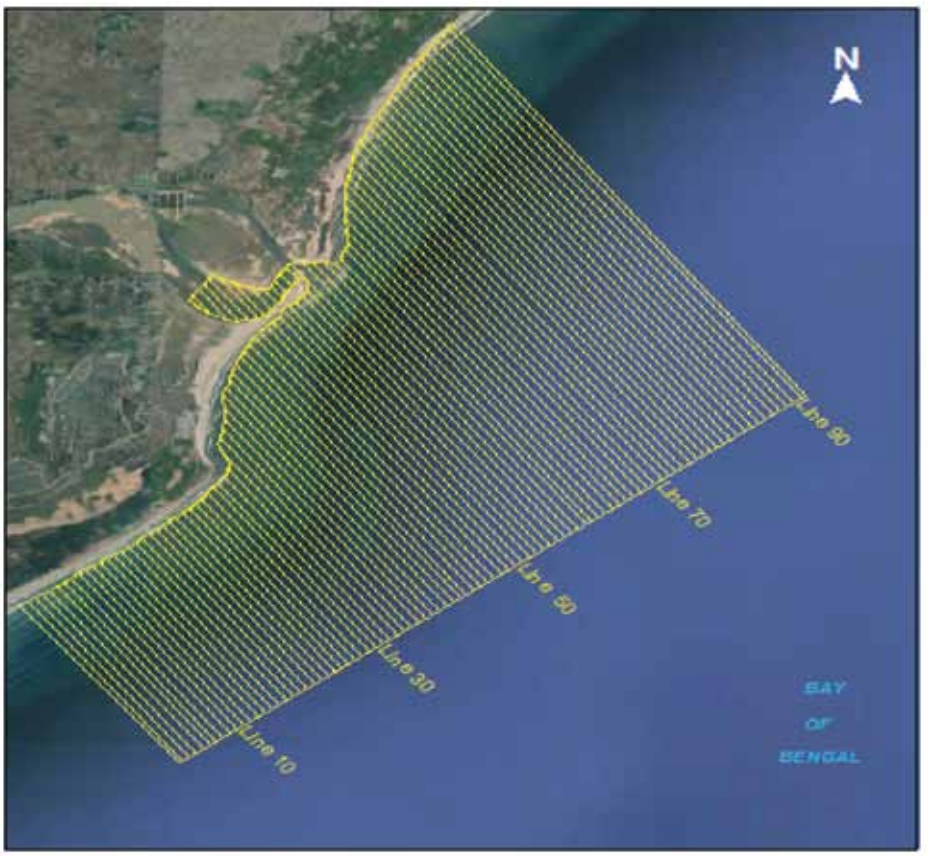

Figure 4. Survey transects for bathymetric study.

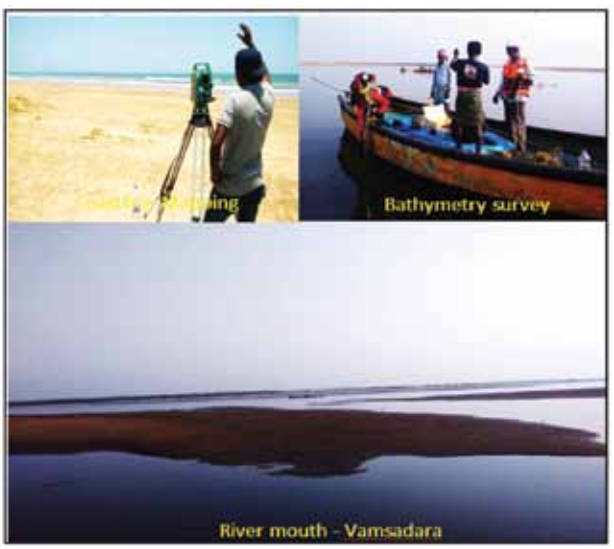

Figure 5. Photograph showing river mouth and field activities.

the interpolated values are modeled by a Gaussian process, run by prior covariance. It is a reasonably accurate method, generally employed on cartography of seafloor. Kriging helps to obtain the shape of the seafloor as relief map in order to delineate the seabed contours in various scales (Christopheret al., 2016). Kriging is also a recommended method for terrain variation analysis, when compared with other interpolation methods such as inverse distance weighted, ANUDEM, nearest neighbor, spline approaches etc., (Hare et al., 2011; Arun, 2013). It also can compensate for clustered data by giving less weight to the cluster in the overall prediction.

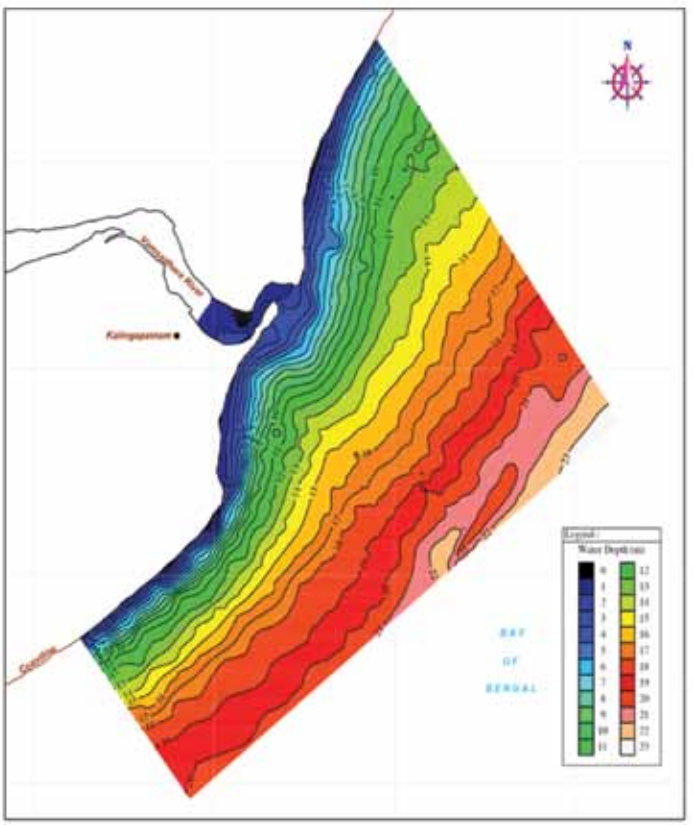

Figure 6a. Pre-Monsoon bathymetry contour map of Kalingapatnam offshore area.

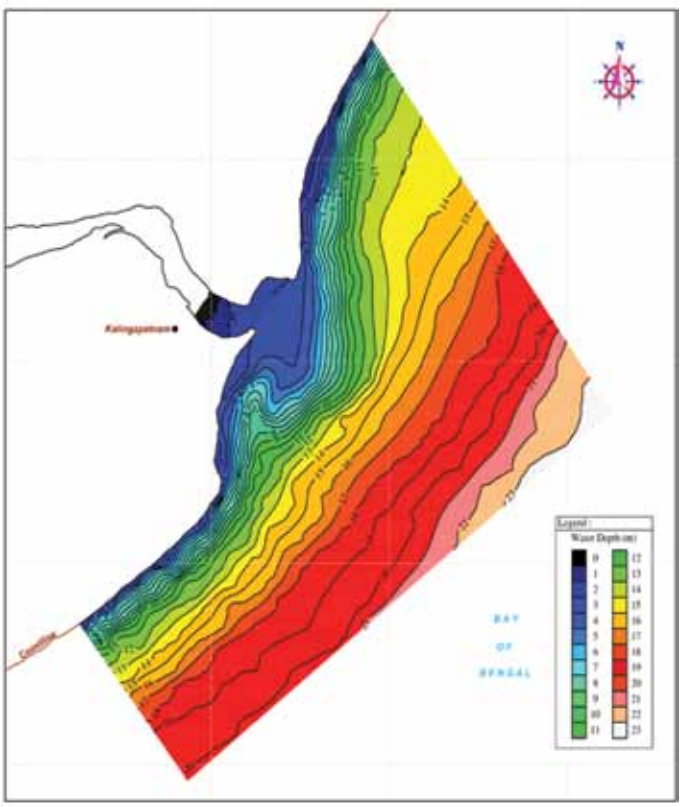

Figure 6b. Post-Monsoon bathymetry contour map of Kalingapatnam offshore area.

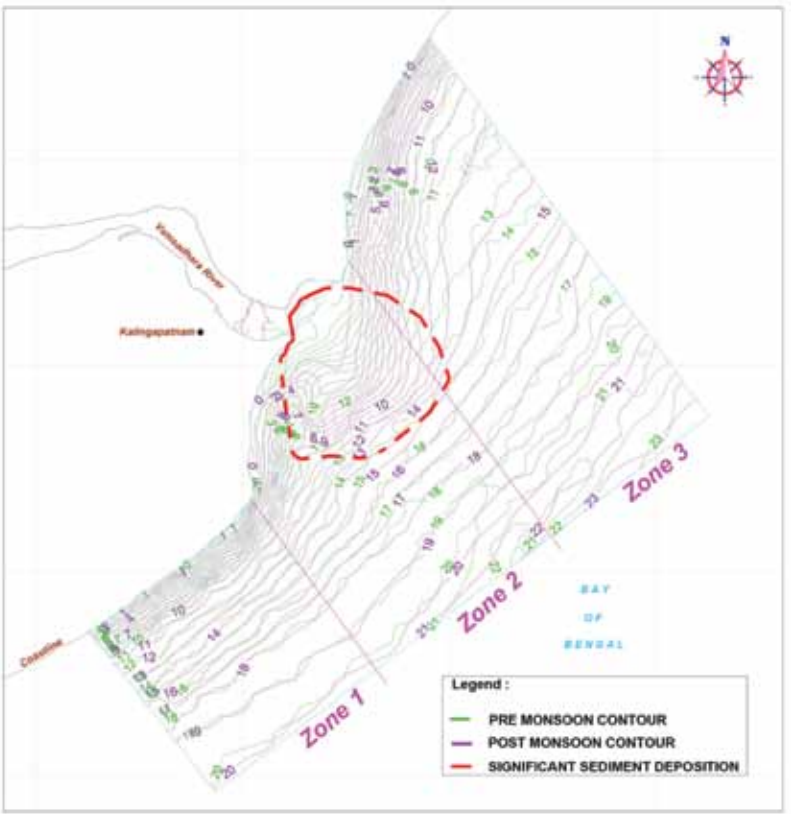

Figure 7. Contour map showing both pre- and post-monsoon bathymetric study in Kalingapatnam offshore area.

Contour maps were prepared from the gridded data at 1 m interval for both seasons (Figure 6a and 6b). The first two dimensions X and Y are the geographical coordinates in UTM. The third dimension (Z) is represented by depth with respect to Chart Datum. The relative spacing of the contour lines indicates the relative slope of the seabed. The pre- and post-monsoon contours are superimposed and analyzed for sediment movement between the two seasons (Figure 7). The development of coastal infrastructure and maintenance are mainly dependent on morphodynamic changes. In this study, the sediment deposition/erosion and its volume has been analysed and computed for each zone separately using the surfer software. The "xyz" data for two seasons were defined as an upper/post-monsoon and lower/pre-monsoon surface for each grid cell. In areas where the surface is tilted at the top or bottom of a grid cell, the software approximates the volume of the prism at the top or bottom of the grid cell column. For very coarse grids, the prisms can contain a significant volume.

RESULTS AND DISCUSSION

The results reveal that in zone 1, the seabed up to 450 m from shore is rather steeper than the seabed further seaward during both monsoons. A slope of 1:45 has been observed till 10 m depth and 1:130 between 10 m and 20 m contours. The analysis of seabed contours for both seasons do not show much variation generally as the same depth contours are running at same distance and pattern in this zone. The maximum depth of 20 m exists at a distance of about 2 km from shore. The sediments accumulation and erosion occurred on seabed between pre- and post- monsoon in this zone is calculated as 11, 78,000 m^3 deposition and 2, 99,000 m^3 erosion. Similarly, zone 2 is the area where river Vamsadhara meets sea. The near-shore area close to river mouth is identified as shallower in post monsoon bathymetry. The sediments are deposited and spread at various directions which show significant variation on post monsoon bathymetry at 1.3 km southward from river mouth (Figure 7) (Fennessy et al., 1994). The seabed near river mouth was observed as a slope of 1:80 till 10 m contour during pre-monsoon and after it has been observed as 1:130 during post-monsoon. The seabed shows a slope of 1:200 further seaward during pre- monsoon and 1:185 in post- monsoon. The depth contours do not show much variation in its pattern and location between 15 m and 20 m. In general, the depth of 20 m is observed at a distance of about 3 km from the river mouth. The total volume of sediment deposited after monsoon is calculated as 1,69,26,000 m^3 in which eroded volume is 2,47,000 m^3.

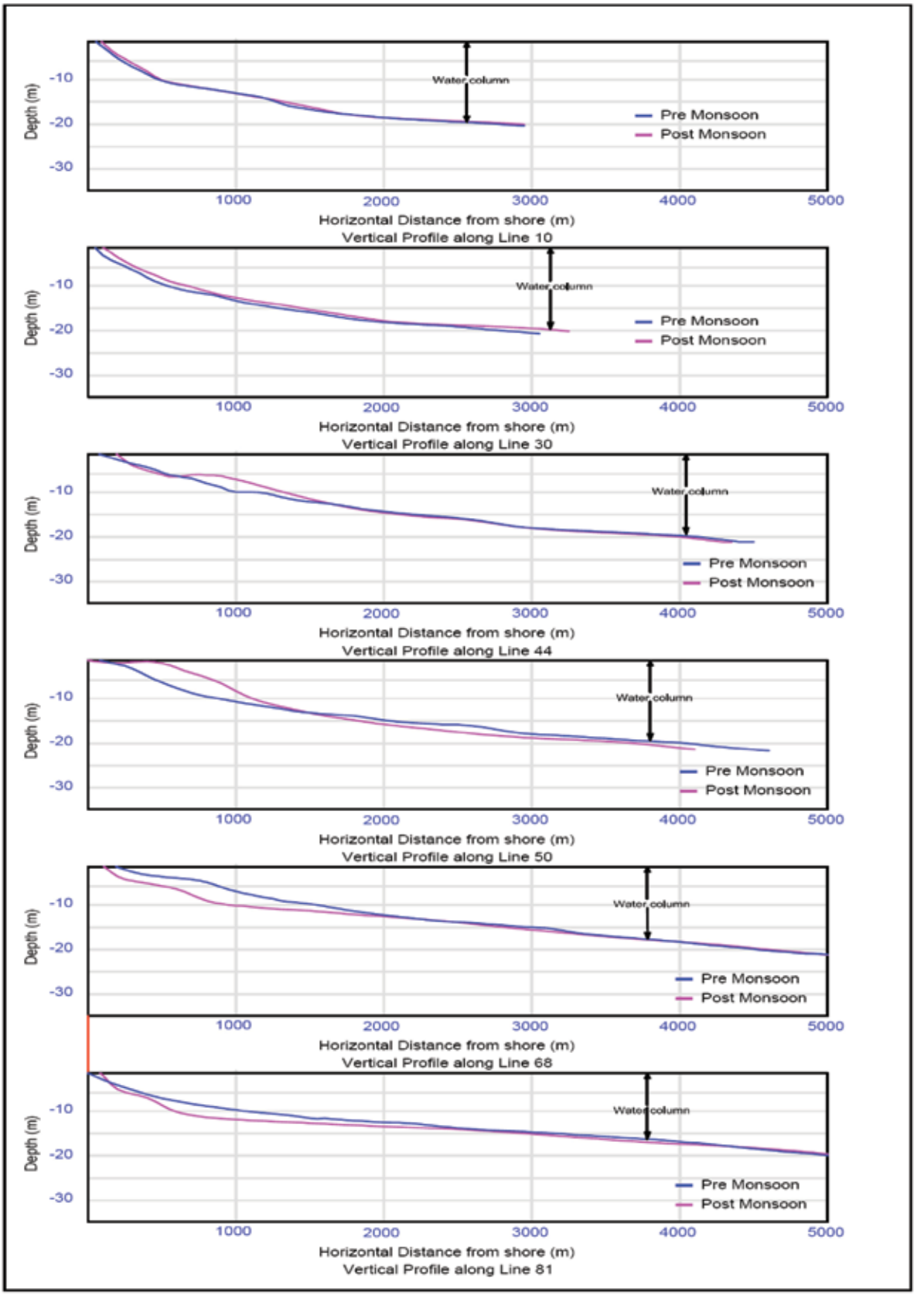

Figure 8. Typical vertical profiles during Pre- and Post –Monsoons

Table 1. Details of vertical profiles at 2 Km interval.

Lines	Start depth	End depth	Straight line distance	Vertical difference (start to finish)	Minimum depth on path	Maximum depth on path	Azimuth	Slope/ tilt
Line 10	0.13 m	20.50 m	2.94 km	20.4 m	0.13 m	20.50 m	144° 48' 48.3"	0.40°
Line 30	0.40 m	20.76 m	3.04 km	20.4 m	0.39 m	20.76 m	144° 49' 14.4"	0.38°
Line 50	1.22 m	21.77 m	4.58 km	20.6 m	1.22 m	21.77 m	144° 49' 29.8"	0.26°
Line 70	0.29 m	22.43 m	5.94 km	22.7 m	-0.29 m	22.43 m	144° 49' 42.8"	0.22°
Line 90	1.84 m	23.32 m	6.75 km	21.5 m	1.84 m	23.32 m	144° 49' 58.7"	0.18°
Post Monsoon								
Lines	Start depth	End depth	Straight line distance	Vertical difference (start to finish)	Minimum depth on path	Maximum depth on path	Azimuth	Slope/ tilt
Line 10	0.47 m	20.20m	2.944 km	19.7 m	0.47 m	20.20 m	144° 48' 43.3"	0.38°
Line 30	0.41 m	20.44m	3.044 km	20.9 m	0.41 m	20.44 m	144° 49' 44.8"	0.39°
Line 50	0.15 m	21.41 m	4.62 km	21.3 m	0.15 m	21.48 m	144° 49' 3.5"	0.26°
Line 70	1.89 m	23.11m	5.947 km	25.0 m	1.89 m	23.11 m	144° 49' 52.5"	0.24°
Line 90	1.08 m	23.08m	6.787 km	22.0 m	1.08 m	23.08 m	144° 49' 48.8"	0.19°

The seabed up to 10 m contour in zone 3 is also rather steeper than the seabed further offshore like zone 1 and zone 2. But, the near-shore part of this zone has quite higher sediment erosion than other two zones. The seabed beyond 15 m contour does not show significant erosion or deposition. The 20 m contour is running at a distance of about 3.5 km from the shoreline. The total deposited sediment volume computed between pre- and post -monsoon for this zone is 64, 51,095 m^3. The total erosion is computed as 71, 90,239.46 m^3. The vertical profiles were analyzed between 1-30 transects in zone 1, 31-60 in zone 2 and 61- 91 in zone 3 during pre- and post-monsoons. The cross-sections are plotted and studied between water depth and horizontal distance referred from shore (Figure 8). Various seabed gradient parameters were derived from each transects for detailed analysis (Table 1).

It has been observed that the sediments deposited in the river mouth are comparatively higher than other location. The sediment accumulation could be assigned to sediments carried out by the river Vamsadhara. Generally, the point where river meets sea is a place of sedimentation zone which is governed by river flow, wave action and type of sediments. Temporal wave, current, tide measurements, river discharge measurements along with its numerical model studies will give a clear picture on rate of sediment deposit, sediment pattern and frequency at river mouth. The vertical profiles show the significant sediment deposition between line 30 and 50 in the near shore area. This indicates that the south of river mouth gets deposited significantly than the northern side of river mouth. Further study on near-shore drift current will help to understand the stability/mobility of sediment movement at this region (Rijn, 1984). The vertical profiles beyond line 68 show the erosion phenomenon in the near shore region. The reason for erosion in this region could be the northerly current movement. This study explains that though the near shore has northerly sediment drift, the river flow dominates towards south for particular extent and distributing the sediments during monsoon period.

CONCLUSIONS

The analysis of both pre- and post- monsoon bathymetry, demonstrates that the seabed has steeper slope in the near shore area till 10 m water depth and gentle slope further seaward. The depth contours are running parallel to the coast at all zones during both seasons. The overall data suggests that zone 2 and 3 experiences substantial sediment movement than zone 1. The zone 2 has major sediment deposition and zone 3 shows key erosion after monsoon. However, the sediment migration in these zones occurs predominantly in the near shore areas. Since the adequate natural depth subsists in the near shore, these zones are suitable for coastal developers to construct coastal based infrastructure such as fishing harbour, thermal power plant, desalination plant etc. In zone 1, the capital and maintenance dredging would be lesser which is suitable for intake and out fall pipeline systems for coastal based power plants and desalination systems. Though, the zone 2 is suitable for fishing harbour and construction of wharf/ jetties in the river banks, the capital and maintenance dredging operation will be little higher. However, a suitable dam at a distance of about 10 km from the river mouth will reduce the maintenance of dredging in the river mouth at zone 2. Further meteorological modeling would be required for planning of suitable break waters and other marine structures at all the three zones before construction.

Compliance with Ethical Standards

The authors declare that they have no conflict of interest and adhere to copyright norms.

REFERENCES

Arun, P.V., 2013. A comparative analysis of different DEM interpolation methods. The Egyptian J. Remote Sensing and Space Sci., 16, 133–139.

Christopher, J., Amante and Barry, W. Eakins, 2016.Accuracy of interpolated bathymetry in digital elevation models. J. Coastal Res., 76, 123-133.

Fennessy, M.S., Brueske, C.C. and Mitsch, W.J., 1994. Sediment deposition patterns in restored freshwater wetlands using sediment traps. Ecol. Engg., 3, 409–428.

Fröhle, P., and Kohlhase, S., 2004. The role of coastal engineering in integrated coastal zone management. Coastline Reports, 2, 167 – 173.

Hare, R., Eakins, B. and Amante, C., 2011. Modelling bathymetric uncertainty. Int. Hydrographic Rev., 6, 31–42.

Kader, A., Rahman, Z., Chowdhury, M.M., Hoque, E., Shyamal, and Chandra, B., 2013. Bathymetric study of the Bay of Bengal based on open source satellite and sounding data. Int. J. Geomatics and Geosci., 4, 116-124.

Lavery, A.C., Chu, D. and Moum, J.N., 2010. Measurements of acoustic scattering from zooplankton and oceanic microstructure using a broadband echosounder. ICES J. Marine Sci., 67, 379–394.

Lyzenga, D., 1985. Shallow-water bathymetry using combined Lidar and passive multispectral scanner data. Int. J. Remote Sensing, 6, 115-125.

Manik, H.M., Mamun, A. and Hestirianoto, T., 2014.Computation of single beam echo sounder signal for underwater objects detection and quantification. Int. J. Advanced Computer Sci. and Applications, 5(5), 94-97.

Mohamed, H., Negm, A., Zahran, M. and Oliver C. Saavedra, 2016. Bathymetry determination from high resolution satellite imagery using ensemble learning algorithms in shallow lakes: case study El-burullus lake. Int. J. of Envt. Sci. and Development, 7, 295-301.

Richard, A., Randall, T., Kerhin, Wells, D., and Cornwell, J., 2000. Bathymetric survey and sedimentation analysis of Loch Raven and Pretty boy reservoirs. Coastal and Estuarine Geology file report No. 99-4.

Rijn, V., 1984. Sediment transport, Part I: Bed Load Transport. J. Hydraulic Engg., 11, 1431-1456.

Sathishkumar, R., Gupta, T.V.S.P. and Babu, M.A., 2013. Echo sounder for seafloor objects detection and classification. J. Engg., Computers and Applied Sci., 2, 32-37.

Smith, W.H.F. and Marks, K.M., 2014. Seafloor in the Malaysia airlines flight MH370 search area. Trans. Am. Geophys. Union, 95, 173–174.

Thompson, D.M., Nathaniel, G., P. and Hansen, M., 2015. Analysis of bathymetric surveys to identify coastal vulnerabilities at Cape Canaveral, Florida. U.S. Department of the Interior, U.S. Geol. Surv., Open-File Report, 2015-1180, 1-24.

Yaacob, R., Ahmad, M.H., Mustapa, M.Z., Sapon, N., Shaari, H., Lokman Husain, M.L. and Nait, N., 2017. Study on coastal morphodynamics in the vicinity of coastal breakwater of Kuala besut during pre and post monsoon. Int. J. Advances in Sci. Engg. Tech, 5, 1-6.

Received on: 19.7.18; Revised on: 12.12.18; Accepted on: 21.12.18

J. Ind. Geophys. Union (March 2019)
v.23, no.2, pp: 173-180

Assessment of land degradation and desertification due to migration of sand and sand dunes in Beluguppa Mandal of Anantapur district (AP, India), using remote sensing and GIS techniques

B. Pradeep Kumar, K. Raghu Babu*, M. Rajasekhar and M. Ramachandra

Department of Geology, Yogi Vemana University, Kadapa, Andhra Pradesh, India.
*Corresponding author: dr.kraghu@gmail.com

ABSTRACT

Land degradation and desertification by means of sand migration, is one of the major problems facing the world today. Degradation is the process of conversion of productive land into waste land or degraded to desertified land. Degradation is influenced by the natural and anthropological causes in arid and semi-arid regions. According to a report by the Indian Space Research Organization (ISRO), 96 million hectors or 30 percent of India's agricultural land, is affected by the land degradation. The present study deals with identification, mapping and assessment of desertified areas in Beluguppa Mandal of Anantapur district, using geospatial techniques, aided by Landsat satellite images. The main reason for land degradation and desertification of this area is the migration of sand and sand dunes by aeolian process. Present study is focused to define the desertification in the study area during 18 years period beginning 2000 and onwards. Hence, temporal data of Landsat satellite image of past 18 years (i.e., 2000-2018), were collected and processed, to know how much of land is covered by migrated sand dunes and get desertified. By using geospatial technologies like satellite remote sensing (RS) and geographical information system (GIS), identification and mapping of desertified areas and progress of desertification were made in the present study. The results of the present study clearly reveal that 26 hectares of agriculture land is desertified in Srirangapuram village, and an area of 14 hectares of agriculture land is desertified in Narinjagundlapalle village in Beluguppa mandal of Anantapur district, A.P.

Key Words: Desertification, waste land, Semi-Arid, Landsat, Geospatial techniques, Anantapur district

INTRODUCTION

Land degradation and Desertification is one of the major environmental problem facing the world today. Nearly one fifth of the world population suffocates from desertification conditions. In fact, 33 percent of earth surface is degraded and exhibits desert like conditions. Arid, semi-arid and sub-humid regions all together form part of drylands. In the United Nations conference at Nairobi during 1977, the issue of Desertification (UNCOD) was described as the desertification happening because of destruction of biological potential of the land. Subsequently, the evolution of the desertification and its definition have been revised by many researchers (Thomas and Meddleton, 1994; Eswaran et al., 2001; Reynolds and Stafford-Smith, 2002; Anonymous, 2005; Budihal et al., 2006; Reynolds et al., 2007; Safriel, 2007; Ajai et al., 2009; Bai, et al., 2011; Arya et al., 2014; Amal Kar, 2016).

However most comprehensive and widely accepted definition of "Desertification" refers to land degradation happening in arid, semi-arid and sub-humid areas, resulting from the factors including climatic changes and human activities (UNEP 1992).The fact is that the ecosystem is seriously affected by the desertification (Lam et al., 2011). Many of the anthropogenic process, shifting of cultivation and deforestation, non-sustainable land use practices, mining, urbanization, road construction and other activities that sternly disturb the natural ecosystem. Therefore, combating desertification is essential to ensure the long term productivity of inhabited drylands (UNEP 1992). There are five types of indicators, (i) physical, (ii) climatic, (iii) biological, (iv) hydrological, and (v) socio-economic, which are used for monitoring and assessment of desertification or land degradation and their prediction (Dhinwa et al., 2016). In India, states like Rajasthan, Delhi, Gujarat, Goa, Maharashtra, Jammu and Kashmir, Odisha, Madhya Pradesh, Karnataka, Telangana and Andhra Pradesh are facing such problems like land degradation and desertification conditions.

The present study in Beluguppa Mandal of Anantapur district, situated in the south central part of Andhra Pradesh, falls under the semi-arid climatic regions. Drought and desertification are known as the common features of the arid and semi-arid regions, as mentioned before. The main reason of desertification in the study area is shifting of sand and sand dunes by the aeolian process. RS along with GIS have been used for desertification mapping the study area (Ajai et al., 2007, 2009). This mapping will help to take action plans and mitigation of desertification of the study area.

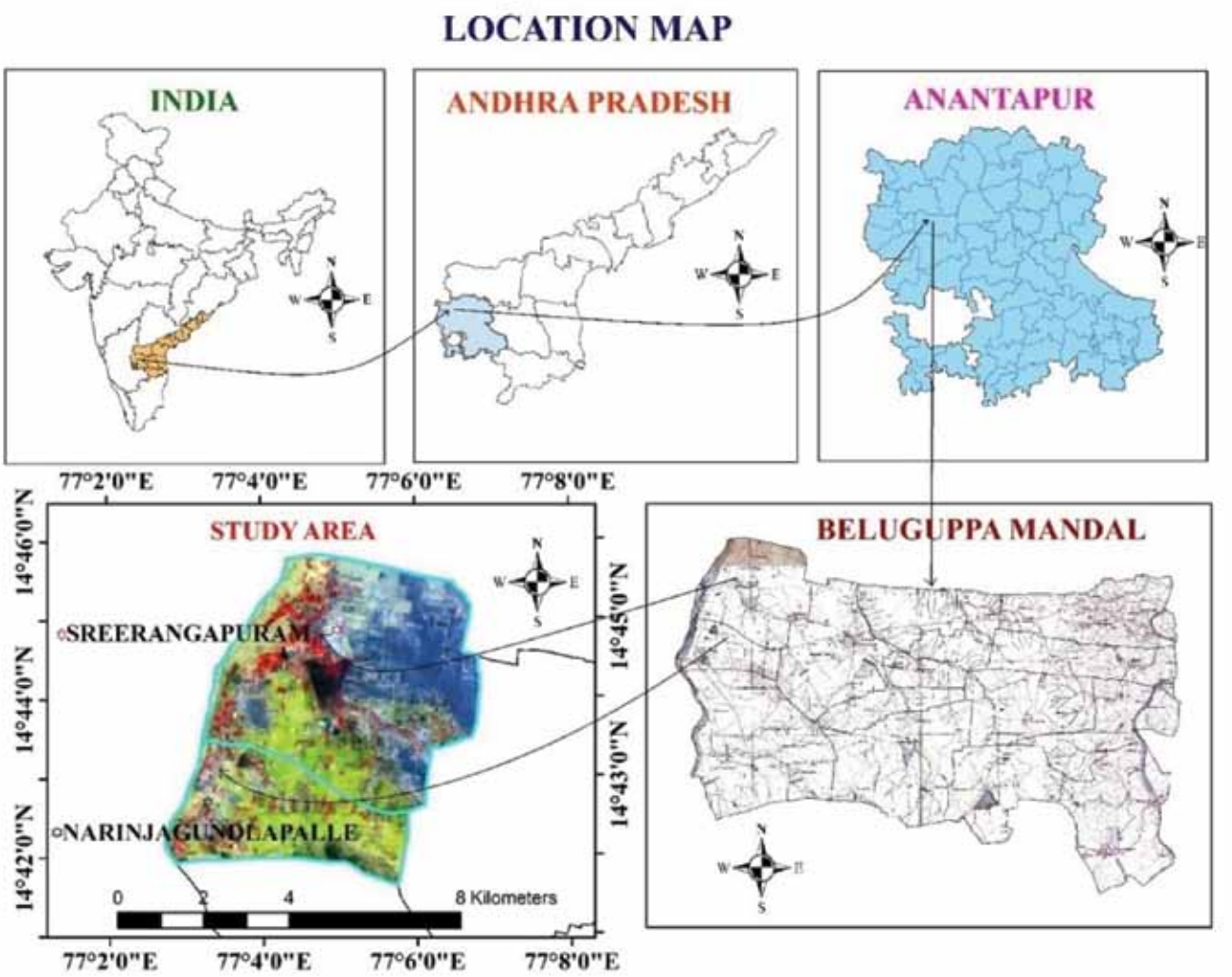

Figure 1. Location map of the study area.

STUDY AREA

Anantapur district which falls in the rain shadow area of Western Ghats and in the interior of Deccan Plateau, is the one of the chronically drought affected district in the country. The district is bounded by Kadapa District in the north-east, Kurnool District in the North, Chittoor District in the south-east, and Karnataka State on the West. Being located in the rain-shadow region of Andhra Pradesh, the district is drought-prone. It has geographical area of 19,130 Sq. Km. The district with an average annual rainfall of about 520 mm is lowest in the state and is identified as the second driest part of the country, next to Jaisalmer. Anantapur experience tropical climate with temperature ranging from 24 to 46° C in summer seasons which continuous from March to May. In Anantapur, most of the people depend on agriculture for their livelihood. In this district, there are two main cropping seasons: Kharif crop season (Monsoon) during July to September or October and Rabi season (winter) during November to April. The villages Sreerangapuram and Narinjagundlapalle of Beluguppa Mandal in the Anantapur district are the foci of the present study. The Mandal Beluguppa is bounded by Kanekal Mandal towards north, Kudair Mandal towards East, Kalyandurgam Mandal towards South, and Rayadurgam Mandal towards west. The study area Beluguppa Mandal is located in the Survey of India (SOI) topographical maps of 57 F/1, 57 F/2 and 57 F/6. (figure1). It has geographical area of 341 sq.km. There are two major rivers that flow through this Mandal; one is Hagari or Vedavathi and another one, Penna River. Hagari or Vedavathi River which flows on western part and Penna River is in eastern part, both are seasonal or ephemeral rivers and thus, they get dry during most of the year. Hagari River flows through Mandal's of Bommanahal, D-Herehal, Kanekal, Beluguppa, Gummaghatta and Brahmasamudram in Anantapur District and then enters in Karnataka state. Most of the Soil types in Beluguppa Mandal are Black Soils and Red soils.

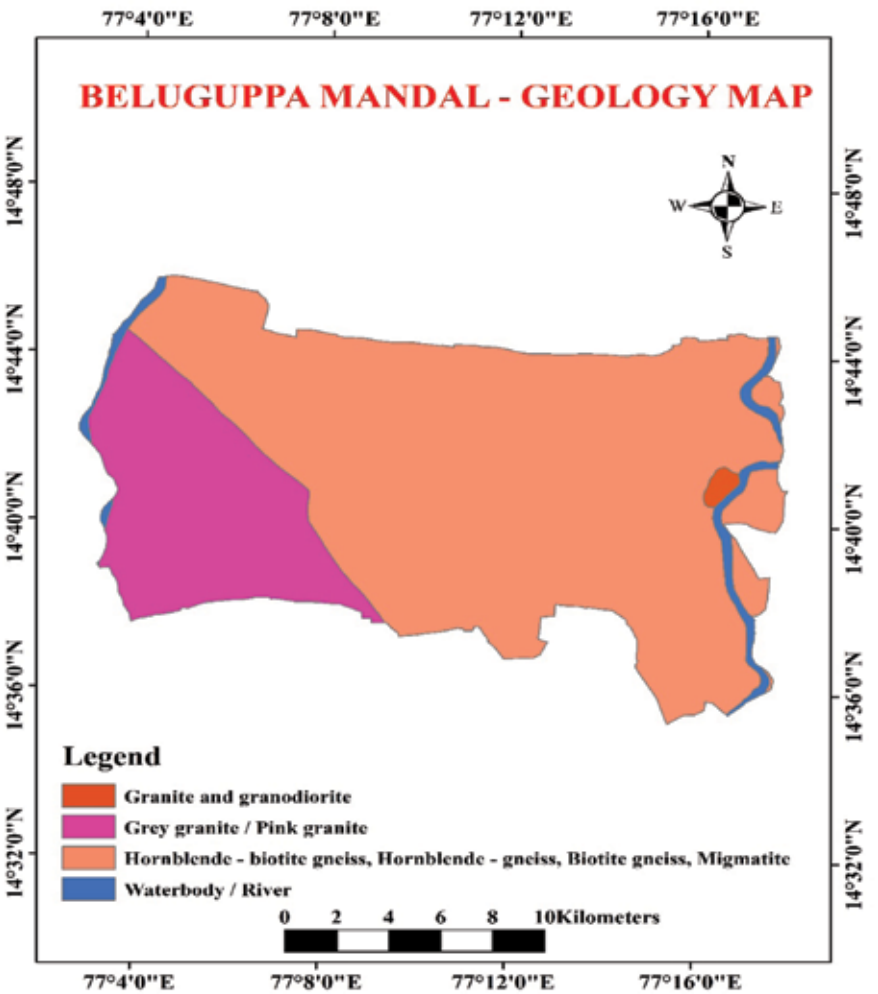

Figure 2. Geological map of the study area.

GEOLOGY OF THE STUDY AREA

Geological formations in Anantapur district are mainly divided into two distinct and well-marked groups: younger groups of sedimentary rocks belonging to the Proterozoic age and the older groups of metamorphic rocks that belong to the Archean age. Figure 2 shows the Geological map of the study area. The major rock types present in the study area are Peninsular Gneissic Complex consisting granite, granodiorite, felsic hornblende-biotite gneiss, hornblende gneiss, biotite gneiss and migmatites, which are present in eastern part of the study area and belong to Archean age. Grey granite/pink granite is present in the south western part of the study area.

GEOMORPHOLOGY

The villages of Beluguppa Mandal under the present study, are associated with active geomorphic changes by the aeolian processes. Sandy soils and alluvium is seen along the Hagari or the Vedavathi River areas. Here, the sand and sand dunes are spreaded by the action of wind. Sand and sand sheets or sand dunes are developed here under a range of environmental and climatic conditions. Sand dunes play very important role in the change of environmental ecosystems, which may be classified in many ways, like size and shape of the dunes, occurrence of environment, degree of internal complexity and the direction of wind. There are five main types of dunes, transverse, oblique, barchans, longitudinal and parabolic. Transverse and linear dunes are found in the area of the present study. Because of low rain fall in the area, the soil type is sandy soil. The low moisture also means that silt and sand-sized particles are easily blown away, while the remaining particles eventually form a tightly packed layer, known as desert pavement (Pradeep Kumar et al., 2018). The geomorphology of the study region shown in Figure 3.

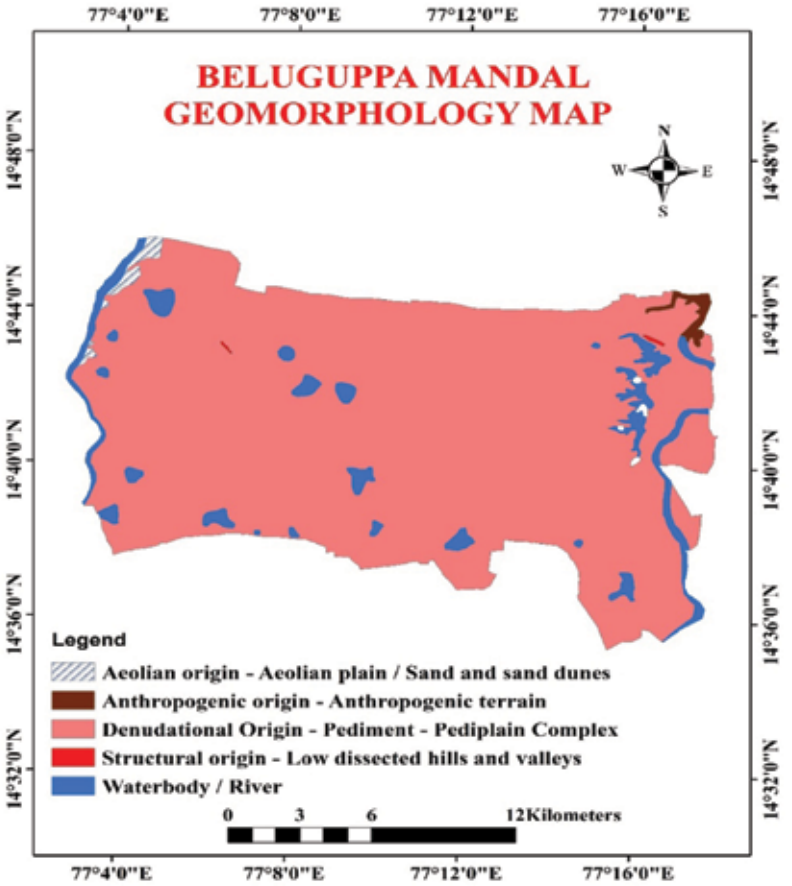

Figure 3. Geomorphology of the study area.

Table 1. Data used

	Data used	Spatial resolution	Year of acquisition	source
Satellite Data	Landsat 4-5	30m	2000	http://www.usgs.glovis.gov
	Landsat 7	30m	2010	
	Landsat 8	30m	2018	
Ancillary Data	SOI maps- 57F/1, 57F/2, 57F/6	1: 50, 000	1962	Survey of India
Collateral Data	Soils, Climate etc.			Groundwater Department, Anantapur District, Andhra Pradesh.

DATA

To prepare desertification status map of Sreerangapuram village of Beluguppa Mandal of Anantapur district (Andhra Pradesh, India), ancillary data like Survey of India (SOI) topo sheets, with 1: 50,000 scale and Landsat data, freely downloaded from (http://www.usgs.glovis.gov) is used. For the preparation of Geology and geomorphology map of the study area, required data has been downloaded from NRSC (National Remote Sensing Center) (http://www.nrsc.gov.in) website (Sources: Table 1).

METHODOLOGY

The present study aims to identify the land degradation or desertification areas of Sreerangapuram and Narinjagundlapalle villages of Beluguppa Mandal. Ancillary data of SOI (Survey of India) topographic maps with 1:50000 scales were used to demarcate the mandal boundary as the base map. Required remote sensing satellite data has been collected from USGS website. Landsat data (ETM+, TM and OLI) of eighteen years has been collected from 2000 to 2018 and layer stacking is done by using ERDAS Imagine

Table 2. Details of the Sreerangapuram and Narinjagundlapalle villages.

Name of the Village	Longitude	Latitude	Total areal extent
Sreerangapuram	77° 04' 02.36"	14° 44' 44.89"	27.06 Sq.km (2706 Hectares)
Narinjagundlapalle	77° 03' 08.10"	14° 42' 37.61"	11.35 Sq.km (1135 Hectares)

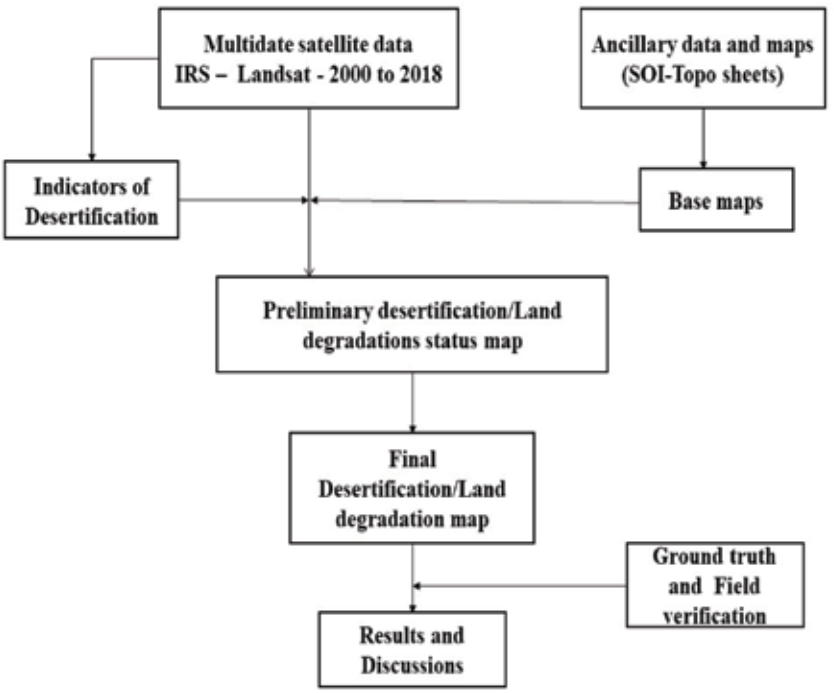

Figure 4. Methodology for preparing DSM (Desertification Status Map).

2014. Before processing the satellite images, the detailed field survey is carried out in the Beluguppa Mandal and GPS (Global Positioning System) points were collected for getting the exact locations of sand dunes or sand migrated areas (Table 2). The downloaded satellite imageries are layer stacked process through ERDAS Imagine 2014 software and given natural color compound 4, 3, 2, and 7, 6, 4. Using this high resolution data in Geographical Information System (GIS), shape files are created and the images were geo-referenced with coordinate system WGS1984. In the Landsat image, the Hagari or Vedavathi River is focused, where the sand is originated and migrated from the river banks to the adjoining villages. The red tone in the image, specifies the vegetation. Usually water absorbs light, so it appears black or dark blue, mud is in brown and suspended sand and sand dunes appears in white color. The detailed methodology is given in Figure 4.

Data has been processed for the preparation of DSM (Desertification Status Maps). Geometry calculation technique is used for knowing the rate of migration of sand/sand dunes. By using the ArcGIS 10.4, and Landsat imagery (layer stacked by using ERDAS), the study areas was demarcated and a polygon line was drawn through the edge of sand migrated areas.

RESULTS AND DISCUSSION

The study area of Sreerangapuram and Narinjagundlapalle villages in Beluguppa mandal with the land extent of 27.06 Sq. km and 11.35 Sq. km in area, desertified to the extent of about 2.73 Sq.km and 0.85 Sq. Km respectively. These areas are faced with migration of sand and sand dunes because land degradation and desertification. Hagari or Vedavathi River is the place of origination of the sands for this migration, which flows through the western side of the study region. During the months June to august strong surface winds flows west to eastern side, because of this strong surface winds, the sand has been migrated to the agricultural fields which reduced the soil fertility and caused desertification conditions. The satellite image (Figure 5) and Plate 1 give the clear picture of migration of sand and sand dunes in the study area. Different size and

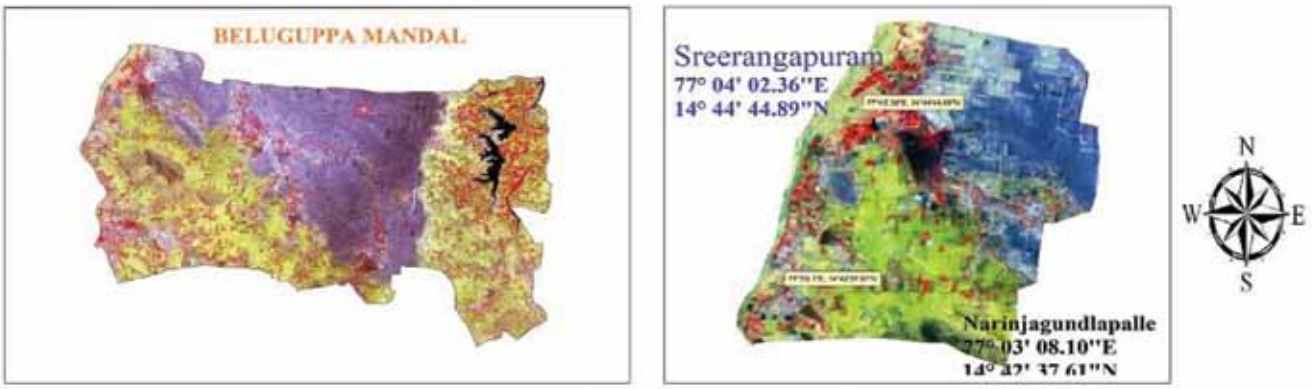

Figure 5. Satellite image of Beluguppa Mandal showing the sand migration/desertification.

Plate 1. Field photos collected in the sand migrated/desertified villages of Sreerangapuram and Narinjagundlapalle villages of Beluguppa Mandal

shapes of the sand dunes present in these villages, where linear and transverse type of dunes are very common. In the Landsat images, different colour indicates various things like: different shades of red and green colour indicates agricultural or vegetation, water absorbs light so it shows in blue or black in colour, brown or tan colour represent light vegetated ground and the sand is in yellow to white in colour (Ajai et al., 2009). Plate 1 shows the location of the study area and the intensity of sand migration in the field.

Changes in 18 years span are calculated through geometry calculation technique used in this study, which clearly reveal (Table 3) that the sand and sand dunes were migrated continuously and desertification process is very active in this areas. For example, the Sreerangapuram village has a total extent of 27.06 Sq.km area, in which the sand migrated area is about 2.44 Sq.km that means 244 hectares of land is desertified in the 2018 year. Similarly, Narinjagundlapalle village has a total extent of 11.35 Sq.km of land and in that, 0.49 sq.km of land is migrated, which means 49 hectares of land losses the soil fertility and desertified.

In a decade from 2000-2010, in Sreerangapuram village, sand migration increased from 2.44 Sq.km to 2.62 sq.km, which is about 262 hectares. Similarly, in Narinjagundlapalle village, it increased from 0.49 sq.km to 0.63 sq.km, i.e. 63 hectares of land is degraded/ desertified. In subsequent decade (from 2010 to 2018), in Sreerangapuram village , it further increased from

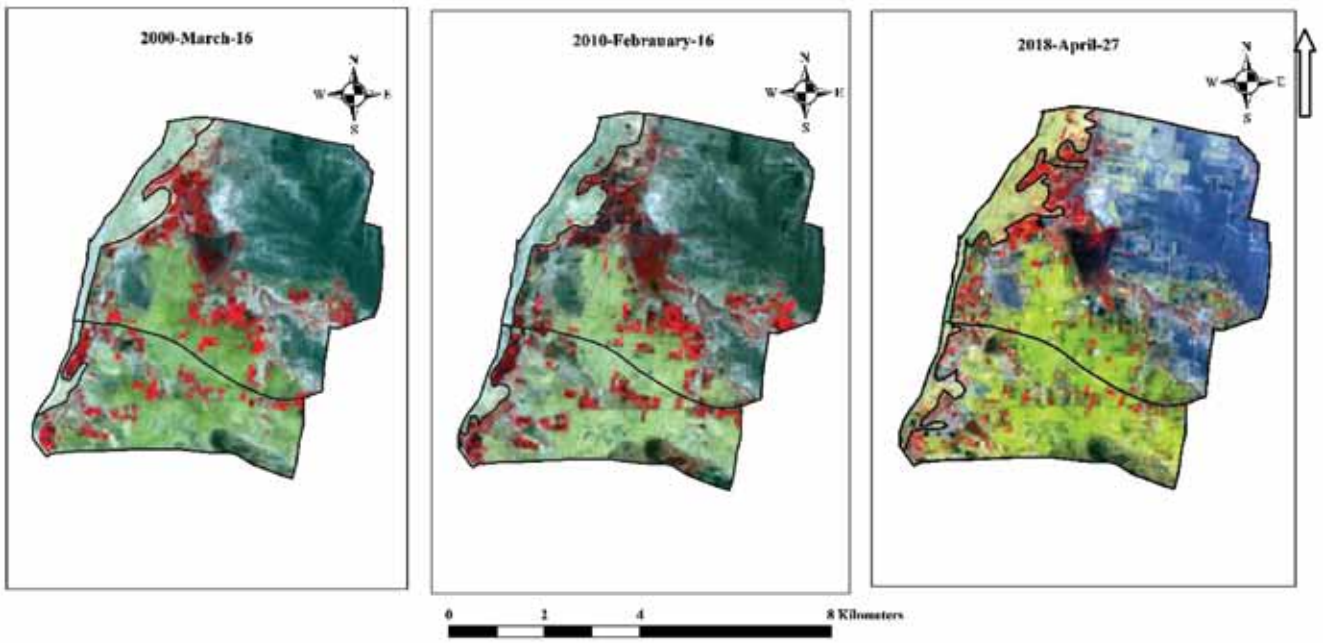

Figure 6. Temporal Landsat imagery of the year 2000, 2010 and 2018, showing migration of sand dunes in Sreerangapuram and Narinjagundlapalle villages

Table 3. Show the GEOMETRIC calculation for the migration of desertification

Village Name	Year			Result
	2000	2010	2018	
Sreerangapuram	2.44 Sq.km (244 Hectares)	2.62 Sq.km (262 Hectares)	2.73 Sq.km (273 Hectares)	Out of 2706 Hectares of land 273 Hectares of land is desertified.
Narinjagundlapalle	0.49 sq.km (49 Hectares)	0.63 Sq.km (63 Hectares)	0.85 Sq.km (85 Hectares)	Out of 1135 Hectares of land 85 Hectares of land is desertified.

2.62 Sq.km to 2.73 Sq.km, that would mean that up to 273 Hectares of the land is desertified. Similarly, in the Narinjagundlapalle village, it increased from 0.63 Sq.km to 0.85 Sq.km. Thus, this study suggests that the migration of sand/sand dunes and desertification has increased enormously, which is likely to pose serious threat to the agricultural as well as for livelihood.

CONCLUSION

In this study, temporal Landsat data from 2000 to 2018, has been used to analyses the trends in land degradation and desertification severity over the past eighteen years. The study reveals that the migration of sand and sand dunes is the main reason for desertification in Beluguppa Mandal of the Anantapur district. This migration is increasing at alarming rates. Remote Sensing Landsat data has been successfully used to develop Desertification Status Maps. The present study reveals that sand desertification in the study area increasing drastically by the change in environmental conditions. The Sreerangapuram village, it has changed by 0.29 sq. km in the past 18 years and similarly, Narinjagundlapalle villages by 0.36 sq.km in the past 18 years. These maps will be very useful to take action plans on controlling desertification. Some of the recommendations can include reduction of the surface wind speeds, in order to avoid sand migration on crop or agricultural field, proper irrigation plans to help to impede the desertification and rehabilitation of slightly or severely decertified lands for productive utilization for agriculture purpose.

ACKNOWLEDGEMENTS

We sincerely pay thanks to Department of Geology, Yogi Vemana University for providing the Laboratory, Remote Sensing data and ERDAS and GIS software during the progress of the work.

Compliance with Ethical Standards

The authors declare that they have no conflict of interest and adhere to copyright norms.

REFERENCES

Ajai, Arya, A.S., Dhinwa, P.S., Pathan, S.K. and Ganesh Raj, K., 2009. Desertification/ Land degradation status mapping of India. Curr. Sci., 97(10), 1479-1483.

Amal Kar, 2016. Desertification. Central Arid Zone Research Institute (CAZRI). January 2016). Yes Dee Publishing, Chennai, Editors: R.S. Dwivedi and P.S. Roy, 295-320.

Anonymous, 2005. Bellary district at a glance: 2003 – 2004. Directorate of economics and Statistics, Govt. of Karnataka, Bangalore.

Arya, V.S., Hardev Singh, Hooda, R.S. and Arya, A.S., 2014. Desertification change analysis in Siwalik Hills of Haryana using Geo-Informatics. The international archives of the Photogrammetry, Remote Sensing and Spatial information sciences, XL-8.

Bai, X.Y., Wang, S.J. and Xiong, K.N., 2011. Assessing spatial-yemporal evolution processes of Karst Rocky desertification land: Indications for restoration strategies. Land Degrad. Develop., DOI: 10.1002/ldr.1102.

Budihal, S.L., Ganesh Raj, k., Reddy, R.S., Natarajan, A., Paul, M.A., Bandyopadhyay, S., Thomas, J.V., Arya, A.S., and Ajai, 2006. Assessment and mapping of desertification status in Bellary District, Karnataka state, using IRS Data. International Society for Photogrammetry and Remote Sensing. ISPRS Archives, XXXVI(4).

Dhinwa, P.S., Dasgupta, A. and Ajai, 2016. Monitoring and assessment of desertification using satellite remote sensing. J. Geomatics, 10(2), 210-216.

Eswaran, H., Lal, R. and Reich, P.F., 2001. Land degradation: an overview. In: Bridges, E.M., I.D. Hannam, L.R. Oldeman, F.W.T. Pening de Vries, S.J. Scherr, and S. Sompatpanit (eds.). Responses to Land Degradation. Proc. 2nd. International Conference on Land Degradation and Desertification, Khon Kaen, Thailand. Oxford Press, New Delhi, India.

Lam, D.K., Remmel, T.K. and Drener, T.D., 2011. Tracking desertification in California using remote sensing: A sand Dune Encroachment Approach. Remote Sens. 3, 1-13.

Pradeep Kumar, B., Raghu babu, K., Rajasekhar, M., Ramachandra, M. and Siva Kumar Reddy, 2018. P – Assessment of land degradation and desertification due to migration of sand dunes- a case study in Bommanahal Mandal, Anantapur district, Andhrapradesh, India using Remote Sensing and GIS techniques, 6(6), 1144- 1151, E-ISSN-2321-9637 –IJRAT

Reynolds, J.F. and Stafford-Smith, M., 2002. Global Desertification: Do Humans Create Deserts? In: Stafford-Smith, M. and Reynolds, J.F., Eds., Do Humans Create Deserts? Dahlem University Press, Berlin, 1-22.

Reynolds, J.F., Smith, D.M., Lambin, E.F., Turner, B.L.2nd., Mortimore, M., Batterbury, S.P., Downing, T.E., Dowlatabadi, H., Fernández, R.J., Herrick, J.E., Huber-Sannwald, E., Jiang, H., Leemans, R., Lynam, T., Maestre, F.T., Ayarza, M. and Walker, B., 2007. Global Desertification: Building a Science for Dryland Development Science 316, 847. DOI: 10.1126/science.1131634.

Safriel, U.N., 2007. The assessment of global trends in land degradation. In: Sivakumar M.V.K., Ndiang'ui N. (eds) Climate and Land Degradation. Environmental Science and Engineering (Environmental Science). Springer, Berlin, Heidelberg.

Thomas, D.S.G. and Middleton, N.J., 1994. Desertification: exploding the myth. John Wiley and Sons Ltd., Chichester, UK. Xiv+194 pages. ISBN 0-471-94815-2.

UNEP, 1992. A status of desertification and implementation of the United Nations plan of action to combat desertification. Report of the executive director, Nairobi, United Nations Environment Programme.

Received on: 5.12.19; Revised on: 16.12.19; Accepted on: 22.2.19

J. Ind. Geophys. Union (March 2019)
v.23, no.2, pp: 181-197

SHEAR ZONES: A Tutorial[+]

T.R.K. Chetty
CSIR- National Geophysical Research Institute, Hyderabad – 500 007
Email: trkchetty@gmail.com

1. Introduction

In the last three decades, some revolutionary concepts have emerged which led to change in earlier thinking significantly in Structural geology and also have important implications to the scenario of Global tectonics. The notable one amongst them is the Shear Zones. In the light of their significance, several areas are being revisited, studied and reinterpreted. It has been well recognized that large tracts of Archean terrains were reworked during the early Proterozoic in many parts of the world. In many cases, the reworking occurred along essentially linear zones in the earth's crust, found to be made up in detail of many shear zones, often recording large amounts of overthrust or transcurrent displacement. Individually, shear zones like faults may be compressional (thrust), extensional (normal or lag), strike-slip or oblique-slip. The determination of the movement direction, not always obvious, is critical to the kinematic interpretation. The most useful guide to the movement direction is the orientation of elongation lineations (parallel to the axis of greatest extension) in zones of high strain.

2. Significance of shear zones

Shear zones are useful in several ways. They are: (i) the prime targets for mineral exploration. Mineralisation is commonly associated with specific geometrical features such as bends and intersections, and (ii) the sites of very large strain. They offer some of the strongest tools to unravel the complex deformation features of the Earth's crust, (iii) the sites for igneous intrusions like alkaline rocks and anorthosites, etc., (iv) the only permeable pathways for the large continental crust and they act as effective fluid conduits during active deformation, (v) the potential hazardous sites because of enhanced concentration of radon gas in soils, sometimes related to the uranium concentration, (vi) the belts of extensive mylonitisation, repeated reactivation and chemical transfer, (vii) a possible correlation between the shear zone and U and The content suggests a progressive increase in U enrichment with deformation, (viii) the terrane boundaries, (ix) the zones of marked geophysical anomalies, (x) the hazardous sites in terms of seismicity and Engineering geology, (xi) the zones of grain size reduction and metamorphic retrogression and finally, (xii) the shear zones form natural laboratories for understanding fluid transport, deformation and metamorphic processes.

The structure of shear zones is typically dependent on fluid-rock ratios. The mineralogical and chemical changes in shear zone rocks are a function of strain and fluid transport. Shear zone rocks show substantial adjustments in elements such as TiO_2,, Fe_2O_3, FeO, MnO, MgO, CaO, Na_2O and K_2O. For instance, mylonites, the characteristic features of ductile shear zones, are enriched in - TiO_2, P_2O_5, MnO, Zr, Y, V, Fe_2O_3 and MgO; and depleted in alkalies and silica. From the foregoing, it is clear that - *"Sufficient care should be taken in sampling of rock specimens for laboratory studies. Samples from shear zones must be treated separately. Interpretations in Geosciences, be it geological, geochemical, geochronological or geophysical, are likely to be misled if the presence of shear zones is not considered."*

3. Definition

Shear zones are by definition much more strongly deformed than the surrounding rocks. It is a zone of faulting in which the displacement is accommodated across and along a zone rather than on a single plane. A shear zone is a tabular zone in which strain is notably higher than in the surrounding rock. In other words, it is a planar zone of concentrated (dominantly simple shear) deformation which by itself, or in association with other zones, helps to accommodate, or wholly accommodates an imposed regional or local, strain rate beyond the strength of the country rock. Shear zones are typically planar to gently curved, but some of them show complex geometries.

[+] Invited Tutorial

These are typically produced when volumes of rock, metamorphosed or intruded at high temperatures, are reworked under lower temperature conditions. Traditionally, only ductile shear zones were only described as shear zones to distinguish them from clean-cut faults. In modern terminology, the term shear zone encompasses both clean-cut faults and ductile shear zones (Ramsay, 1980). The shear zones range in scale from microscopic or grain scale to the scale of a few hundred kilometers in length and a few kilometers in width, as reported from the Precambrian gneisses of Greenland (Bak et al., 1975). They exist at all scales: microscopic or grain scale; a few hundred kms in length and a few kms in width. They are long relative to their width, generally 5:1. They can extend up to mantle depths. Shear zones can occur as intersecting and anastomosing pattern, depending on the nature: Compressional (Thrust), extensional (Normal or Lag), Strike-Slip or Oblique Slip (Wrench).

Traditionally, shear zones are believed not to show any loss of coherence, between the wall rock and the shear zone itself. A marker layer, though deflected in the shear zone, should not be broken at the contact. Therefore, a ductile shear zone cannot be regarded as a fault in the ordinary sense of the term. However, the distinction is difficult, if not impossible, for most field examples especially when the tangential displacement is very large in comparison with the width of the ductile zone. In such shear zones marker units may undergo extensive boudinage and the continuity of the markers may be unrecognizable in the mylonite belt. Following Ramsay (1980), we can designate this entire class of structures as shear zones, with faults and ductile shear zones as the end members. It also depends on the scale we are looking at these structures. A line, for instance, on a million-scale map represents nearly 1 km width on the ground, which indicates that it is a zone of planar elements or crushed material. Even on outcrop scale, although we find it as a line in the field, if we project the same on to a microscopic scale, it invariably becomes a zone. So, it is justified to refer the entire spectrum of faults as shear zones.

4. Recognition of shear zones

Identification of shear zones is not simple. Field geologist's perspective is, in general, limited to out crop scale. The shear zones are invariably marked by heterogeneous strain and in association with the common occurrence of less deformed areas of different sizes. Misidentification of mylonites, pseudotachylites, schists is also a common feature among geologists. It may be noted that large shear zones can be identified easily on maps of regional scale particularly through satellite images. However, it is cautioned that shear zones with steep to moderate dips are distinctly visible while the flat lying shear zones, which are common, would not be easily recognisable on the image. It is observed that the concept based approach in mapping shear zones has become more successful. First, identify the shear zones in the form of lineaments on the image and start looking for evidences in the field. Identification of shear zones is crucial. If not, one may be misled totally in their interpretation be it in structural geology, P-T-t history, geochemical signatures, isotopic systematics or geophysical anomalies.

It may be noted that shear zones may act as both closed and open geochemical systems, irrespective of their size. The geometry of individual shear zones is dependent on both the degree of pre-existing anisotropy and the orientation of the new anisotropy with respect to strain field. It is also recognized that apparent multiple deformation events occur within a shear zone arising from single progressive deformation event.

"Several areas have been revisited, changed earlier thinking and reinterpreted."

5. Classification of shear zones

The shear zones can be classified into three classes (Figure 1).

(i) Faults / Brittle shear zones – are a special variety of shear zones, where a clear discontinuity exists between the sides of the zone and the shear zone walls are almost unstrained or perhaps brecciated. Gouges and cataclasites are produced. As a rule of thumb, brittle shear zones form in the upper crust at temperatures below about 300° C.

(ii) Brittle-ductile shear zones – are associated with some ductile deformation in the walls, which show permanent strain for a distance of up to 10 meters on either side of the fault break. There is a possibility that the ductile part of the deformation history formed at a different time from that of the fault discontinuity. Another type of brittle-ductile shear zone is the extension failure. The deformation zone shows an en-echelon array of extension openings, usually filled with fibrous crystalline material. The openings usually make angle of 45^0 or more with the shear zone and some times shearing in a sigmoidal form.

(iii) Ductile shear zones – are those in that the deformation and differential displacement of the walls is accomplished entirely by ductile flow. No discontinuities can be observed on the scale of the rock outcrop. Marker layers in the country rock can be traced through the shear zone; they are deflected and may change in their thickness, but mostly they remain unbroken. Ductile shear zones are extremely common in deformed crystalline basement rocks (granites, gabbros, gneisses, etc.) of all grades of metamorphism. Crystal plastic deformation processes, e.g: pressure solution, dislocation creep, grain boundary sliding and diffusion, along with recrystallization and neomineralization, dominate to make mylonites; which are characteristics of ductile shear zones. Field examples of all the varieties are provided in Figure 2.

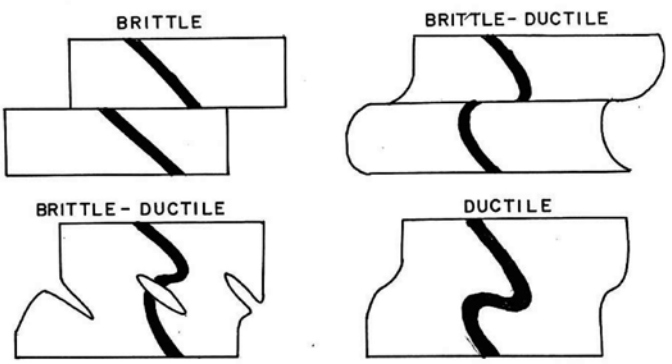

Figure 1. Diagrammatic classification of shear zones.

Figure 2. Field examples of shear zones in granitic rocks around Hyderabad: (a) Brittle shear zone; (b) Brittle-ductile shear zone; and (c) Ductile shear zone

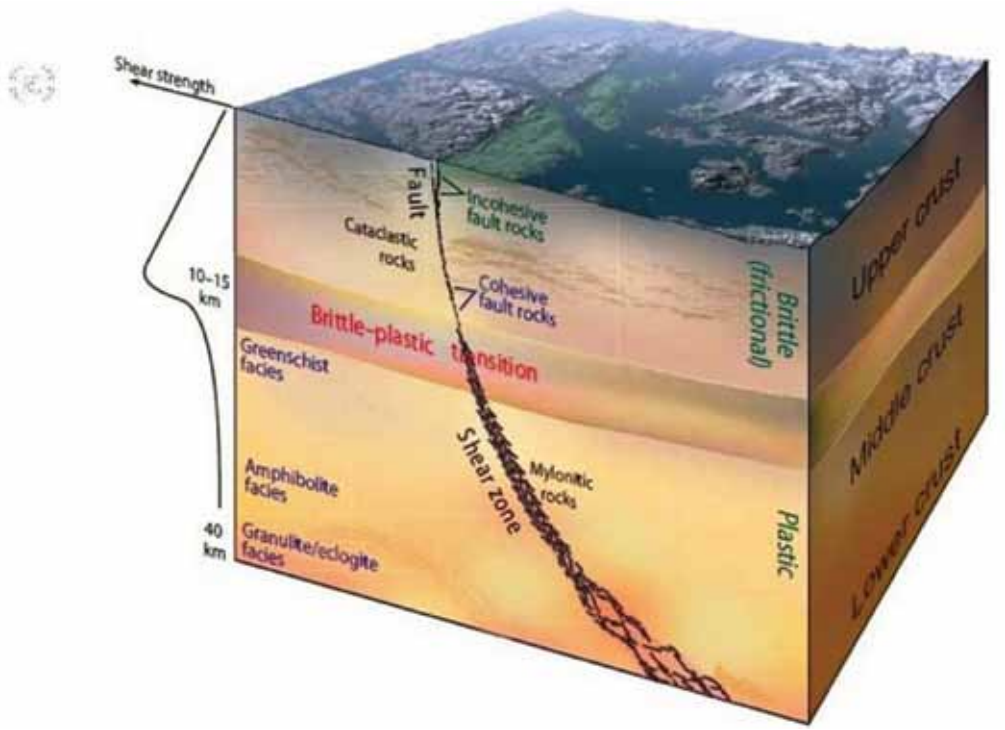

Figure 3. Simplified model of the connection between faults, which normally form in the upper crust, and the classic ductile shear zones. The transition is gradual and known as the brittle–plastic transition.The depth depends on the temperature gradient and the mineralogy of the crust. For granitic rocks it normally occurs in the range of 10–15 km (source: Fossen, 2010).

In general, ductile – and brittle-ductile varieties are the deep level counterparts of brittle shear zones and faults at higher levels in the crust. These shear zones may range in scale from the microscopic or grain scale to the scale of few 100 km in length and a few metres or a few tens of kilometers in width, eg. Precambrian gneisses of Greenland (Bak et al., 1975) and crustal shear zones in Africa (Daly, 1986). Ductile shear zones can be further classified into two types: (a) discrete shear zones which cut across rocks, otherwise undeformed by the particular phase of deformation; and (b) shear zones located at the margins of mobile belts or at the margins of sub zones within the belts (Coward, 1980). The former are unrelated to the local tectonics and the later develop necessarily to maintain compatibility between zones of different intensities of deformation. Ductile shear zones are formed at mid-crustal levels of around 15-20 km depth as indicated by the high metamorphic grade of the associated fabrics. There is increasing evidence from deep seismic reflection surveys and theoretical considerations of crustal rheology that major detachment horizons of this kind exist within middle and lower crust. It should be borne in mind that faults and shear zones are closely related structures. In fact, the general perception of shear zones as the deep counterpart or extension of faults is well illustrated in Figure 3. The depth depends on the temperature gradient and the mineralogy of the crust. For granitic rocks it normally occurs in the range of 10–15 km. Both shear zones and faults are strain localization structures. Both involve displacement parallel to the walls, and both tend to grow in width and length during displacement accumulation.

6. General characteristics of Shear Zones

Typically, the shear zones are characterized by the development of mylonitic fabric – in granitic material for instance, the closely spaced foliation is defined by alternating layers of recrystallized quartz grains, milky ribbons of fine grained, recrystallized feldspar and fine platy biotite. The following are the common characteristics in shear zone rocks: (a) The foliation surfaces contain a very strong lineation (stretching lineation) defined by the elongation (and / or boudinage) of minerals like hornblende, micas, quartz, feldspar, etc. as well as mineral aggregates, (b) S-C mylonites are very common, indicating non-coaxial deformation history, (c) The amount of strain is highly variable resulting in the occurrence of mylonitic series (Proto- to ultramylonite), (d) Grain size reduction is typical, (e) Retrogression is usual, (f) Development of new grain-growth, particularly biotite, kyanite, staurolite and muscovite, (g) The shear zones occur as intersection and anastomosing patterns, (h) Generally, they are associated with large geophysical anomalies, and (i) Association with igneous intrusions is a common feature. The typical

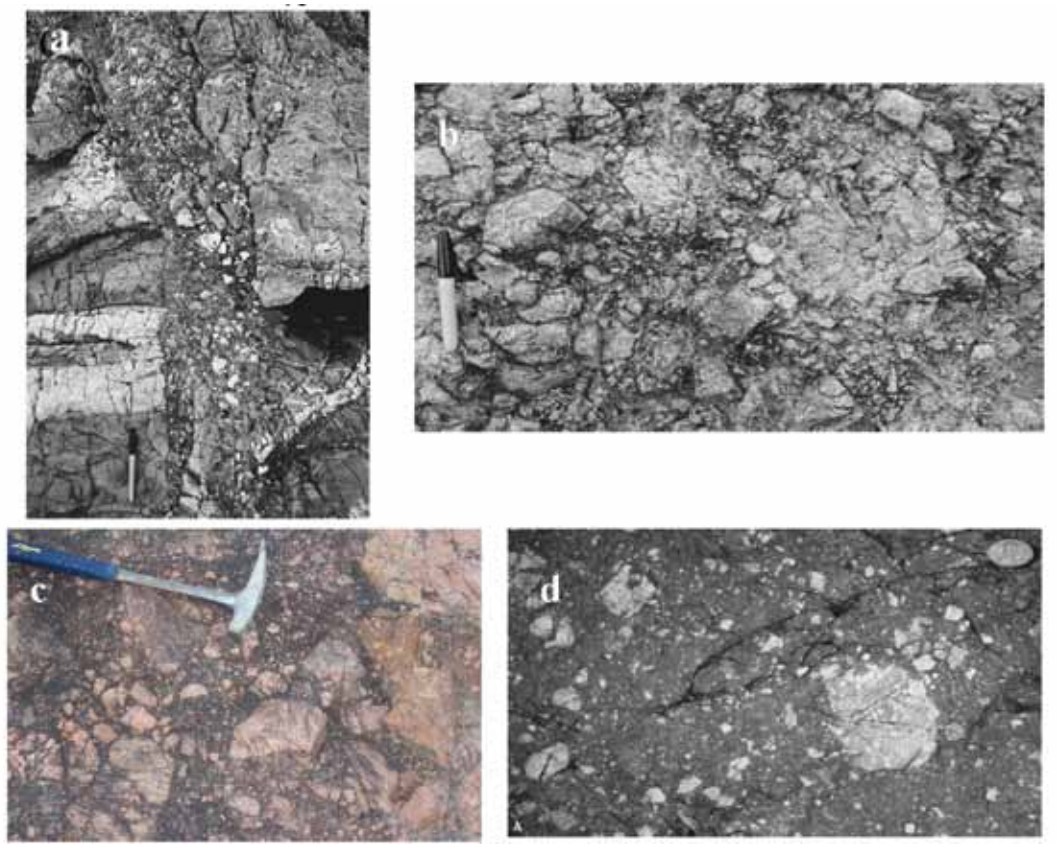

Figure 4. (a) Brittle shear zone cutting across the layered sequence, (b) Brecciated granite, (c) Fault gouge, (d) Cataclasite.

features associated with different types of shear zones are illustrated below.

6.1 Brittle Shear Zones

Brittle shear zones form in the shallow parts of the crust, generally within 5-10 km of the Earth's surface, where deformation is dominated by brittle mechanisms, such as fracturing and faulting. Brittle deformation is also favoured by the relatively rapid strain rates that occur during seismic events (many earthquakes occur within the upper 10-15 km of the crust). Accordingly, and shear fractures, and brecciation. Brittle shear zones can also be termed as fault zones and are characterized by closely spaced faults, numerous joints marked by fault gouge and other breccia series (Figure 4).

Breccia

Brecciated rock is composed of angular fragments of host rock greater than about 1 mm, and as much as several meters across and is noncohesive. Creation of a random array of nonsystematic mesoscopic fractures that surround angular blocks of rock creates fault breccia. In general, breccias have random fabrics, implying that they do not contain a distinctive foliation. Continued displacement across the fault zone may crush and further fragment breccia, and/or may break off microscopic asperities protruding from slip surfaces in the fault zone, thereby creating a fine-grained rock flour described as fault gouge. Gouge and (micro) breccia are noncohesive fault rocks, meaning that they easily fall apart when collected at a fault zone or hit with a hammer.

Gouge

Gouge is incohesive fault rock that result from shallow level movements in a zone. Sometimes, they have a weak foliation. They tend to be limited to narrow zones often within wider mylonitic or cataclastic zones. Gouge is a rock composed of material, whose grain size has been mechanically reduced by pulverization. Grains in fault gouge are less than about 1 mm in diameter. Like breccia, gouge is noncohesive. Shearing of gouge along a fault surface during progressive movement may often create foliation within the gouge. Clay formed by alteration of silicate minerals in fault zones may be difficult to distinguish from true gouge.

Figure 5. Brittle-ductile shear zones in the field defined by en echelon quartz veins. A single set of veins defining a shear zone crossing diagonally across the photograph.

Cataclasite

Cataclasite is a cohesive brittle fault rock that differs from gouge or breccia in that the fragments interlock, allowing the fragmented rock to remain coherent even without cementation. Cataclasites generally have random fabrics (i.e., no strong foliation or lineation). A cataclasite lacks a foliation and has angular clasts in a fine-grained matrix which consists of newly developed minerals, mainly white mica, chlorite and/or calcite. A similar classification to that used in mylonites is also applied to cataclasites, based on the proportion of matrix in the rock. In protocataclasite, 10–50% of the rock is matrix; in cataclasite (*sensu stricto*) 50–90% is matrix; and in ultracataclasite, 90–100% is matrix. This can also grade into mylonite after initial cataclasis. Unlike breccia, it is a solid rock that does not disintegrate when struck with a hammer.

Pseudotachylites

Pseudotachylites result from melting along sliding planes during an earthquake event. It requires dry rock and is limited to the seismogenic zone. The melt is ejected from the generating planes into adjacent rocks. Consequently, these appear as small, cross cutting black veins of igneous material in the shear zone.

6.2 Brittle-ductile shear zones

Brittle-ductile shear zones (Figure 5) form when (i) the physical conditions permit brittle and ductile deformation to occur at the same time, (ii) different parts of a rock have different mechanical properties, (iii) a shear zone "strain hardens," (iv) a short-term change in physical conditions, such as in strain rate, causes the rock to switch from ductile to brittle mechanisms or vice versa, (v) physical conditions change systematically during deformation.

6.3 Ductile Shear Zones

Ductile shear zones are formed by shearing under ductile conditions, generally in the middle to lower crust (10 – 20km) and in the asthenosphere. For the most common crustal rocks (e.g., granite), brittle deformation at shallow crustal levels gives way downward into ductile deformation at the brittle-ductile transition. Most ductile shear zones form under metamorphic conditions, and the resulting sheared rocks are metamorphic in character, typically possessing foliation and metamorphic minerals. Rocks within a ductile shear zone may be so changed by the intense shear, by metamorphism, and by fluids passing through the shear zone that it becomes very difficult, if not impossible, to decipher the original rock—the protolith.

Mylonites are the most commonly encountered rocks in ductile shear zones and also the one most likely to be misidentified as schist. There is one additional fault rock, a pseudotachylite which is a frictional melt generated during the earthquake rupture of strong dry rocks in the upper crust. Moine Thrust belt is the classic area from where much of the structural geology has come while studying this belt a century back – a famous geologist by name Lapworth (1885) has come across a peculiar rock type

lying mostly along the thrust plane. Lapworth describes the rocks in the following way. "The most intense mechanical metamorphism occurs along the grand disloction (thrust planes), where the gneisses and pegmatites resting on those planes are crushed, dragged and ground out into a finely laminated schist, composed of shattered fragments of the original crystals of the rock set in a cement of secondary quartz, the lamination being defined by minute inosculating lines (fluxion lines) of Kaolin or chloritic material and secondary crystals of mica". Then he has coined the term "Mylonite" for such rock type and defined it, for the first time, as "Mylonites are the schist-like products of dominantly ductile reworking of the country rock within a shear zone". Depending on the size of the zone, mylonites can vary in width from centimeters to tens of kilometers. They are further subdivided into three broad classes, depending on the degree of reworking. They are, with increasing shear strain: Protomylonite, mylonite and ultramylonite. The boundary between each class is set by the percentage of reworked matrix, relative to clasts of parent country rock minerals. In a protomylonite, the matrix makes up less than 25%, a mylonite between 25% and 90% and ultramylonite more than 90%. The term ultramylonite does not necessarily mean an ultrafine grain size always. It is simply the degree of reworking. Thus ultramylonites mark the most highly strained areas within a shear zone.

The classical ideas about the process of development of mylonites have been greatly modified subsequently and were demonstrated that the dominant process of grain refinement in mylonites is by syntectonic recrystallisation and neomineralization. The well-known mortar structure of mylonites develops by syntectonic recrystallisation and not by cataclastic processes. Typically, a mylonite consists of elongated and drawn out clasts (augen) in a fine-grained matrix. It is the matrix that flows by crystal processes. The clasts tend to be the stronger minerals, for example in the granite gneiss, the stronger K-feldspar clasts form the augen and the softer phases, quartz and phyllosilicates form the matrix. The phyllosilicate orientation and the elongation of the matrix quartz causes the mylonitic foliation. At low temperatures, e.g. greenschist facies, the feldspar clasts, both plagioclase and K-feldspar, elongate by fracturing and the fragments retrogress to a white mica, chlorite, quartz assemblage which is incorporated into the matrix. As the change from mylonite to ultramylonite is effected, the granite gneiss changes into a finely laminated phyllosilicate quartz assemblage which may resemble a slate and which deforms ductile environment. The effect of retrogression is to change the brittle feldspar into a weaker and consequently ductile mineral assemblage. At higher temperatures, the feldspar deforms ductilely, plastically elongate and undergo grain refinement by recrystallisation, rather than by fracturing and neomineralization. Quartz grains always refine by recrystallisation under all mylonite conditions. In a quartzite or quartz bands the harder grains of quartz may remain as elongate augens and the softest as ribbons.

The diagnostic features of mylonites include intrafolial folds, rotated clasts, internal shear bands forming a second foliation and oblique grain growth, all of which have a constant sense of symmetry related to the direction of shearing. Also, mylonites have another feature viz., a stretching lineation, which is absent in schists. Two lineations are encountered in mylonites, one unique to mylonites, the stretching lineation, and the other, an intersection lineation, which is found in both mylonites and schists. The later results from the intersection of one foliation on the plane of another. This lineation has no kinematic significance. The stretching lineation indicates the direction of flow in a mylonite. This can be distinguished from an intersecting lineation as it is marked by elongate minerals such as hornblende or by elongated or pulled out clasts such as feldspars, quartz and calcite.

7. Depth of shear zones

The brittle to ductile shear zone rock sequence: gouge-cataclasite-mylonite forms a depth sequence (Figure 6). Gouge forms at shallow crustal depths where temperatures are so low that clay mineral growth in the matrix and precipitation from fluids is not sufficient to "weld" the fault rock together. This is likely to be favoured by temperatures lower than 100-150^{o}C. At higher temperatures, welding occurs and a cataclasite would be developed. The cataclastic / mylonite boundary is taken as the temperature at which the ductile / brittle transition occurs in a granite type mineral assemblage. This was first noted by Sibson (1977) and the transition ranges between 250-300^{o}C. This implies that the earthquakes, which are a manifestation of catastrophic brittle failure, occur at temperatures lower than the transition range. This is confirmed by later seismic studies.

Considering the above, the depth of shear zones becomes a controversial issue, especially for strike slip zones which cannot be directly imaged by reflection seismics. However, the depth can be worked out indirectly from the depth of normal and thrust movements, but in general, all strike slip zones are coupled with them. The depth to which individual normal and thrust faults, can reasonably be estimated. For example, the faults cutting through the upper mantle are rare, many of them decouple along the Moho and many others within the crust. Therefore, few strike slip zones cut into the mantle, more end at the Moho and most end within the midcrust. From these considerations, three possible main orders can be outlined: (a) First order – major strike slip mobile zones coupled to entire thrust and extensional (basin)

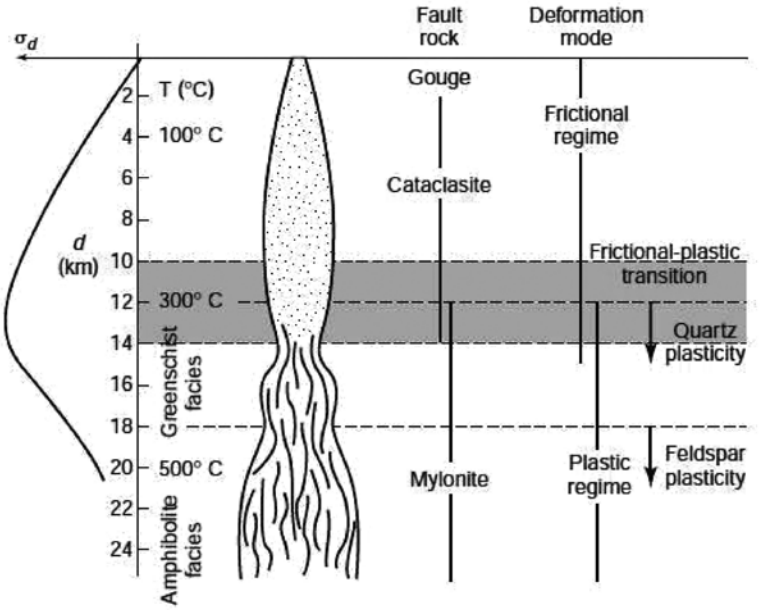

Figure 6. Integrated model for a displacement zone that cuts deep into the crust, showing the frictional and plastic regimes, the frictional–plastic transition, and crustal strength (σd); *this is sometimes* called the Sibson-Scholz fault model. Fault rocks typically found at crustal levels are indicated.

belts (orogenic belts) and the coupling of which effectively divides the continental lithosphere into platelets, (b) Second order – main strike slip shear zones occur within a thrust or extensional belt and terminate at the Moho, and (c) Third order – minor, shorter zones within these belts that terminate at shallower depths. They are the most abundant. The variation in depth will influence magma generation within a strike slip zone and also the source of deep fluids entering an individual zone or an array. It will also have a bearing on reactivation tectonics.

The model for depth variation in shear zones was formalized by Sibson (1977), who shows that a shear zone broadens with depth (Figure 6). The reason for the broadening, especially a ductile one, could be due to relative differences in strength (viscosity) between fault rocks and the enveloping rock with depth. This is based on experimental as well as from the field evidences. For instance, the shear zones in the Moine Thrust in N.W. Scotland, are typically less than 10 m wide in shallow zones, while the deeper shear zones extend over 100 m in width.

If a major, deep shear zone has a vertical component of movement, it will exhume itself during movement and bring up the deeper part of the zone. The prime example for this is the Alpine Fault in New Zealand. However, there is insufficient data to formalize a depth-width relationship. The fault rock profile across the Alpine fault shows a temperature increase into the hanging wall. Uplift has concentrated on the footwall and parts of the zone are progressively accreted on to the hanging wall as uplift progresses. Consequently the lateral sequence cataclasite-augen-mylonite-green, mylonite-schistose, mylonite-early schist is a depth sequence arising from the accretion. The zone is approximately 200 m wide in cataclastic field widening to 700 m at the ductile / brittle transition as indicated by the augen and green mylonites and finally widening to 1 km at the temperature at which the early schists developed (Johnson and White, 1982). However, there is insufficient data to formalize a depth-width relationship.

8. Development of folds in shear zones

Flow within a shear/mylonite zone is extremely inhomogeneous because of variations in the competency of individual bands that may reflect variations in grain size – fine grained bands of quartz concentrate deformation to a greater extent than coarse grained ones. The result of this is to develop local dilatant and compressive zones in a mylonite. The former may concentrate fluids and the latter will initiate intrafolial folds as shown in Figure 7.

The folds develop in shear zones as simple buckles with their axes perpendicular to the movement direction, i.e. perpendicular to the stretching lineation, which they fold. The axial plane of these folds rotates from an inclined position at about 45° to the foliation into parallelism with it as shear strain increases. The short limb is progressively thinned during the rotation and may shear out to leave isolated fold hinges.

In addition to inhomogeneous flow between bands, there is also inhomogeneity along the plane of a band.

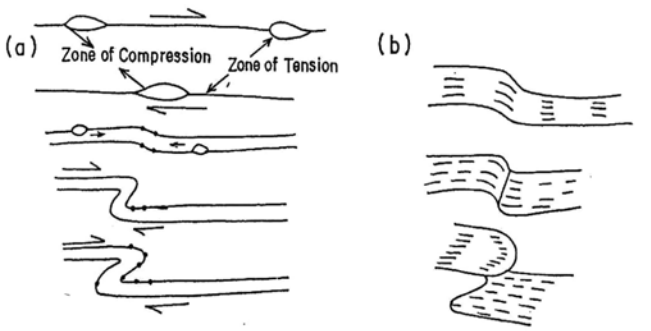

Fig. 7 (a) The development of intrafolial folds due to local stress notches along the mylonite foliation due to differential shearing along the foliation (after Rhodes and Gayer, 1978).

(b) Progressive tonguing out of the intrafolial fold to form a sheath fold (Minnigh, 1979).

Figure 7. Concentration of deformation along the shear zones and the development of folds.

This causes bowing of the axial plane and the folds become grossly non-cylindrical. The combination of both inhomogeneities is to tongue out the folds in the flow direction, i.e. parallel to the stretching lineation. Carreras et al. (1977) termed them as "sheath folds" because they resembled a knife sheath in profile. If sectioned perpendicular to the stretching lineation, they have an eye appearance, sometimes known as "eye folds". The "eye" like cross section is similar to Type I interference pattern that results from the superimposition of two fold events (Ramsay, 1967) and have often been interpreted as such. Sheath folds are not the product of fold super imposition.

The size of a sheath fold depends upon the size of a shear zone. They may range from the microscopic scale in ultramylonite bands up to the kilometric scale (a km in width and several kms long) in major shear zones, e.g., mobile belts (orogens), which have great thickness of mylonite. The amount by which a shear zone tongues (length: width ratio) is a measure of shear strain (Cobbold and Quinquin, 1980). The effect of the tonguing process is to rotate the axial plane from being perpendicular to the stretching lineation; to having large segments parallel and small segments oblique to the stretching lineation depending on the amount of tonguing. Any folds in the country rocks will also be rotated towards parallelism with the stretching lineation.

Once sheath folds tongue out they effectively become a part of the mylonite again but are a heterogeneity in the zone. Consequently, they tend to nucleate another intrafolial fold, which is initially perpendicular to the stretching lineation and consequently "refolds" the sheath fold and in turn becomes tongued itself and is then "refolded" and the process repeated again and again. Quite complex fold pile-ups result from this refolding process and all during a single deformation.

"The concentration of fold axes perpendicular and parallel to the stretching lineation with the former folding the lineation and the later having an apparent superimposition appearance, formerly always and now often, led geologists to conclude that there had been at least two distinct periods of folding post dating the initial development of the mylonite foliation, which is not correct. This is well evident from the history of Moine Thrust studies (Evans and White, 1984), where the previously postulated first three deformation events were found to be due to a single event of progressive deformation."

9. Apparent multiple deformation events arising from single shearing event

The shear band structures rotate the mylonite foliations and also rotate intrafolial folds and present pseudo appearance that all folding is post deformational. Consequently in a classical interpretation of geometrical analysis, such folds are taken to represent four multiple deformation events. But in reality, all these structures are produced from a single shearing event. Thus, if a mylonite is misidentified as a schist, the following four regional deformation events are thought to have occurred: D1- development of the schistose foliation, D2- folding of this and development of the lineation, as a b-lineation, parallel to the fold axis, D3- refolding of the above folds and lineation about a perpendicular axis with local development of an axial planar foliation, D4- large scale regional folding (because they are not seen) to form the shear band foliation, whose constant asymmetry is used to deduce the position of the large scale invisible folds.

"The above analysis of apparent multiple deformation events shows that an entire mess can be made of the regional structural geology if major mylonite belts (shear or mobile zones) are misidentified as schist belts arising through regional shortening."

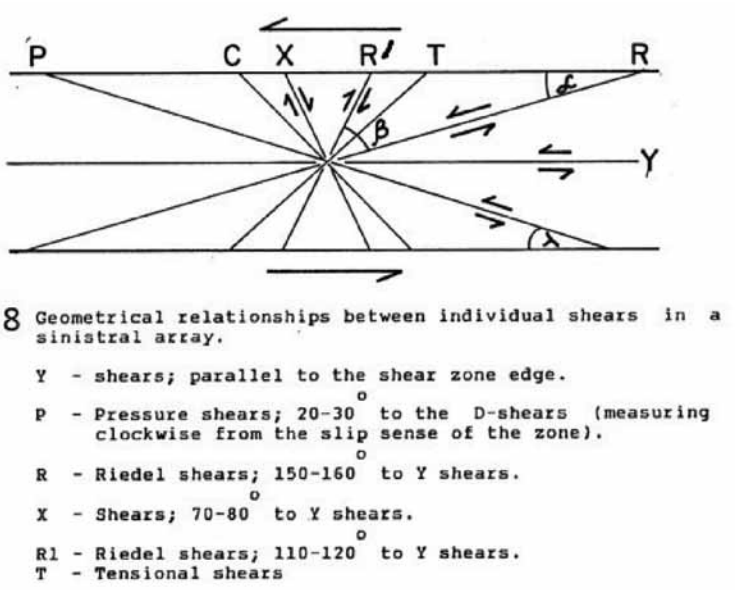

Figure 8. Strike slip arrays in a major shear zone and their geometrical relationships.

10. Three dimensional geometry of shear zone arrays

Shear zones are commonly arranged in networks or sets composed of a number of individual shear zones. They may occur in subparallel sets, may deflect toward one another and link up in an anastomosing pattern, or may crosscut and displace one another. Some shear zones have a curviplanar or folded geometry. Such geometry may indicate that an originally planar shear zone was folded or warped by subsequent deformation. Alternatively, many shear zones form with an original curviplanar geometry, encompassing and wrapping around more rigid, less deformed rocks.

In nature, most individual shear zones are members of an array or of a set in a larger array. Therefore, it is important to consider the fault arrangements in strike slip, extensional and thrust arrays with particular reference to fluid flow and / mineralization and then turn to the depth to which the shear zones cut the lithosphere and in turn will affect the fluid compositions.

Strike slip arrays

There will be individual strike slip zones in the arrays and have a similar sense of movement. Similar geometrical features are produced in experiments of the simple shear of clay blocks. That shows, the same geometrical relationship exists within strike slip zones, irrespective of scale from the mega scale down to the microscale. The relationship is shown in Figure 8.

The arrays consist of normal faults, extensional zones, tensional fractures, 135° to the Y-shears. Reverse faults, fold axes; 45° to Y-shears. The above angles show only slight variations with increasing strain. Y-, P-, R- shears all have the same sense of displacements as that of major shear zone, i.e. in sinistral, while X and R^1 shears have the opposite sense of shear. Each of the individual shear zones have the same internal structures as described earlier. Thus each, in a shear/mylonite zone, has its own uniquely oriented intrafolial folds, shear bands etc. If it is a cataclastic zone, it will have within its own Y-, R-, R^1- and P shears and extensional zones, i.e. shears within shears develop. An example can be from Abitibi greenstone belt where Y-, R-, and R^1 shears are described by Dimroh et al., (1983).

Zone of maximum dilatancy occur where a Y-shear transfers across another Y-through a R-shear and especially where the terminations of two Y-shears are cross-linked by a normal fault (a large extensional or dilational jog) (Figure 9). In cataclastic environments, the R- segments are characterised by extensive veining. In ductile shear zones, they display greater veining and replacement than that of normal faults. The transfer of displacement between two Y-shears also takes place through a P-shear with complete stresses on the P-segment. If there is cataclastic environments in such transitional zone, intense crushing and veining is produced. The most concentrated zones for enhanced fluid flow are the extensional jogs. As will be seen small jogs can give rise to "breccia pipes" and large ones which form the pull apart basins will run into normal faults and extensive fracturing at depth.

"From an exploration viewpoint, extensional jogs offer the best potential for mineralisation, especially vein mineralisation, then R and P shears. The last is more likely to have dispersed mineralisation. The depth to which veins develop especially in the transitional zone depends on the pore fluid pressures and can be calculated."

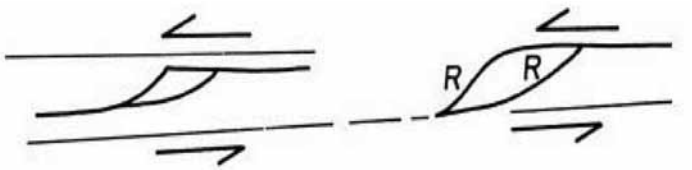

Figure 9. Development of large extensional or dilational jogs when two Y-shears are cross-linked by a normal fault.

Reverse / Thrust Zones

The structure of shear zones in the basement rocks are only considered here but not the ones in cover sediments. The reader is referred to an excellent review by Boyer and Elliot (1982) for the geometrical arrangement of faults in cover sequences.

Shear zone arrangements in thrusted basement are well studied in the South Arunta block on the Alice Springs on 1: 100,000 Geological sheets. They consist of steeply north dipping zones together with some back thrusts dipping to the south and which again have an anastomosing pattern but lack the regularity that appears in strike slip arrays. Cross cutting faults occur more or less, at right angles to the general trend of the anastomosing reverse faults and have a vertical dip. These are transfer or transform strike slip shear zones that accommodate lateral variations in regional shortening (they are also referred to as lateral or sidewall ramps in the thrust literature). The reverse faults show down dip stretching lineations and all internal structures, e.g. sheath folds, shear bands etc. that reflect thrusting. However, in the transfer zones, the lineation is oblique, being parallel to that in the reverse shear zones and again all structures within the zone reflect the oblique shearing. Also of importance, are the transfer faults as they are vertical structures and are the shortest path length for fluids. Once recognized, they can be prospected as straightforward slip zones.

The nature of normal fault arrays in the basement rock is not clearly understood. Much information is available from the oil industry on the structure of normal faults in basins. Deep structures show that they exhibit a similar geometry as that of thrust terrains. There are also transfer strike slip zones accommodating differential extension and as in thrust terrain, they should also be prospected as strike slip shear zones for any mineralization. Andersonian analysis indicates that the vertical segments of the listric normal faults are the most dilatant and are known sites for extensive veining. However, exploration along detachment zones of extensional terrains shows that dispersal mineralization can occur in the flat detachment zone as a result of dilatancy, associated with cataclasis and veining in mylonites.

Extensional faults also propagate into the footwall during continued extension and as a result of maximum thinning and inversion (uplift) towards the basin axis, i.e. into the hanging wall direction of the main listric faults. Metamorphic grade also increases in this direction. This metamorphism differs from that in compressional terrains (thrust) it is of the low pressure regional facies and often confused with contact metamorphism.

Coupled Zones

The transfer faults in the above extensional and thrust terrains are examples of coupling where the strike slip zones are needed to accommodate differential horizontal movements. Coupling does not only aid Andersonian analysis and this, in turn can be used to identify coupling on a regional scale. The best example of coupled shear zones has been reported from Broken Hill of Australia. Another example is from South Africa where the coupling of strike slip zones joins a series of thrust belts.

11. Kinematic indicators in Shear zones

Our understanding of microstructures as kinematic indicators in shear zones and mylonite zones increased considerably during the 1970s and 1980s. Understanding the connection between structural asymmetry and kinematics represented an important breakthrough in the study of strongly sheared rocks. The key point is that many mylonites contain structures that show monoclinic (low) symmetry, exhibiting asymmetric structures. The asymmetry is related to the rotational component or non-coaxiality of the deformation.

The monoclinic structures that give information about the sense of displacement or sense of shear represent crucial kinematic indicators. Some of the key kinematic indicators include: (i) Deflected markers (Foliations and other marker horizons), (ii) S-C structures, (iii) Porphyroclast systems, (iv) Grain-tail complexes, (v) Foliation fish and foliation boudinage, (vi) Crystallographic orientation, and (vii) Fibres and veins.

(i) Deflected markers

It is well observed that the pre-existing markers (linear or planar) become rotated into shear zones during shearing. Even if the shear zone margins are not seen, rotation of planar markers (foliation/marker horizon) from an area of low strain to an area of high strain, provides a

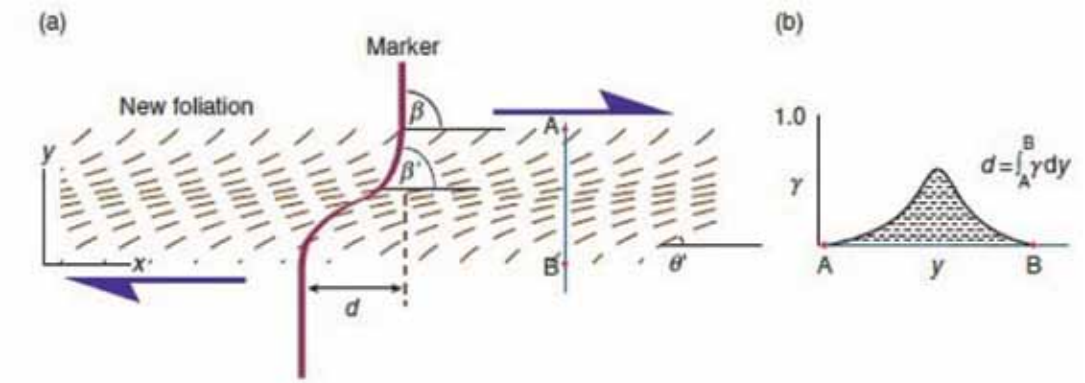

Figure 10. (a) Shear zone with genetically related foliation. The foliation makes 45^0 with the shear zone along the margins. This angle is reduced as strain increases toward the centre of the zone. Y^0 is the angle between the shear zone and the foliation, (b) The displacement can be found by measuring or calculating the area under a shear strain profile across the zone if the deformation is simple shear (source: Fossen, 2010).

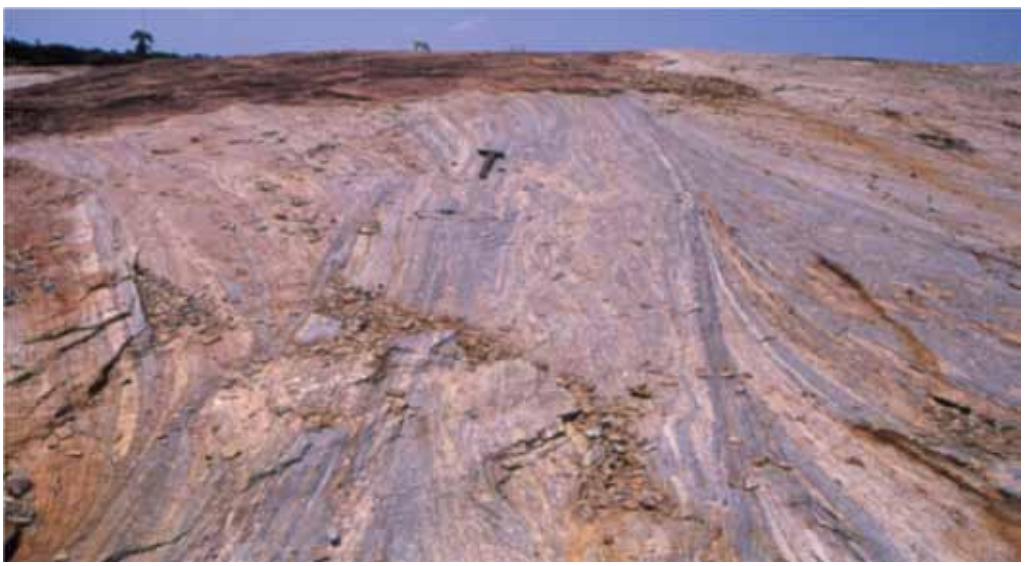

Figure 11. A field example of high grade gneissic rocks in southern Granulite terrane, exhibiting a 1m wide shear zone with deflected gneissic foliation (S-C fabrics).

very reliable criterion for sense of shear determination (Figure 10). Existing country rock foliations rotate into a shear zone and if shearing is homogeneous continue to rotate so that at high shear strains they become parallel to the shear zone edges and through reworking become mylonite foliation (Figure 11). In isotropic country rocks such as granite, a foliation first develops parallel to the flattening plane of the regional strain ellipsoid and then rotates into parallelism with the zone edge as above. However, deformation is seldom homogeneous especially in a zone with a width greater than a meter or so. Small-scale shears marking narrow zones of more intense deformation and strain localization develop at the edges, often described as C-planes and they coalesce to form the braided internal structure of the shear zone and enclose the pods of country rock. The enclosed pods will have a foliation, S, oblique to the mylonite foliation, which should be recognized during mapping as less deformed pods and consequently their internal foliation should cause no difficulties in a regional synthesis.

(ii) C-S and C-C′ Structures

Most mylonites show at least one well-developed foliation that is generally at a low angle to the boundary of the shear zone. Previously, this foliation was called the mylonitic foliation, and it is otherwise known as the S-foliation; S is derived from the French word for foliation, "schistosité." Its angle with the shear zone boundary may be as little as a few degrees, at which point, it is hard to distinguish from a

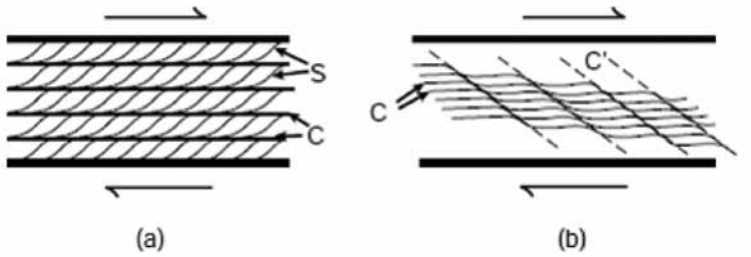

Figure 12. Characteristic geometry of (a) C-S and (b) C-C′ structures in a dextral shear zone.

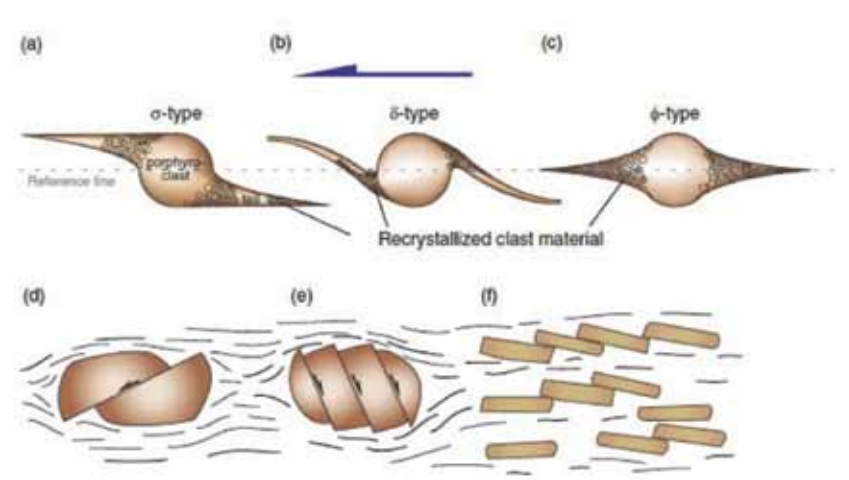

Figure 13. (a) and (b) show monoclinic symmetry (with the rotation axis being perpendicular to the page). (c) The tail is symmetric about the reference line due to coaxial deformation, (d) Fractured porphyroclast with synthetic fracture, (e) Antithetic shear fractures, (f) Tiling (imbrication) of porphyroclasts. All structures (except (c) are consistent with sinistral shear (source: Fossen, 2010).

foliation that parallels the shear zone boundary, called the C-foliation (Figure 12); C comes from "cisaillement," which is French for shear. Often, a third foliation is also developed showing discrete shear displacements that is oblique to the shear zone boundary is called the C′-foliation. The C-surface is parallel to the shear zone boundary and is a surface of shear accumulation (i.e., not parallel to a plane of principal finite strain). The S-foliation is oblique to the shear-zone boundary and may approximate the *XY-plane of the finite strain ellipsoid.* The C′-foliation in (b) displaces an earlier foliation (C or composite C/S).

(iii) Porphyroclasts

Porphyroclasts of feldspar, quartz, mica or other minerals can develop a mantle of recrystallized material that also forms tails, as illustrated in (Figure 13a–c). Coaxial deformations produce tail geometries that are symmetric with respect to the general mylonitic foliation (see Figure 13c). Porphyroclasts with recrystallized tails show sigma-type where the tails do not cross the reference line (Figure 13a) and the tails cross in delta-type (Figure 13b).

(iv) Foliation within mylonites

Two foliations may develop within the mylonites: a localized foliation, axial planar to the intrafolial folds and a more penetrative foliation, that is due to oblique shearing in the zone and has nothing to do with folding. The former is a typical fold related foliation due to local shortening, associated with the intrafolial folds and rotate towards the mylonite foliation as the axial plane of the intrafolial fold rotates into parallelism with the mylonite foliation. The second oblique foliation is commonly encountered in mylonites especially in phyllonites. The foliation is due to localized, internal oblique shearing with the same sense of movement as the main zone, and which leads to extension in the zone in the direction of overall flow. The relationship between this foliation, the mylonite foliation and the movement direction can be referred to as a shear band foliation (White et al., 1986). It further develops along the direction of Riedel shear (R-shear), which is a high shear strain phenomenon, forming well after the mylonite development. The shear bands back rotate with increasing strain and cause the mylonite foliation

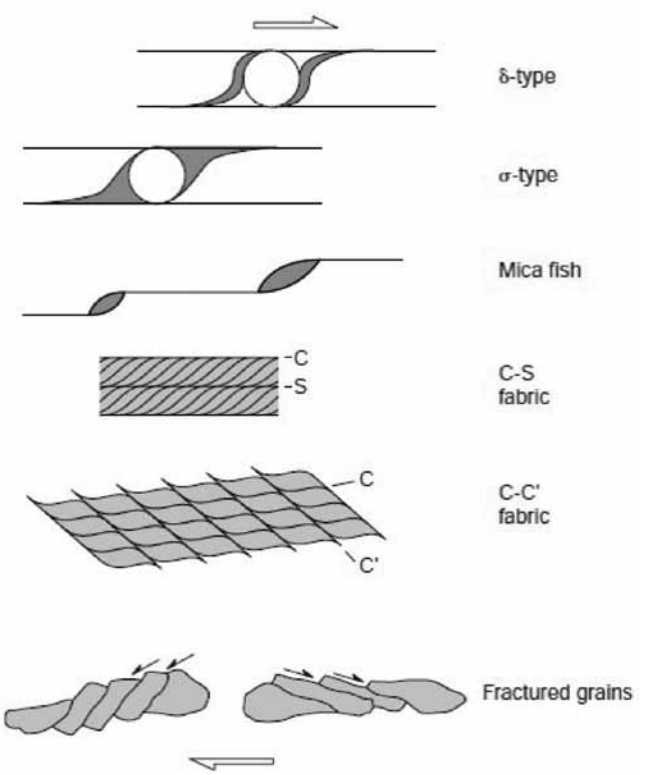

Figure 14. Summary diagram of shear-sense indicators in a dextral shear zone. A copy of this figure on a transparency (for left- and right-lateral shear) makes a handy inclusion in your field notebook (source: Pluijm et al., 2004).

to become oblique to the shear zone edge. The mylonite foliation increasingly steepens as the shear bands back rotate. It is not uncommon for a second set of shear bands to cut a back-rotated earlier set.

(v) Pods or less deformed clasts

In a shear zone with a braided internal morphology, shear strain gradients develop around the pods of enclosed country rock of intended igneous rocks. The result is to develop large shear stresses around these which depending upon the shape will tend to cause dilation at their ends, if they have a low length/width ratio, or pull the pods apart if the length/width ratio is high. The pods tend to break into halves and then quarters and so on later subsequently with increasing shear strain. Often, they develop boudin structures and internal fractures and are perpendicular to the trend of the zone.

With rounded pods extensional fractures or dilatant zones develop at the edges perpendicular to the flow direction with fracturing or dilatancy preferentially occurring at the largest pods. These effects should be remembered when exploring large zones, which contain well preserved pods of country rock or of intruded igneous rocks. A similar behavior is displayed by hard clasts, e.g. feldspars in mylonites at lower temperatures.

Of all kinematic indicators, C-S and δ-clasts are most readily interpretable. For more details of other kinematic indicators such as Grain-tail complexes, Foliation fish and foliation boudinage, Crystallographic orientation, and Fibres and veins and their significance the reader is referred to a book by Passchier, and Trouw (2005). Shear sense in ductile shear zones can be reliably determined when two or more different indicators give a consistent sense of displacement. The summary diagram (Figure 14) shows shear-sense indicators that are commonly encountered in a ductile shear zone.

"Always consider as many sense-of-shear indicators as possible to establish the shearsense."

12. Geometry and Nature of shear zones

Shear zones are commonly arranged in networks or sets composed of a number of individual shear zones. They may occur in subparallel sets, may deflect toward one another and link up in an anastomosing pattern, or may crosscut and displace one another (Figure 15). Some shear zones have a curviplanar or folded geometry. Such geometry may indicate that an originally planar shear zone was folded or warped by subsequent deformation alternatively, many shear zones form with an original curviplanar geometry, encompassing and wrapping around more rigid, less deformed rocks.

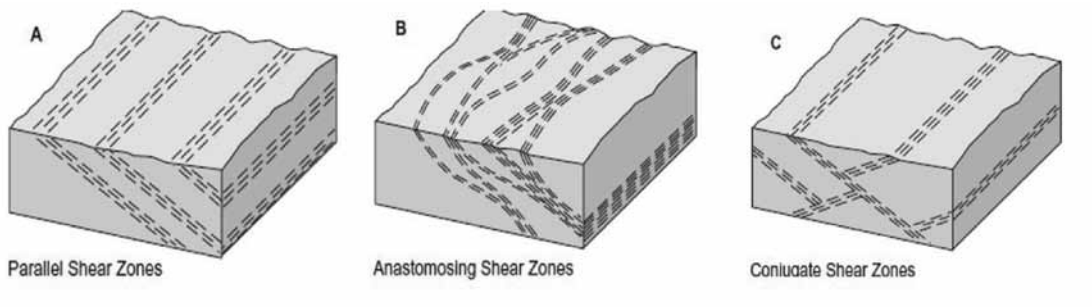

Figure 15. Regional geometry of shear zones.

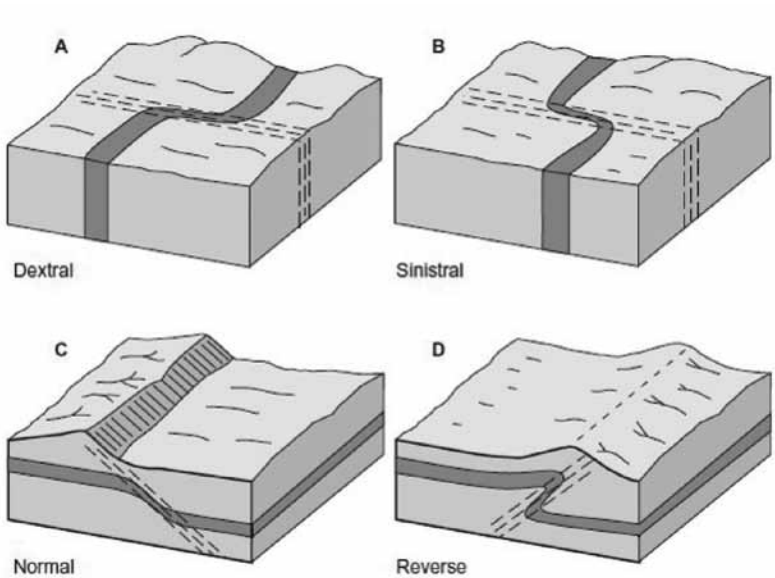

Figure 16. Deflection and offset across shear zones: (A) right-handed or dextral, (B) left-handed or sinistral, (C) normal, (D) reverse. Oblique shear zones have components of both strike-slip and dip-slip (source: Davis et al., 2012).

Determination of relative displacement of rocks on opposite sides of a shear zone reveals the sense of shear within the zone. Similar to fault terminology, shear zones can also be strike-slip, normal, reverse, and oblique-slip (Figure 16). Strike-slip shear zones may be right-handed (dextral) or left-handed (sinistral). Normal-slip shear zones are marked by hanging wall displacement downward relative to the footwall. Reverse- and thrust-slip shear zones are marked by hanging wall displacement upward relative to the foot wall. Oblique shear zones have components of both strike-slip and dip-slip.

13. Reactivation tectonics

In many cases, the brittle-ductile character of a shear zone indicates either that the physical conditions systematically changed during deformation or that the shear zone formed under one set of conditions and was later reactivated under much different conditions. Reactivation tectonics can be easily recognisable when conditions change from ductile to brittle environment. The brittle structures, such as fractures, will overprint an earlier ductile fabric in the shear zone and are easily identifiable. It is more difficult recognizing a shear zone formed during a change from brittle to ductile conditions, because early, brittle structures may be totally overprinted and "healed" by later ductile fabric and metamorphic minerals.

14. Shear zones at Plate Boundaries

Shear zones form in a wide variety of tectonic settings (Figure 17), including plate boundaries of all types. They are undoubtedly forming at depth today in any region with abundant earthquake activity or other manifestations of active deformation (Davis et al., 2012). For example, shear zones are present along seismically active strike-slip zones, such as the San Andreas Fault of California, the Alpine fault of New Zealand, and the numerous strike-slip faults that dissect China and Tibet north of the India-Asia continental collision. Shear zones also mark the sites of past strike-slip zones, such as the South Armorican shear zone of western France and the Great Glen fault of Scotland.

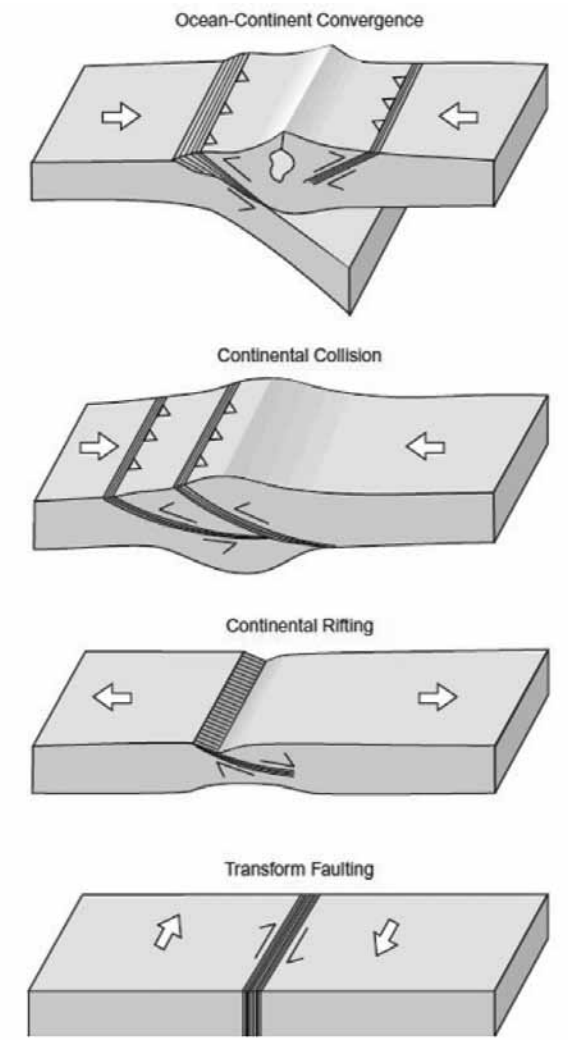

Figure 17. Shear zones occurring in a wide variety of tectonic settings, particularly at plate boundaries of all types.

Shear zones that develop during plate convergence and crustal shortening commonly have thrust displacements that typically bring older, deeper rock up against younger and higher level rock sequence. The best examples are large and spectacular thrust shear zones that occupy nearly the entire length of the Alpine Zagros, Himalayan belt, derived from the collision of Africa and India with the southern flank of Europe and Asia. On the other hand, shear zones that accommodate crustal extension place high-level rock in the hanging wall down against deeper rocks of the footwall. Extensional shear zones are interpreted as forming at depth in regions of active continental rifting, such as the African rift, Greece, and the Basin and Range province of western United States.

15. Controls on fault and shear zone development

Three sets of controls on fault and shear zone development exist: lithospheric-scale, network geometry-scale, and grain-scale. Each scale range tends to be the focus of different research communities, e.g. geodynamicists, structural geologists and microstructural geologists, respectively. However, in order to gain a complete understanding of fault and shear zone processes and their controls, it is necessary to consider the relationships and interactions of processes across all scales.Field-based studies

The fault rock sequence gouge - cataclasite - mylonite forms a depth sequence. Gouge forms at shallow crustal depths where temperatures are so low that clay mineral growth in the matrix and precipitation from fluids is not sufficient to "weld" the fault rock together. This is likely to be favoured by temperatures lower than 100-150°C. At higher temperatures welding occurs and a cataclasite results. The cataclastic / mylonite boundary is taken as the temperature at which the ductile / brittle transition occurs in a granite type mineral assemblage. This was first noted by Sibson (1977). According to him, the transition ranges at around 250-300°C. This implies that the earthquakes

which are a manifestation of catastrophic brittle failure, occur at temperatures lower than the transition range. This is confirmed by later seismic studies.

Many shear zones are simple and well-defined structures, yet our knowledge and understanding of how they form and develop, is far from complete. For simplicity, it is often assumed that they form in homogeneous rocks such as granite. In practice, shear zones form at the weakest point or along the weakest layer in the rock, such as micaceous layers, partly molten zones, veins, fractures, fine-grained layers, dikes etc. This will have to be addressed separately for each shear zone.

Shear zones can develop quite differently, depending on rock properties, fluids, deformation mechanisms and metamorphic reactions, but generally go through an early phase of widening. For further advanced studies on shear zones, the reader is recommended for an excellent review (Fossen and Cavalcante, 2017), published recently, that provides the most useful and fundamental aspects of shear zones, their evolution from incipient to large structures, and discuss challenges that need to be studied in the future.

ACKNOWLEDGEMENTS

I am thankful to Dr. O. P. Pandey, Editor, Journal of Indian Geophysical Union for his invitation to contribute this article. I must also submit here that this article is not exhaustive, but provides only important elements related to shear zones. I am hopeful that this would be of some help for many students, teachers, researchers and other professionals in their scientific pursuits and applications.

Compliance with Ethical Standards

The authors declare that they have no conflict of interest and adhere to copyright norms.

REFERENCES

Bak, J., Sorensen, K., Grocott, J., Korstgard, J.A., Nash, D. and Watterson, J., 1975. Tectonic implications of Precambrian shear belts in Western Greenland, Nature, 254, 566-569.

Boyer, S. and Elliot, D., 1982. Thrust Systems, AAPG Bulletin 66(9), 1196-1230.

Carreras, J., 1997. Shear zones in foliated rocks: geometry and kinematics, in: Sengupta, S. (Ed.), Evolution of Geologic Structures in Micro- to Macro-scales. Chapman and Hall, London, 185–201.

Cobbold, M. and Quinquis, M., 1980. Development of sheath folds in shear regimes. J. Struct. Geol., 2, 119-126.

Coward, M.P., 1980. The Caledonian thrust and shear zones of NW Scotland. J. Struct. Geol., 2, 11-17.

Daly, M.C., 1986. Crustal shear zones and thrust belts: their geometry and continuity in Central Africa. Phil. Trans. R. Soc. Lond., A317, 111-128.

Davis, G.H., Reynolds, S.J. and Kluth, C.F., 2012. Structural Geology of Rocks and Regions, John Wiley and Sons, Inc. third edition.

Dimroth, E., Imreh, L., Goulet, N. and Rocheleau, M., 1983. Evolution of the south-central segment of the archean Abitibi Belt, Quebec. Part II: Tectonic evolution and geomechanical model. Canadian J. Earth Sci., 20, 1355-1373.

Evans, D.J. and White, S.H., 1984. Microstructural and fabrioc studies from the rocks of the Moine Mappe, Eriboll, NW Scotland. J. Struct. Geol., 6, 369-389.

Fossen,H., 2010. Structural Geology, Published in the United States of America by Cambridge University Press, New York.

Fossen, H. and Cavalcante, G.C., 2017. Shear zones – A review, Earth-Science Reviews. , 171, 434–455.

Johnson, D.J. and White, S.H., 1982. Shear heating associated with movement along the Alpine Fault zone, New Zealand, Tectonophysics, 92, 241-252.

Lapworth, C., 1885. The high land controversy in British geology; its courses, course and consequences. Nature, 32, 558-559.

Passchier, C.W. and Trouw, R.A.J., 2005. Microtectonics: Springer, Berlin, 366p.

Pluijm, B.A.V. and Marshak, S., 2004. Earth Structure: An introduction to Structural Geology and Tectonics, Wilkerson second edition.

Ramsay, J.G., 1967. Folding and fracturing of rocks. McGraw Hill, New York.

Ramsay, J.G., 1980. Shear zone geometry: a review. J. Struct. Geol., 2, 83-99.

Sibson, R.H., 1977. Fault rocks and fault mechanisms. J. Geol. Soc. Lond., 133, 191-213.

White, S.H., Bretan, P.G. and Rutter, E.H., 1986. Fault zone reactivations: kinematics and mechanisms. Phil. Trans. R. Soc. Lond., A317, 81-97.

Received on: 20.12.18; Revised on: 21.1.19; Accepted on: 23.1.19

GUIDE FOR AUTHORS

The Journal of Indian Geophysical Union (J-IGU), published bimonthly by the Indian Geophysical Union (IGU), is an interdisciplinary journal from India that publishes high-quality research in earth sciences with special emphasis on the topics pertaining to the Indian subcontinent and the surrounding Indian Ocean region. The journal covers several scientific disciplines related to the Earth sciences such as solid Earth geophysics, geology and geochemistry, apart from marine, atmosphere, space and planetary sciences. J-IGU welcomes contributions under the following categories:

- Research papers and short notes reporting new findings.
- Review articles providing comprehensive overview of a significant research field.

In addition, J-IGU also welcomes short communications, after communications and report on scientific activity, book reviews, news and views, etc.

The manuscript should be submitted electronically as a single word format (.doc file) including the main text, figures, tables, and any other supplementary information along with the signed "Declaration Letter". The manuscript should be submitted by email (jigu1963@gmail.com) to the Chief Editor.

After acceptance of the manuscript the corresponding author would be required to submit all source files (text and Tables in word format) and figures in high resolution standard (*.jpg, *.tiff, *.bmp) format. These files may be submitted to J-IGU as a single *.zip file along with the "Copyright Transfer Statement".

IMPORTANT INFORMATION

Ethics in publishing
J-IGU is committed to ensuring ethics in publication and takes a serious view of plagiarism including self-plagiarism in manuscripts submitted to the journal. Authors are advised to ensure ethical values by submitting only their original work and due acknowledgement to the work of others used in the manuscript. Authors must also refrain from submitting the same manuscript to more than one journal concurrently, or publish the same piece of research work in more than one journal, which is unethical and unacceptable. Editor of J-IGU is committed to make every reasonable effort to investigate any allegations of plagiarism brought to his attention, as well as instances that come up during the peer review process and has full authority to retract any plagiarized publication from the journal and take appropriate action against such authors if it is proven that such a misconduct was intentional.

Similarly, Editor and Reviewers are also expected to follow ethical norms of publishing by ensuring that they don't use any unpublished information, communicated to them for editorial or review purpose, in their own research without the explicit written consent of the author. They are also expected to keep manuscript/ data/ observations/ any other information related to the peer review confidential to protect the interest of the authors. Reviewers should refrain from reviewing the manuscripts in which they have conflicts of interest resulting from competitive, collaborative, or other relationships or connections with any of the authors, companies, or institutions connected to the manuscript.

Conflict of interest
All authors are requested to disclose any actual or potential conflict of interest including any financial, personal or other relationships with other people or organizations within three years of beginning the submitted work that could inappropriately influence, or be perceived to influence, their work.

Submission declaration
Submission of a manuscript implies that the work has not been published previously and it is not under consideration for publication elsewhere, and that if accepted it will not be published elsewhere in the same or any other form, in English or in any other language, without the written consent of the publisher. It also implies that the authors have taken necessary approval from the competent authority of the institute/organization where the work was carried out.

Copyright
After acceptance of the manuscript the corresponding author would be required to sign and submit the "Copyright Transfer Statement".

MANUSCRIPT PREPARATION

The corresponding author should be identified (include E-mail address, Phone/Mobile number). Full affiliation and postal address must be given for all co-authors.

Abstract:
An abstract of not more than 300 words must be included.

Text:
The manuscript should be structured to include a front page containing the title, Author(s) name, affiliation and address of the institute, where the work was carried out, a short title, and 5-to-6 Key words. Author(s) present address, if different from the above mentioned address, may be given in the footnote. The corresponding author should be identified with an asterisk and his/her email ID should be provided. This page should be followed by the main text consisting of Abstract, Introduction, Methods/ Techniques/ Area description, Results, Discussion, Conclusions, Acknowledgements, and References. Tables and Figures with captions should be inserted at the end of main text. It should not be inserted in the body of the text.

Figures/ Illustrations:
All figures should be provided in camera-ready form, suitable for reproduction (which may include reduction) without retouching. Figures in high-resolution (at least 300 dpi) standard formats (*.jpg, *.tiff, *.bmp) are acceptable. Figures should be numbered according to their sequence in the text. References should be made in the text to each figure. Each figure should have a suitable caption.

Tables:
Authors should take note of the limitations set by the size and layout of the journal. Table should not exceed the printed area of the page. They should be typed on separate sheets and details about the tables should be given in the text. Heading should be brief. Large tables should be avoided and may be provided as supplementary information, if required.

Equations:
Equations should be numbered sequentially with Arabic numerals and cited in the text. Subscripts and Superscripts should be set off clearly. Equation writing software that presents each equation as an object in MS Word will be accepted. Style and convention adopted for the equations should be uniform throughout the paper.

References:
All references to publications cited in the main text should be presented as a list of references in order following the text and all references in the list must be cited in the text. References should be arranged chronologically, in the text. The list of references should be arranged alphabetically at the end of the paper.

References should be given in the following form:
Kaila, K.L., Reddy P.R., Mall D.M., Venkateswarlu, N., Krishna V.G. and Prasad, A.S.S.S.R.S., 1992. Crustal structure of the west Bengal Basin from deep seismic sounding investigations. Geophys. J. Int., 111,45-66.

REVIEW PROCESS:

All manuscripts submitted to the journal are peer-reviewed. It is advisable to send the contact details of 4 potential reviewers along with the manuscript to expedite the review process. Editor has the option to select reviewers from the list or choose different reviewers. The review process usually takes about 3 months. All enquiries regarding the manuscript may be addressed to the Editor.

GALLEY PROOF:

Technical editing of manuscripts is performed by the editorial board. The author is asked to check the galley proof for typographical errors and to answer queries from the editor. Authors are requested to return the corrected proof within two days of its receipt to ensure uninterrupted processing. The editor will not accept new material in proof unless permission from the editorial board has been obtained for the addition of a "note added in proof". Authors are liable for the cost of excessive alterations to galley proof.

PUBLICATION CHARGES:

There are no page charges for publication and printing charges for b/w figures. However, in view of substantial cost involved in printing of color figures, author will be charged for printing of pages containing color figures @ Rs. 2,500/- per page. The charges may be revised at any time based on cost of printing and production. Author will receive an estimate/ invoice of the color figures reproduction cost along with the galley proof. It is the responsibility of the author to remit the color figures reproduction cost within one month of the receipt of the estimate/invoice.

The corresponding author will receive a soft copy (pdf format) of his/her published article. Should the author desire to purchase reprints of his/her publication, he/she must send the duly signed Reprint Order Form (accompanies the galley proof and contains price details) along with the corrected galley proof to the Editor. The reprint charges must be paid within one month of sending the Reprint Order Form.

Any payment related to printing of color figures and/or purchase of reprints should be made in the form of a Demand Draft in the name of Treasurer, Indian Geophysical Union, payable at Hyderabad.

You may download the pdf file from: http://www.j-igu.in/IGU-Guide-forAuthors.pdf